NASA CONTRACTOR REPORT

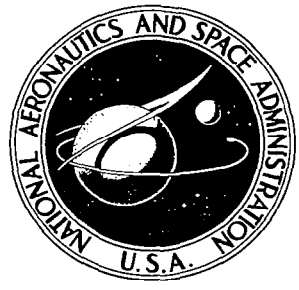

DESIGN AND DEVELOPMENT OF A MULTIPURPOSE, BORESIGHTED STAR TRACKER

by George V. Zito and E. A. Chilton

Prepared by
THE BENDIX CORPORATION
Teterboro, N. J.
for Goddard Space Flight Center

NATIONAL AERONAUTICS AND SPACE ADMINISTRATION • WASHINGTON, D. C. • MARCH 1969

NASA CR-976

DESIGN AND DEVELOPMENT OF A MULTIPURPOSE, BORESIGHTED STAR TRACKER

By George V. Zito and E. A. Chilton

Prepared under Contract No. NAS 5-3780 by
THE BENDIX CORPORATION
Teterboro, N. J.

for Goddard Space Flight Center

NATIONAL AERONAUTICS AND SPACE ADMINISTRATION

For sale by the Clearinghouse for Federal Scientific and Technical Information
Springfield, Virginia 22151 – CFSTI price $3.00

TABLE OF CONTENTS

LIST OF ILLUSTRATIONS

LIST OF ILLUSTRATIONS (CONT)

LIST OF ILLUSTRATIONS (CONT)

LIST OF TABLES

INTRODUCTION

This report covers the development of Multipurpose Star and Planet Trackers by the Navigation & Control Division (formerly Eclipse-Pioneer Division) of The Bendix Corporation for the Stabilization and Control Group of the Goddard Space Flight Center. An Engineering Test Summary is provided as Appendix A.

The Multipurpose Star and Planet Tracker contains several novel features:

1. The Channeltron® image dissector which replaces the plurality of dynodes required by conventional photomultipliers with a single continuous strip electron multiplier.

2. A scanning system in which a multi-lobed scan serves for both acquisition and tracking in a single mode, automatically generating proportional and saturated zones.

3. The use of magneto-resistive bridge multipliers as modulators.

4. Microcircuited timing and demodulator circuits.

Although the tracker was unable to satisfactorily meet the original specification with respect to the signal-to-noise ratio, it will track navigational stars and the center of illumination of the planets Mars, Venus, and Mercury. It will track the brighter of two stars within its 8 degree field of view provided the star is brighter than one visual magnitude and separated from other stars by at least 50 minutes of arc.

The completed tracker weighs only 5 lbs, 14.4 ozs (project goal was less than 8 lbs) and requires 4.65 watts of power (project goal was less than 8 watts). The protype unit and the flight unit have been supplied with alternate mounting configurations to satisfy a wide range of applications.

The single mode approach has much to recommend it. However, for optimum performance certain concessions are required with respect to field size and/or output bandwidth if extremely low error pointing is desired. The Channeltron® image dissector photomultiplier has reached that stage of development where it is competitive with other state-of-the art detectors; incorporated into future trackers it holds promise of providing a highly reliable component for spacecraft instrumentation system.

The design concept originally proposed involved a single mode of operation to preclude the need for switching at the input of the control system. This concept has been adhered to despite occasional excursions into experiments with two mode tracking or alternate schemes which attempted, in one form or another, to satisfy the difficult signal-to-noise requirements initially specified (and subsequently modified). A novel multilobed scan was employed which allows coarse acquisition accuracy near the edge of the wide angle (8^{o}) field of view with increasing resolution and pointing accuracy at and near boresight. Since the specification requirements were for a non-gimballed, boresighted tracker, the scan chosen appears to satisfy this requirement ideally. However, the requirement that the output bandwidth be limited to 5 cycles limits the choice of scanning frequencies available; the "frame" frequency, which produces two rotations in azimuth of the scanning beam, must be sufficiently high to allow rejection of its components by the output filter and yet be low enough to permit adequate dwell time on the star target. Since the detector is essentially shot-noise limited, and although we have recourse to extremely high efficiency photocathodes of the S-20 variety, the dependency of signal-to-noise ratios upon the arrival times of photo-electrons limits the ultimate pointing accuracy. The large angular excursion of the scanning beam (out to ± 4 degrees at a 400 cps rate) in elevation permits a pulse duty cycle to be employed which is inadequate from the standpoint of the electron arrival rate for weak stars. Unfortunately, neither the 400 cps excursion in elevation angle nor the 25 cps excursion in azimuth may be decreased sufficiently in frequency while still accommodating the 5 cps output bandwidth requirements. Either the scan must be switched, reducing its excursion to limits at or near boresight once the star has been acquired, or larger optics or lower output bandwidths must be employed.

The trackers, as furnished, include optical heads with the largest collecting power economically feasible. An F:2 refractive system is employed, with photographic resolution components. Since the photocathode size (0.5 inch) and the desired field of view (8 degrees) fix the focal length at 90 mm, the 45 mm objective was selected as the largest aperture readily available. Lens systems with stops lower in number than F:2 are uneconomical and massive in structure and hence are not within the ground rules established for this program.

The design goals specified included a maximum weight of 8 pounds and a maximum power input requirement of 8 watts. The units delivered weigh less than 6 pounds each and require less than 5 watts for operation. The design goal for target star acquisition was one second, although less than 0.1 second is required by the units delivered. The mechanical configuration of the tracker is such that it may be either mounted from the rear or at the mounting flange close to the center of gravity where the telescope is fastened. No dis-

assembly of the unit is required to change optical heads; instead, the removal of eight screws permits the telescope to be removed and another inserted in its place. Separate X and Y zeroing adjustments are available at the front panel to permit final boresight adjustment after mounting.

The desired star tracker output characteristic is shown in Figure 1 (A), and consists of a limited zone of proportionality surrounded by a zone of signal saturation. This characteristic is generated in the manner shown in Figure 2. A series of scanning spot excursions, at a 400 cps rate, traverse the 0.5 inch photocathode diameter while progressing clockwise at a 25 cps rate, producing an interlaced scan of 32 lobes. Figure 3 shows how this is accomplished by multiplying the 400 cps lobe signal with a 25 cps timing signal divided down from it to produce X and Y deflection yoke voltages, and presents additional information on the scanning signal. Multiplication is carried out by magneto-resistive bridge multipliers. Synchronous demodulation and filtering of the video signal results in the production of a 25 cps error signal, the phase angle of which is related to the angular displacement of the target star in azimuth, and amplitude of which is proportional to the linear displacement of the target star from the center of the field of view. This signal is then resolved into X and Y components and presented to the output terminations as dc error signals.

The Channeltron® image dissector tube is shown in Figure 4; Figure 5 shows the component parts used in its assembly. The Channeltron® element is the resistor-like subassembly near the left hand margin of the photograph. Figure 6 is a photograph of the tracker optical subassembly. The Channeltron® image dissector is bonded to a copperplated Armco iron shield by means of a silicone rubber potting compound. The shield registers upon the deflection yoke housing which in turn registers to the front mounting plate of the tracker; the telescope registers against the opposite surface of the front mounting plate. The central pin emerging from the tube base is the image dissector target electrode. Four machine bosses upon the mounting plate accept the studs which hold the printed circuit electronics packaging. Figure 7 shows this arrangement; the circuit boards have been assembled about the optical head. The central, shielded portion is the high voltage power supply required by the image dissector; the video amplifier section lies to the rear of the assembly; where it picks up the target electrode; the timing circuits lie at the front, immediately about the deflection yoke. Figure 8 is a view of the assembled tracker. Figure 9 is a rear view, with a smaller telescope mounted to the front mounting plate. In both photographs the housing is a spun alcuplate shroud bonded to a mounting flange which accepts the tracker front mounting plate. Tracker No. 2 was furnished with this style housing. Tracker No. 1 was furnished in a rear mounting design compatible with a pre-existing secondary mirror support of a larger telescope the tracker was to guide.

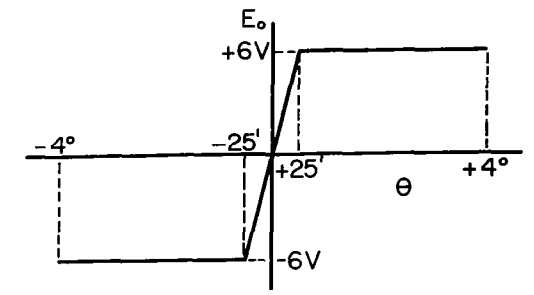

Tracker Output Characteristic

FIGURE 1

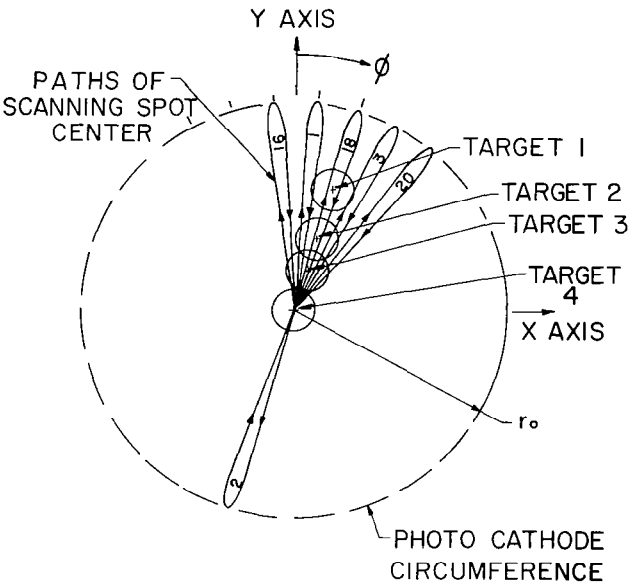

Tracker Scanning Pattern

FIGURE 2

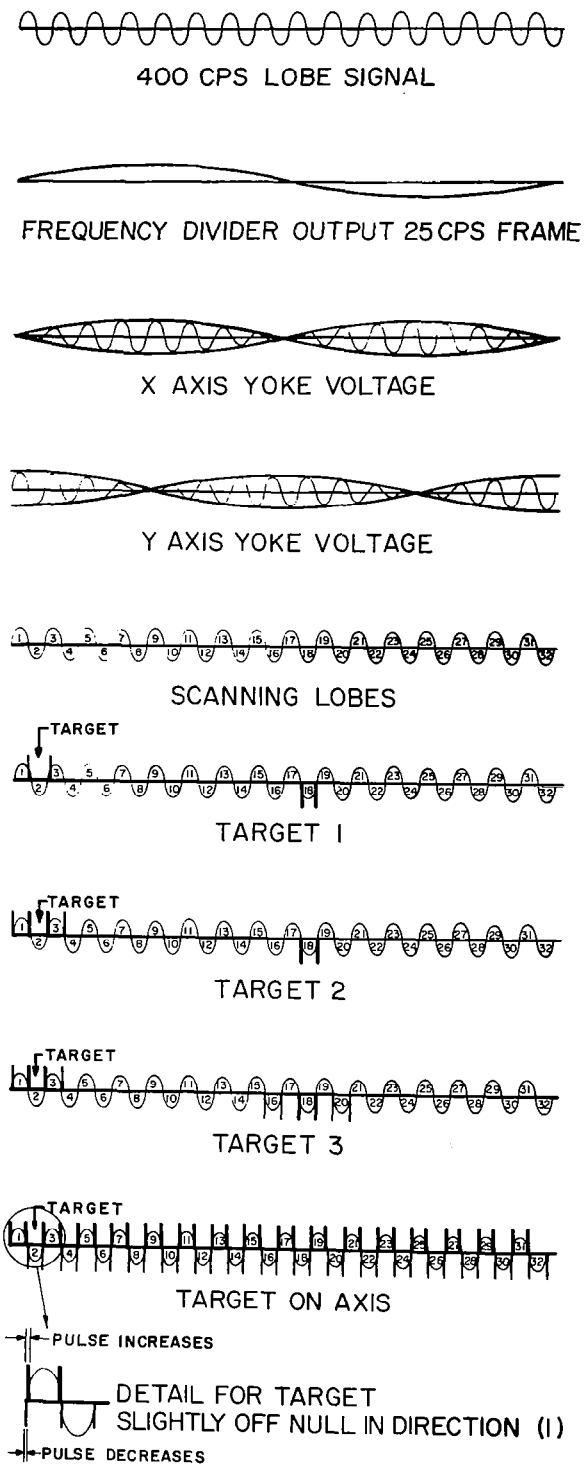

Tracker Scanning Signal

FIGURE 3

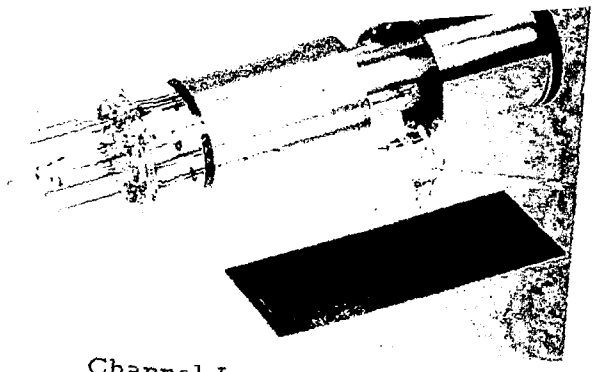

Channel Image Dissector
Photomultiplier

FIGURE 4

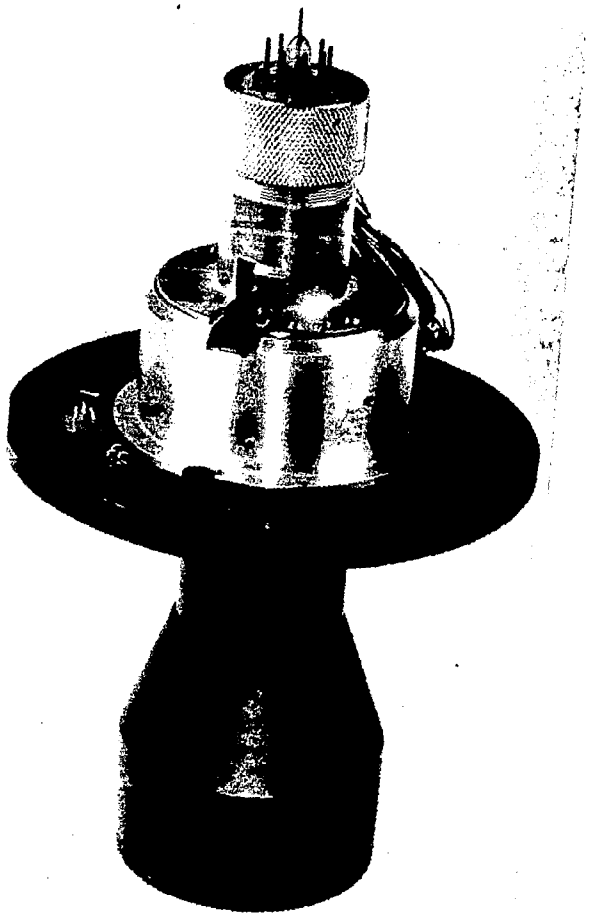

Tracker Optical Head
FIGURE 6

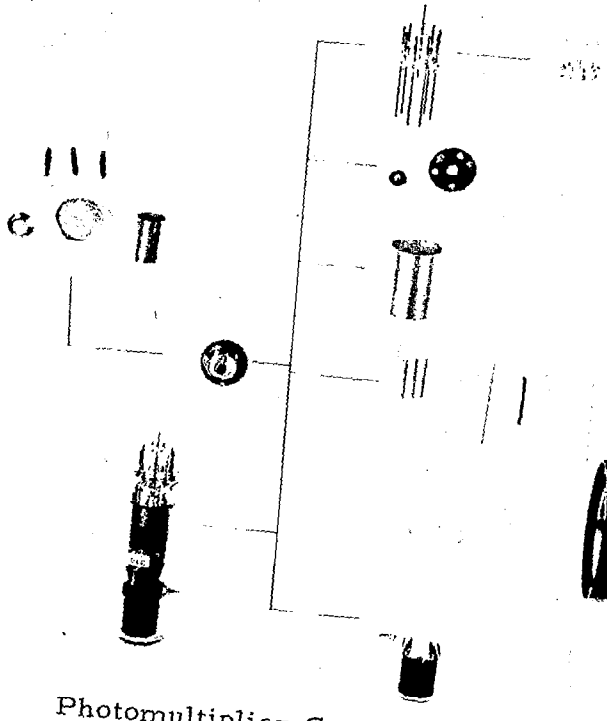

Photomultiplier Components

FIGURE 5

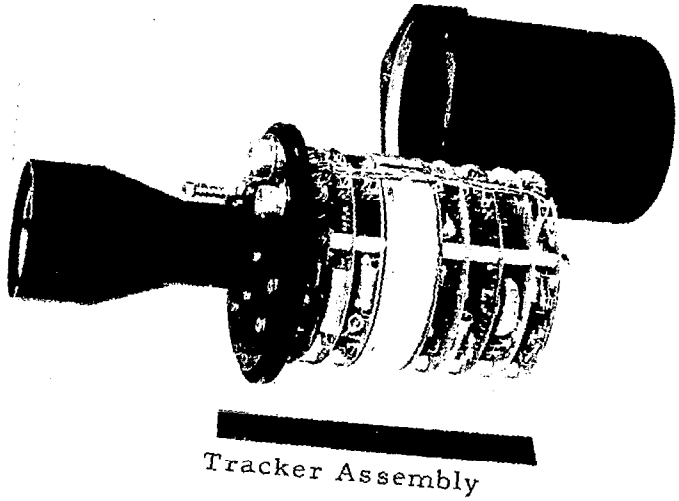

Tracker Assembly

FIGURE 7

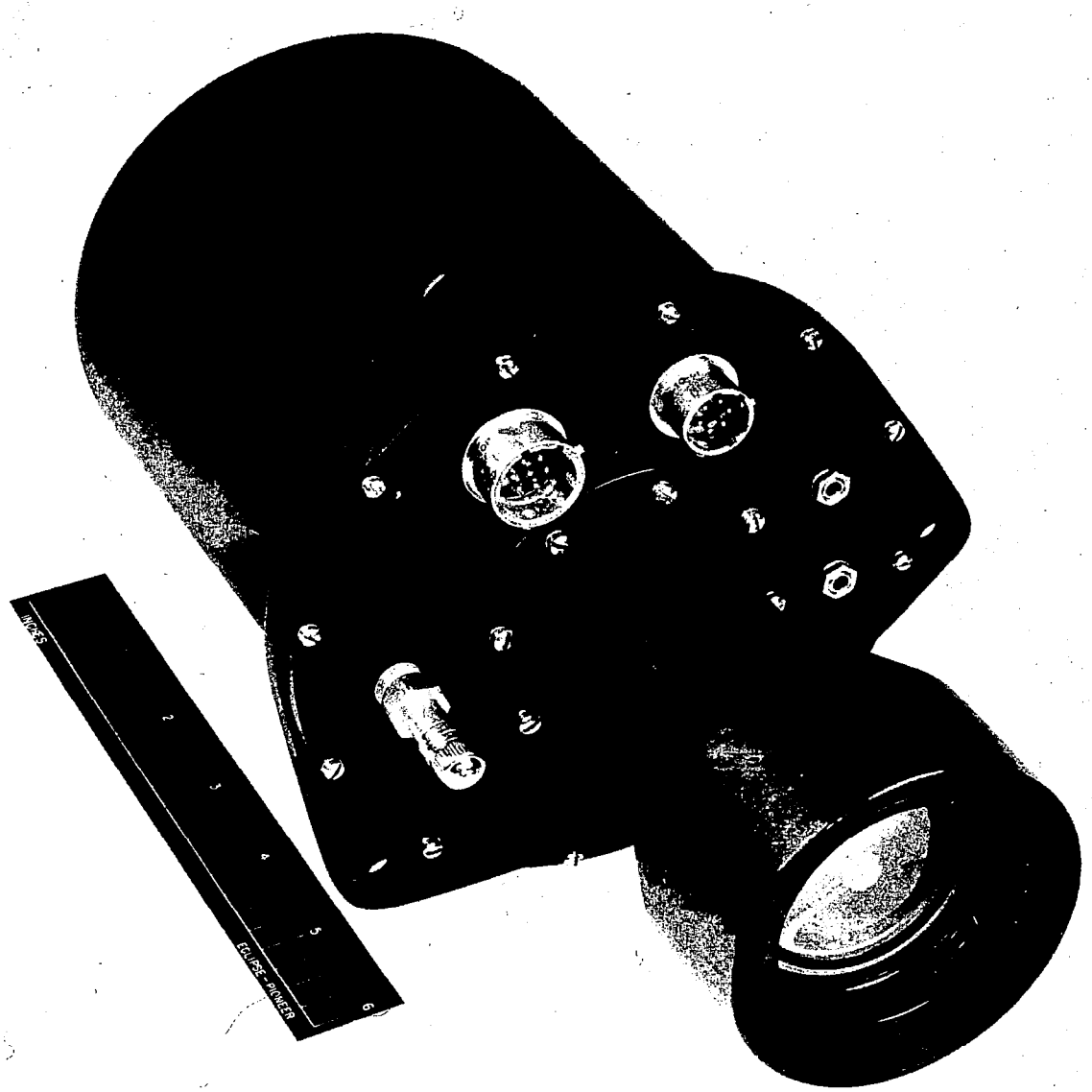

Tracker, Large Optics

FIGURE 8

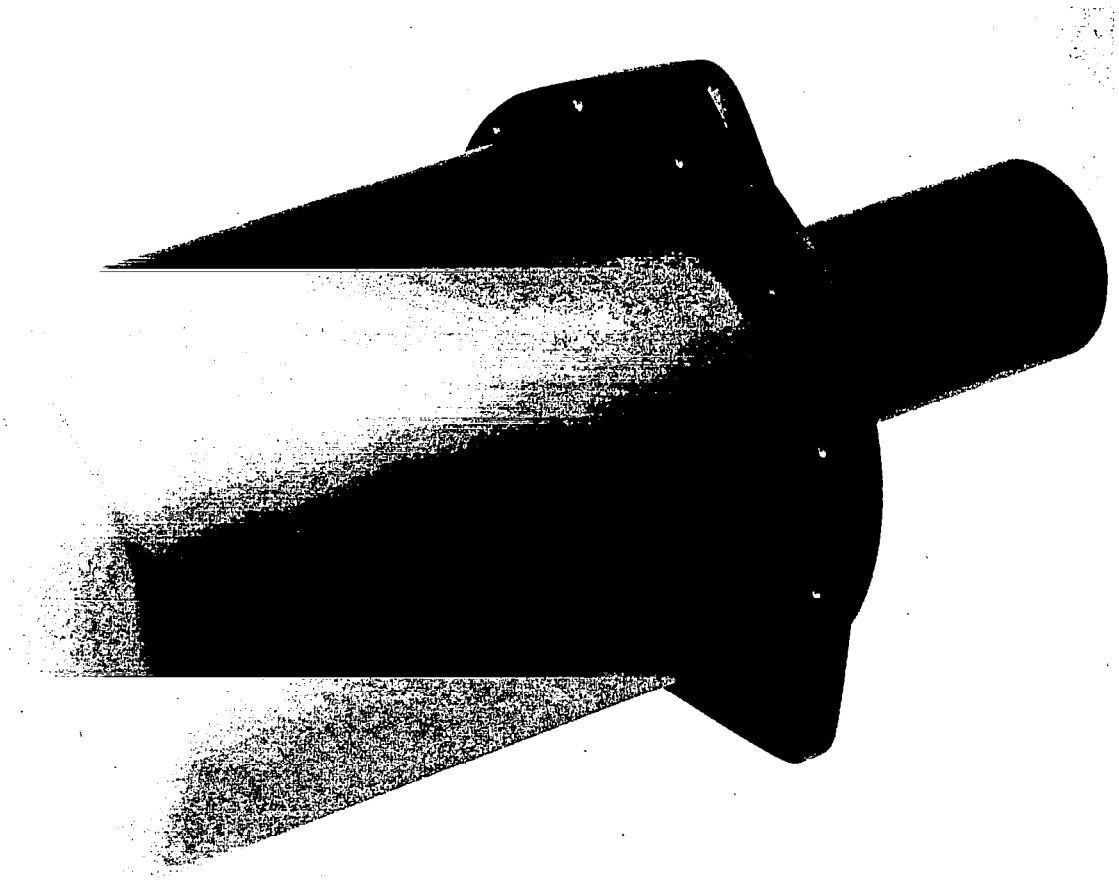

Tracker, Small Optics

FIGURE 9

Figure 10 shows this housing, on the left in the photograph, prior to final finishing. The copper gasket shown in front of the housing permits additional support to minimize excursions of the cantilevered structure. At the right in the photograph is the secondary mirror-support within which the tracker must be mounted. A screw-in flange, shown before this support, is unscrewed from the support after the tracker has been bolted down, and engages the copper flange, driving it into the recess provided in the circumferential boss near the top of the tracker housing. Figure 11 shows the housing bolted in place within the mirror support, with the screw-in flange engaged. The actual secondary mirror of the telescope to be directed is not shown in the photograph; it mounts upon the bosses which appear to be the feet of the support in the photograph, and looks toward the primary reflective optics which are, in turn, looking in the same direction and along the same axis as the star tracker.

The outline dimensions of the tracker are shown in Figure 12, which also shows the location of the various tracker components. The coaxial design registers all optical components, including the telescope, detector, and scanning yoke and appropriate magnetic shields, to concentric circular registers on the front plate for maximum mechanical accuracy. The front plate, in turn, registers with the various housings available to satisfy different mounting constraints.

Two trackers were built and delivered to the Goddard Space Flight Center. The first of these was placed on the Aerobee Air Bearing simulator and tests with the control system performed, using simulated star targets. The second unit was subjected to qualification testing at Bendix and subsequently delivered. The second unit included one additional printed circuit board, Board 9, which eliminated some of the sub-boards used in Tracker No. 1. Aside from the alternate housing configurations, and the inclusion of Board 9, the two trackers are identical in embodiment, and performance tests disclose little difference between the two.

The following discussions are intended to recount, as fully as possible, the design concept of the Multipurpose Star and Planet Tracker, the manner in which this concept was carried out in the final hardware, and the engineering effort involved. Included are discussion of the tracker circuitry and theoretical concepts, discussion of signal-to-noise accuracy and allied optical subjects, and finally, test results and measurement procedures.

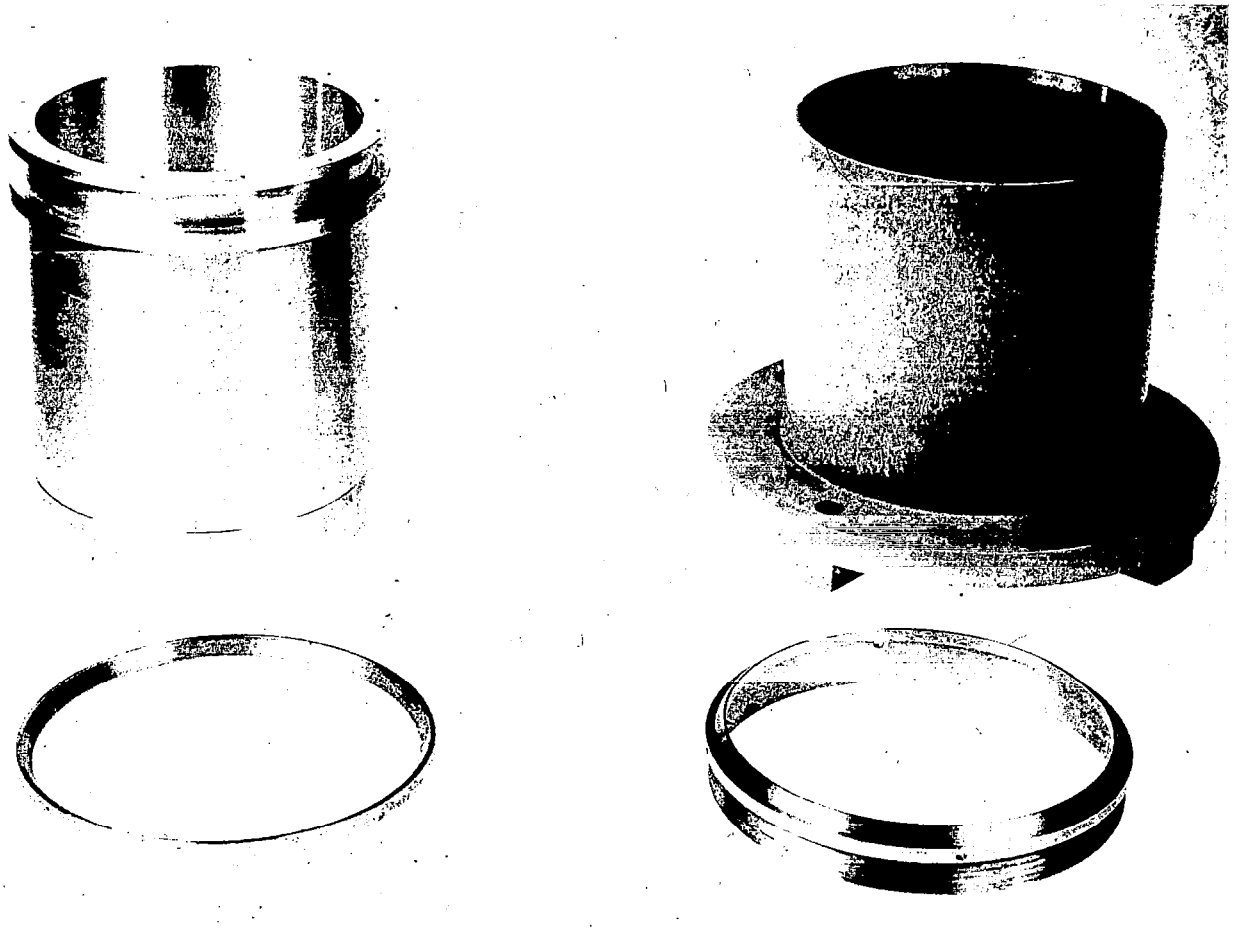

Multipurpose Tracker Housing and Secondary Mirror
Mount of UV Experiment (Aerobee)

FIGURE 10

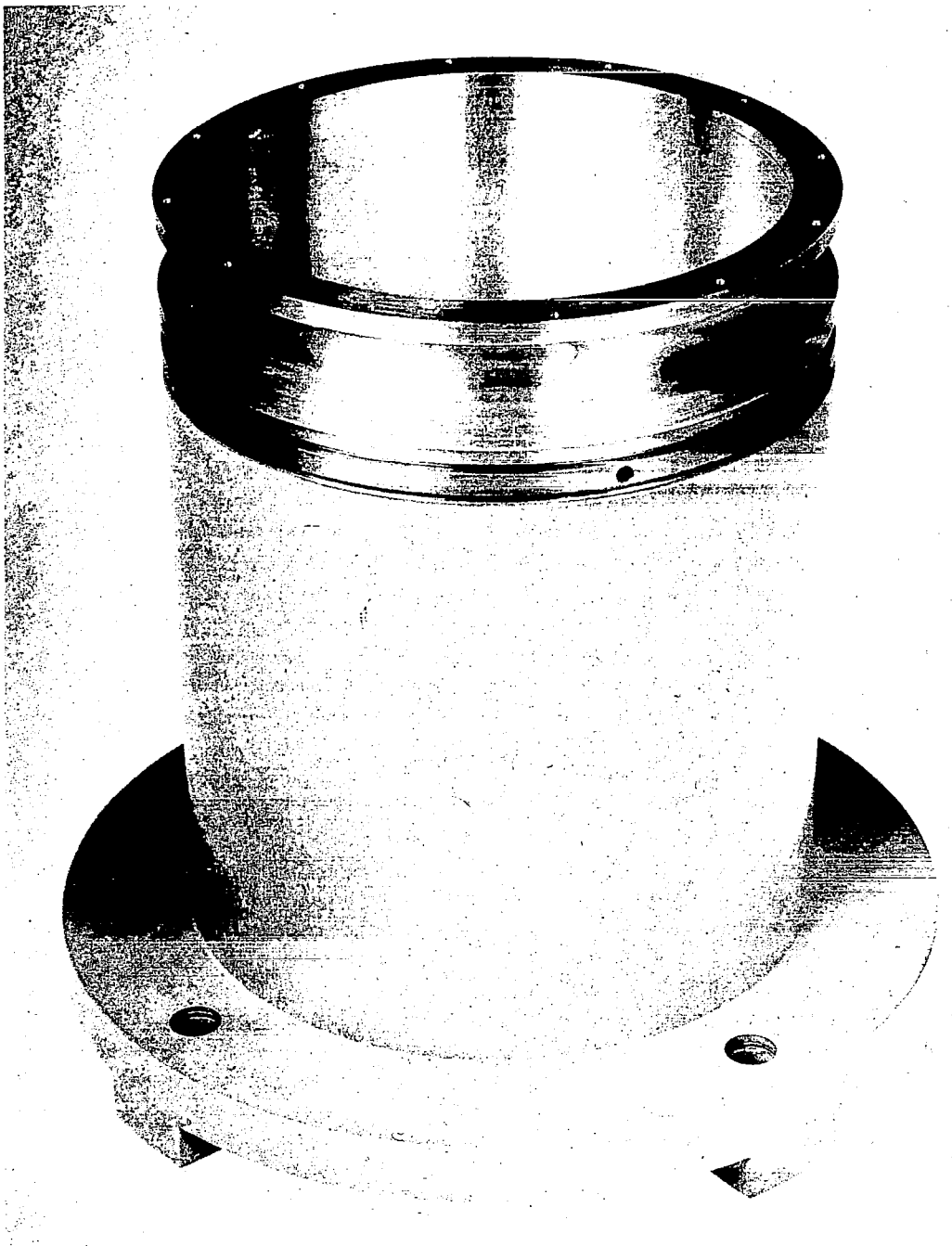

Method of Mounting Multipurpose Tracker To Secondary Mirror of UV Experiment

FIGURE 11

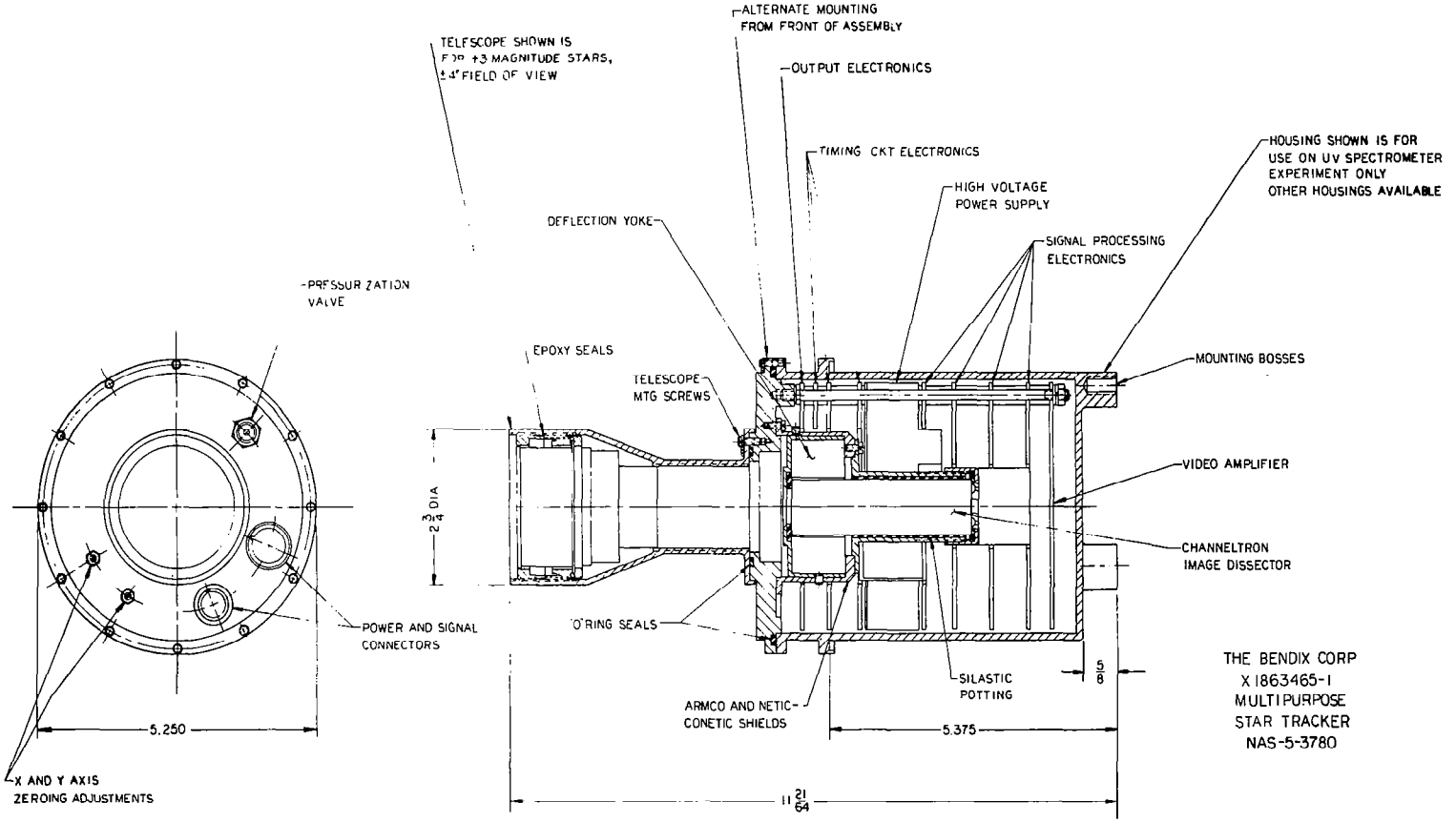

Tracker Outline Drawing

FIGURE 12

THEORY OF OPERATION

The theory of operation of the Multipurpose Star and Planet Tracker is discussed in the following sections. Wherever possible, we have attempted to key the explanations of particular portions of the circuit to their physical embodiments in the delivered trackers. Thus, in the section on Video Amplification, we note that the video amplifier "is located on Board No. 8". The designation of boards by number is an informal expedient, useful in testing the individual circuits involved. Table 1 lists the boards by number, schematic designation, and title. The high voltage power supply module replaced Board No. 4. Figure 13 shows the location of these boards in the tracker.

The system is relatively complex conceptually, although each of its elements lends itself to relatively simple description. For this reason certain portions will be covered several times in different sections. Several simplified block diagrams are used, and the discussion is arranged in an order that permits the reader to grasp certain functional concepts of operation before plunging into circuit details.

A portion of the present material has appeared in other forms, either in progress reports or in papers presented before technical groups in this country or aboard. Where such material has been used, however, it has been carefully edited to conform with the overall discussion format of the present report.

Simplified Block Diagram Discussion

The tracker electronics may be roughly divided into three separate sections:

1: A timing section which generates the necessary timing pulses to provide demodulation and which, in conjunction with the magneto-resistive bridge modulator, generates the scan.
2: A modulator-demodulator section.
3: A video amplifier and associated service circuits, as for example, those circuits required for telemetering star magnitude, star presence, etc., all of which are inherently video functions. The high voltage power supply is included in this category.

A system of double demodulation is employed to extract the star position information from the video signal and resolve it into x and y component. Figure 14 is a simplified block diagram of the elements of the system.

TABLE 1

Designation of Circuit Boards*

BOARD NO.	SCHEMATIC DRAWING	ASSEMBLY DRAWING**	CIRCUITS INCORPORATED
0	1856353	1856351	Tracker final output circuit; 25 cps demodulator and filter
1	1818880	1818863	Timing ckt, oscillator, frequency divider, exclusive OR
1A	1863196	1863198	Timing signal pulse inverters, 25 cps
2	1818881	1818870	Filter circuits for square to sine wave conversion
3	1818875	1818879	Deflection drive preamplifiers
5	1856346	1856342	400 cps demodulators and 25 cps filters
6	1856370	1856373	Frequency multiplier drive amplifiers
6A***	1896310	---	Gain changer
7	1856365	1856368	Frequency multiplier circuits
8	1818887	1818886	Video amplifier, AGC amplifier, pulse standardizer
8A***	1896311	---	Star present circuit
9***	1896329S2	1896329S1	Proportional region detector, star present circuit, gain changer

* Board No. 4 is replaced, in the delivered trackers, with a power supply potted module HV, schematic No. 1863471, assembly drawing No. 1863456 (high voltage supply, dc level translator, buffers).

** See Figure 13 (drawing No. 1863465) for hardware location.

*** Board No. 9, in Tracker No. 2 only, incorporates circuits supplied on Board No. 6A and Board No. 8A, in Tracker No. 1 only.

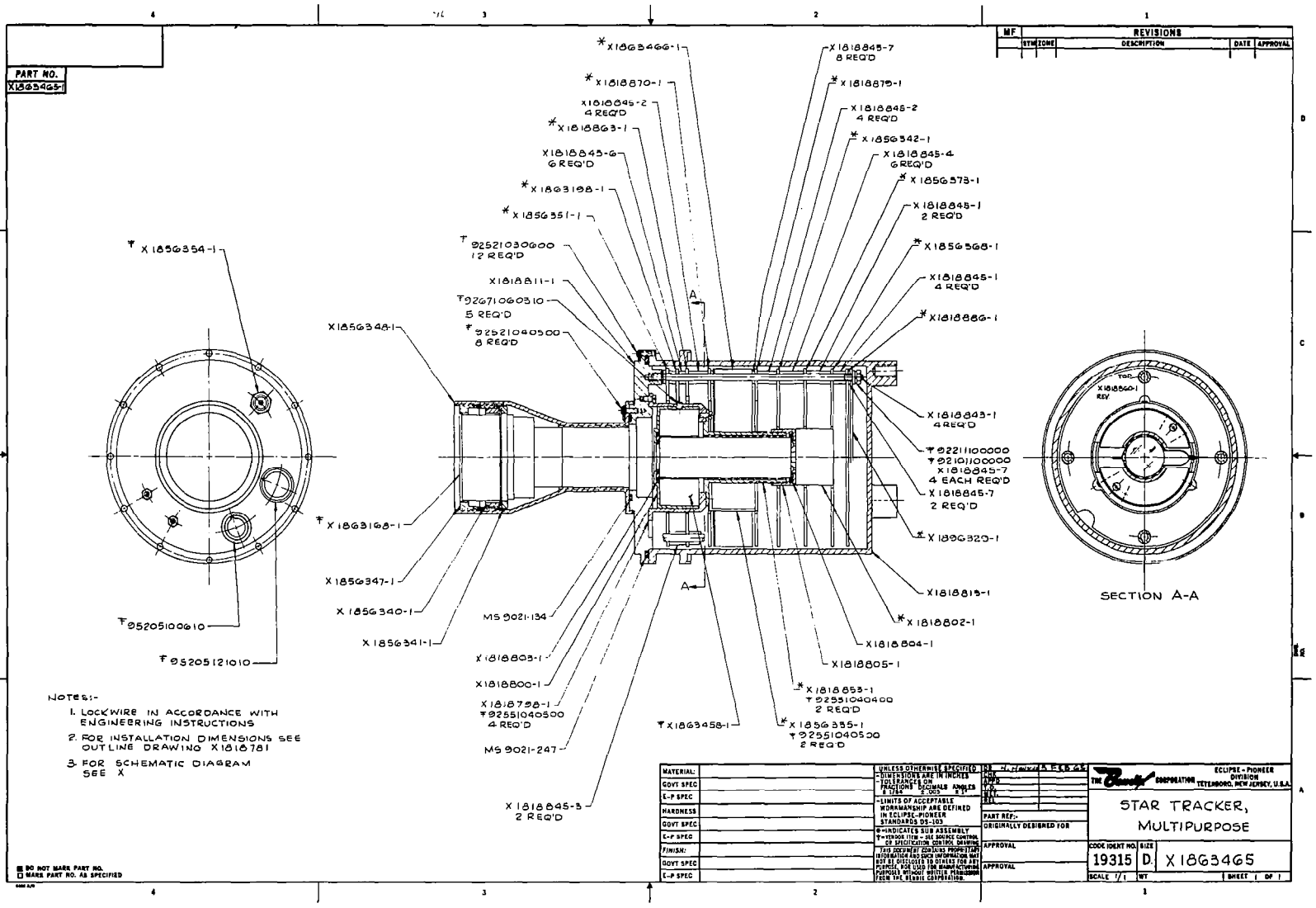

Location of Circuit Boards
FIGURE 13

The timing oscillator is a tunnel diode oscillating at 800 cps; this frequency is immediately divided to 400 cps, however, and does not appear elsewhere in the system. The timing signal at point A is, therefore, at a 400 cps rate. This signal is further divided, by the frequency divider shown, to provide two 25 cps signals, one of which is in phase with the initial 400 cps signal; the other 25 cps signal is shifted 90 degrees. To provide modulator signals the 400 cps signal and both 25 cps signals are converted from square waves to sine waves before injection into the modulators; elsewhere in the system, however, they appear as square waves to facilitate switching functions. The modulator output signals, which drive the orthogonal deflection yoke coils, are in the form shown previously in Figure 3 and consists of 25 cps modulating envelopes at 90 degrees to each other, superimposed upon 400 cps carriers. A series of scanning lobes is produced, 32 in number, as shown in Figure 2. At boresight and close to boresight the scanning aperture projection will make 32 excusions through the star target. What is present at the output of the video amplifier, therefore, is a series of pulses, one each per excursion for the star at null (target on axis), as shown in Figure 3. Progressively off null the number of pulses diminishes, as shown in the other portions of Figure 3. Exactly at null these pulses are centered about the 400 cps crossovers; slightly off null they lead or lag the crossover times.

The 400 cps half-wave periods shown in Figure 3 have been numbered to correspond with the scanning lobes of Figure 2. By synchronous demodulation at a 400 cps rate, the chain of video pulses in the output of the video amplifier are converted to positive and negative going pulses in accordance with their correspondence, position-wise, to the numbered 400 cps half-wave periods. For a star exactly at boresight these pulses are evenly spaced and occur at the zero crossover points of the 400 cps timing signal. Off null, however, there will be an uneven distribution of pulses, at the azimuthal rotation rate (25 cps) at a phase angle determined by the azimuthal position of the star. A 25 cps filter is used at the output of the switched demodulator to extract this signal component from the pulse chain, and it is then applied to the 25 cps switched demodulators. One of these demodulators is being switched at the sine signal rate, the other at the cosine (90 degree phase shift) rate. The error signal is thus resolved into its X and Y components and, passed through the 5 cps output filters, appears as two DC voltages at the tracker output terminals.

Figure 15 is a functional block diagram, useful in understanding the overall operation of the tracker. Here the DC servo loop controlling detector gain has been included. The high voltage is automatically maintained at that value required to obtain 4×10^{-10} ampere into the input of the video amplifier;

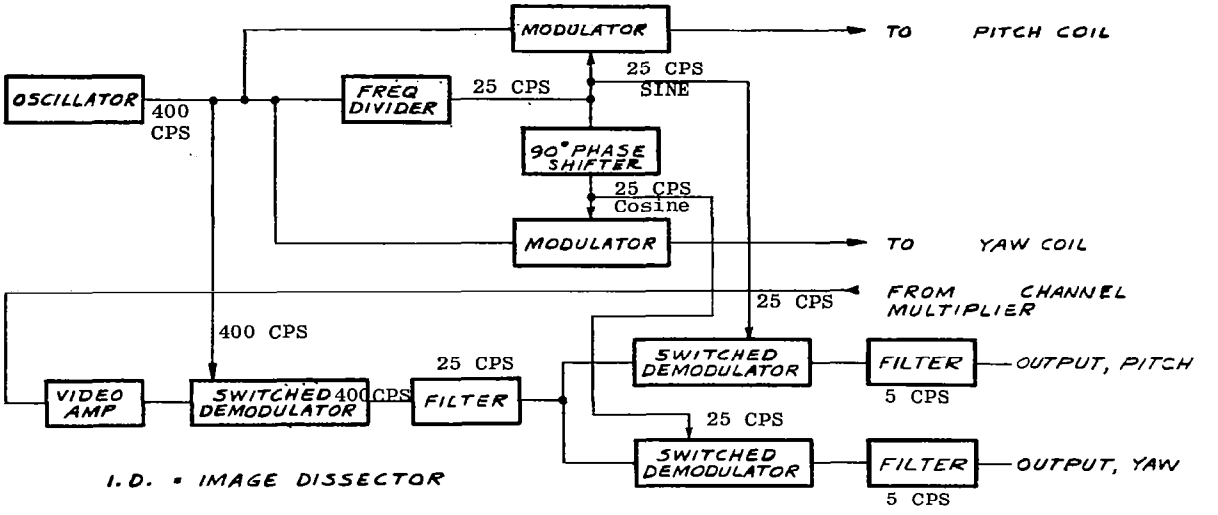

Simplified Block Diagram
FIGURE 14

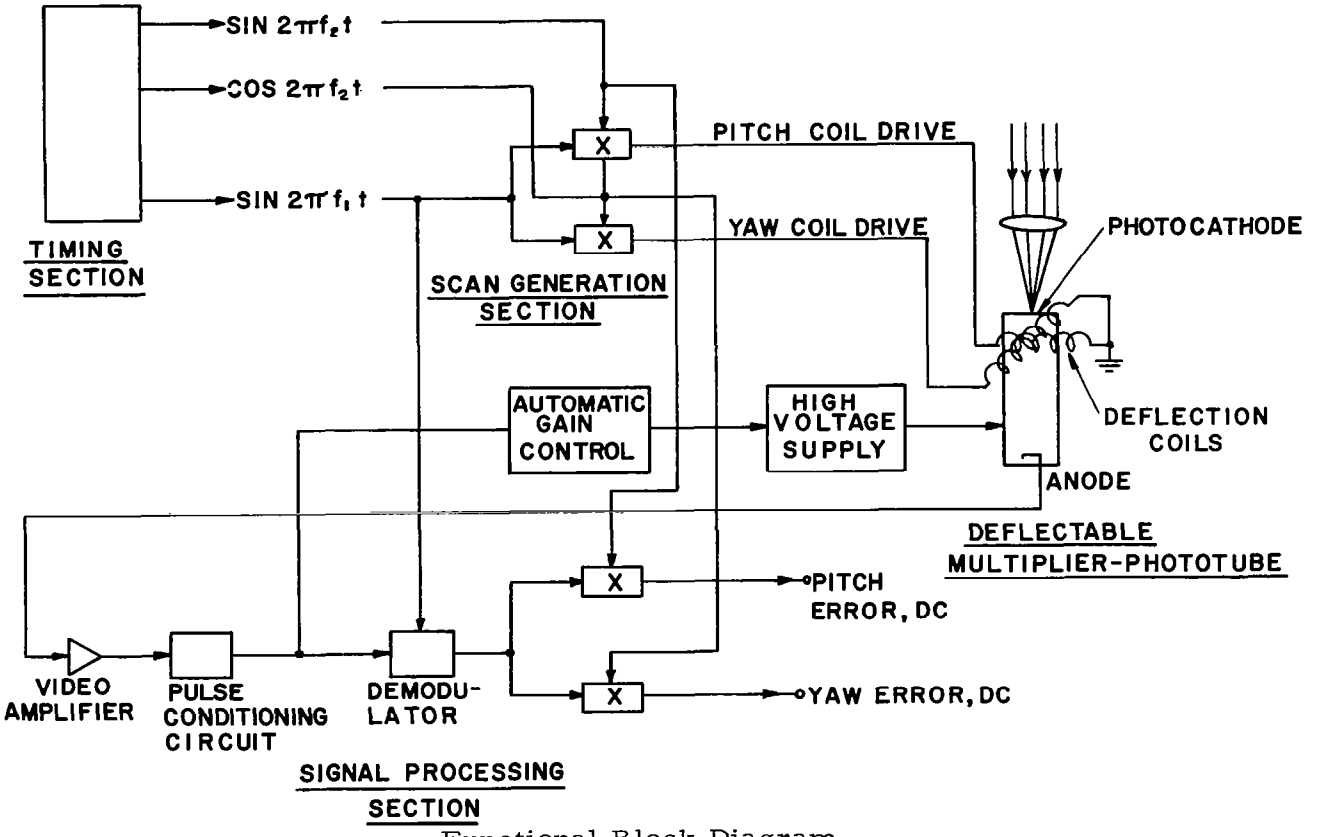

Functional Block Diagram

FIGURE 15

thus, a lower high voltage is supplied to the phototube for a bright star than for a weaker star. This not only allows for video pulse height standardization, but permits the generation of a low value dc signal which is proportional to star magnitude, and which is provided for telemetry purposes to facilitate star identification.

Block Diagram (System)

Figure 16 is a comprehensive block diagram of the star tracker system. Waveforms obtained at various points are given, and representative signal amplitudes. The elements of the block diagram are referenced to the respective printed circuit boards (see Table 1), and the circuit board designations. Figure 16 will be found particularly useful in understanding the discussions which follow in the subsequent subsections of the present section, and the interrelationships of the elements of the Multipurpose Star and Planet Tracker.

Video Amplification

The video amplifier (Figure 17) is located on board No. 8 (Schematic diagram X1818887) and is composed of the video preamplifier, voltage amplifier stages, the pulse amplitude selector circuit, and the overdrive circuit. After discussing these portions of the video amplifier, this section presents the derivation of the video preamplifier current-to-voltage transfer.

Video preamplifier. The problem of matching the video amplifier to the essentially infinite impedance of a Channeltron ® collector has been met by using a low-noise type field-effect transistor as an input stage. This input transistor, Q_1, cascaded with transistors Q_2 and Q_3, produces a high gain dc-coupled voltage amplifier which when used with the resistance divider network R_6 and R_7, and feedback resistor R_1, results in a current to voltage transfer characteristic for the preamplifier of:

$$\frac{e_{out}}{I_{in}} \cong \frac{R_1 (R_6 + R_7)}{R_7} \cong 35 \text{ meg } \frac{(68K + 11K)}{11K}$$

$$\cong 2.5 \times 10^8 \quad \frac{\text{volts}}{\text{ampere}}$$

This derivation may be found later in this section.

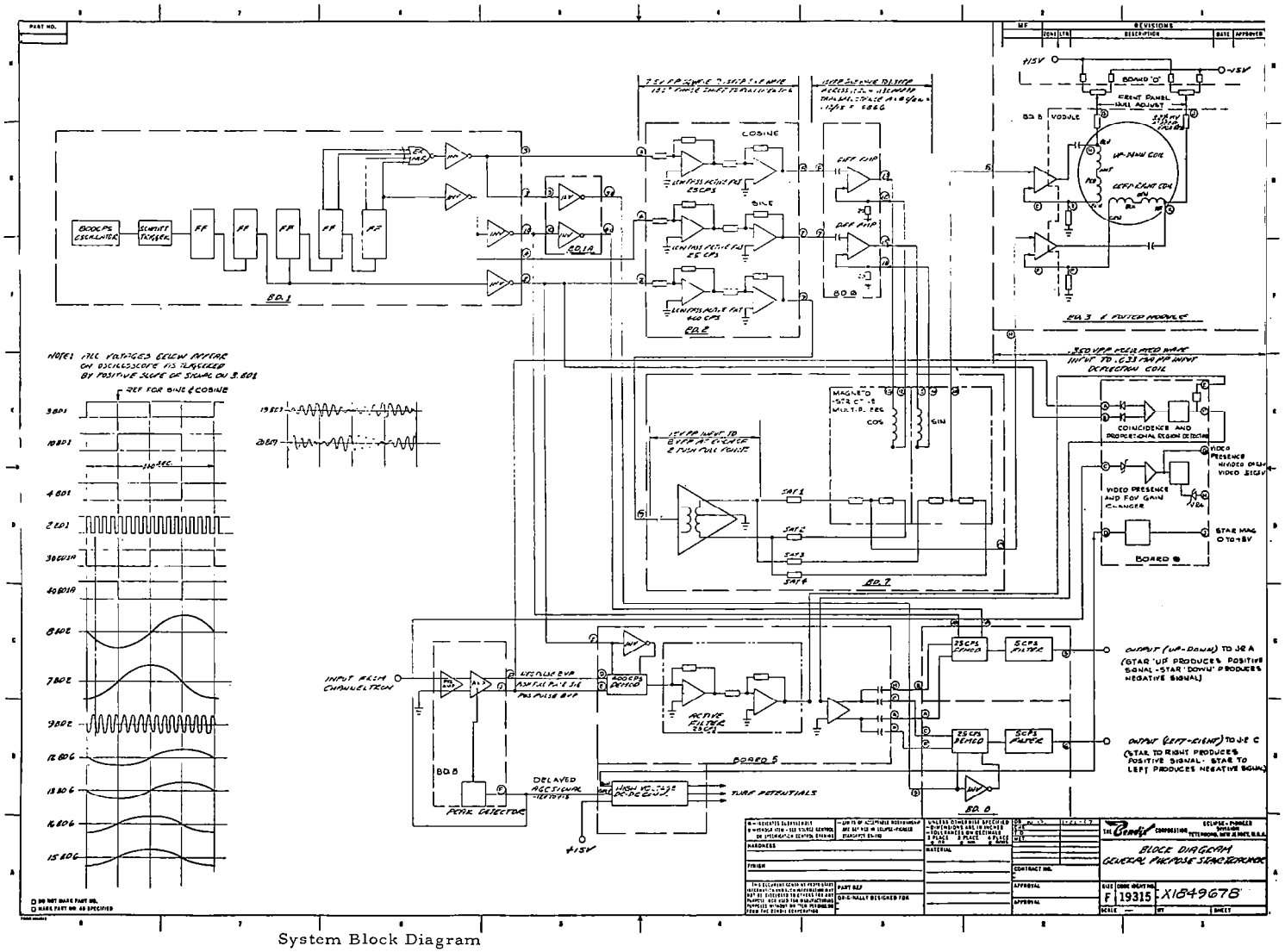

System Block Diagram

FIGURE 16

Under normal operating conditions, current pulses of 4×10^{-10} amperes at the Channeltron ® collector are amplified to 0.1 volt pulses at the pre-amplifier output (Q_3 collector).

Because of its extremely high input impedance and, therefore, its susceptability to pick-up, the entire preamplifier section has been shielded by locating it within aluminum covers on both sides of the printed circuit board.

Voltage amplifier stages. The video preamplifier drives a gain stage comprised of transistors Q_4 and Q_5. The gain of this stage ($R_{10} = 0$) is approximately

$$\frac{R_{11} + R_{12}}{R_{12}} \cong \frac{15K + 1.5K}{1.5K} \cong 11.$$

Thus, 1.1 volt pulses appear at the collector of Q_5. The next gain stage is comprised of transistors Q_6 and Q_7 and these are connected to give "phase split" outputs; that is, a non-inverted, video signal at the collector of Q6 and an inverted video signal at the emitter of Q7. The gain of this stage is approximately

$$\frac{R_{16} + R_{17}}{R_{16}} \cong \frac{3K + 30K}{3K} \cong 11.$$

The phase split outputs are buffered by the common-collector connected transistors Q_8 and Q_9, so that under normal operating conditions a positive video pulse of approximately 12 volts appears at Q_8 emitter and a negative video pulse of approximately 12 volts appears at Q_9 emitter.

Pulse amplitude selector circuit. Under closed loop operating conditions the pulse magnitudes at the collectors of Q_8 and Q_9 are determined by the brighter star in the field of view. Amplifying transistors Q_{10}, Q_{11} are normally biased hard "on" or conducting so that normal size (12 volts) pulses from Q_8 or Q_9 will turn Q_{10} and Q_{11} "off" or into a non-conducting state. Weaker (by one magnitude) stars in the field of view generate pulses that are too weak to over-ride the biases on Q_{10} and Q_{11} and video pulses are transmitted into the processing electronics by the brighter star only.

Overdrive circuit. In the event that the star tracker is suddenly exposed to a bright star after being in a "no star" condition, the output of the video preamplifier will swing "hard over" in a positive voltage direction. This

large positive voltage causes the transistors Q_{14} and Q_{15} that are shunting R_6 to conduct. This has the effect of increasing the video pre-amp feedback voltage thereby reducing the gain and output of the video preamplifier to compensate for the suddenly applied brighter star signal. Q_{15} also transmits clamped voltage pulses directly into the base of Q_{12} which operates to reduce the voltage across the channel in the Channeltron (R) to further reduce the pre-amplifier video signal. Thus, the system is driven to equilibrium at a reduced channel voltage, the preamp transfers normal video pulses, and Q_{14} and Q_{15} return to operation as a high resistance shunt across R_6.

Derivation, video preamplifier current-to-voltage transfer.

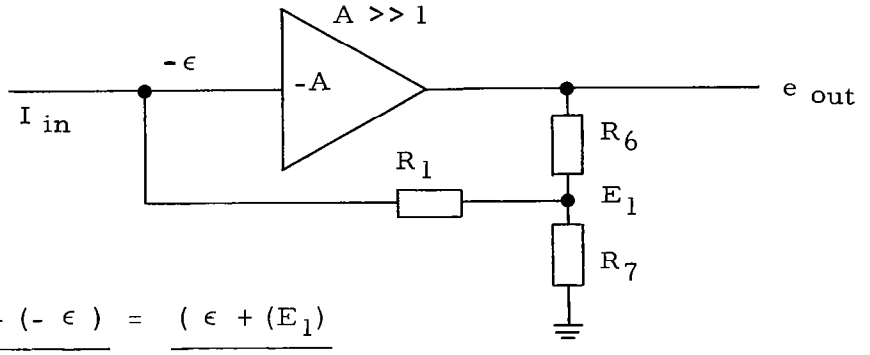

$$I_{in} = \frac{E_1 - (-\epsilon)}{R_1} = \frac{(\epsilon + (E_1)}{R_1}$$

$$e_{out} = -A(-\epsilon) = A\epsilon$$

$$E_1 = \frac{R_7}{R_6 + R_7} \qquad e_{out} = \frac{R_7}{R_6 + R_7} \; A\epsilon$$

$$I_{in} = \frac{-1}{R_1}(E_1 + \epsilon) = \frac{-1}{R_1} \left[\frac{R_7}{R_6 + R_7} \; A\epsilon + \epsilon \right]$$

$$I_{in} = \frac{-\epsilon}{R_1} \left[\frac{R_7 A}{R_6 + R_7} + 1 \right] = \frac{-e_{out}}{AR_1} \left[\frac{R_7 A + R_6 + R_7}{R_6 + R_7} \right]$$

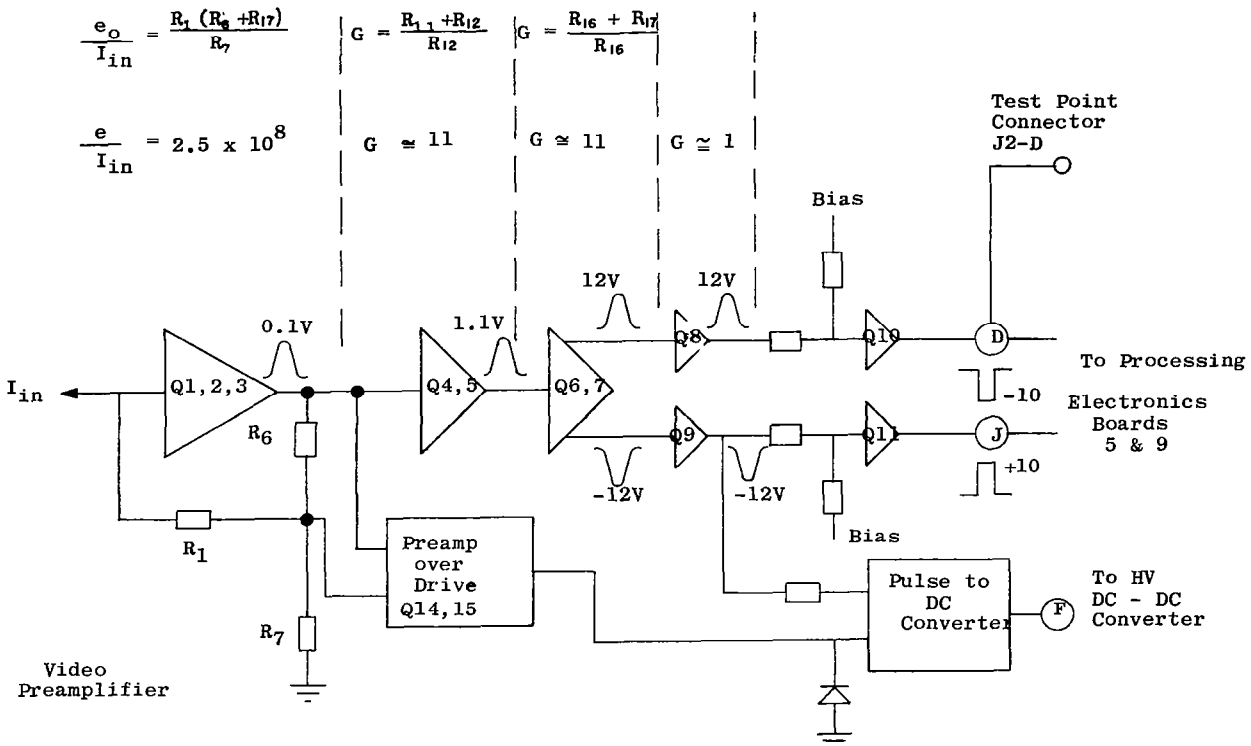

Video Amplifier

FIGURE 17

$$\frac{e_{out}}{I_{in}} = A R_1 \frac{(R_6 + R_7)}{R_7 A + R_6 + R_7} = \frac{- R_1 (R_6 + R_7)}{R_7 + \frac{R_6 + R_7}{A}}$$

$$\frac{e_{out}}{I_{in}} \cong - \frac{R_1 (R_6 + R_7)}{R_7}$$

High Voltage DC Servo

Operation. The operation of the high voltage dc servo system may be understood by reference to Figure 18 and to schematic drawings No. X1818887 (Board #8) and No. X1863471 (High Voltage Power Supply).

In actual operation, scanning the field of view with a star present produces a series of current pulses at the Channeltron® collector. These current pulses are converted to voltage pulses by the video amplifier. Negative video pulses are picked out of the video amplifier at the emitter of Q_9 and fed into a pulse-to-dc converter. The dc voltage developed at the output of the pulse-to-dc converter is fed into a high voltage dc-to-dc converter. The high voltage output of the high voltage dc-to-dc converter is applied across the channel of the Channeltron® and thus controls the current gain of the channel. Under equilibrium conditions, the loop gain is a function of the channel gain (applied channel voltage) and video pulses of approximately 12 volts are available at the emitters of Q_8 and Q_9. If the star magnitude were to change to that of a weaker star, weaker current pulses wo uld be generated down the channel to the collector. Weaker video pulses would be fed into the pulse-to-dc converter which would then generate an increased dc voltage output. This increased dc voltage would be sensed by the high voltage dc-to-dc converter and the high voltage across the channel would be increased. Increasing the high voltage across the channel, increases the channel gain until equilibrium is again reached and the current pulses are at the original magnitude (brighter star condition). Thus, the dc servo system automatically adjusts itself to give fixed magnitudes by the use of a high loop gain that controls the current gain of the channel.

Pulse to dc converter. (See schematic drawing No. X1818887.) Negative pulses are taken from the emitter of Q_9 in the video amplifier and fed through R_{30} to "buck out" the positive bias on the base of amplifier transistor Q_{12} and produce sharp positive pulses at the collector of Q_{12}. The Q_{12} collector pulses are ac coupled into a filtered dc restorer type circuit, comprised of D2, D3, C6, and the negative dc voltage generated by the restorer at the base of Q_{13} is summed with the positive base bias on Q_{13} received through R_{34}. The summed dc current flowing in the base of Q_{13} is amplified by Q_{13} and the resultant dc voltage at the collector of Q_{13} is fed into the input of the high voltage dc-to-dc converter. The voltage at the collector of Q_{13} is capable of being driven in this manner from -12 to +15 volts depending upon whether Q_{13} base drive current is positive or negative, corresponding to "no star" and "bright star" conditions. The dc output at Q13 is also used to drive the "star present" circuit on Board No. 9.

High voltage dc-to-dc converter. (See schematic drawing No. X1863471) The high voltage dc-to-dc converter operation is shown in block diagram form in Figure 19. The dc voltage from the collector of Q_{13} in the pulse-to-dc converter is fed into the high voltage dc-to-dc converter at terminal F. This dc voltage is given a level translation by Zener diode D_6, and filtered by the R_2 C_{6-7} network. It is then buffered by Q_1, and limit clamped by diodes D_8 and D_7. Final buffering of the dc input signal is given by transistor Q_2.

Transistors Q_3 and Q_4, and transformer T_1, are connected to form a static inverter with the primary-secondary windings of T_1, having a high step-up ratio. One side of the static inverter is powered directly by the +15 volt line and the other side (the emitters of Q_3 and Q_4) is returned to the dc voltage level of transistor Q_2, which is actually the translated dc voltage from the pulse-to-dc converter. The voltage across the static inverter is, therefore, controlled by the dc level of transistor Q_2 emitter and in turn controls the magnitude of the voltage across the secondary of T_1. The secondary voltage of T_1, is coupled into a voltage quadrupler which results in a transfer from the inverter input to quadrupler DC output of approximately 100 volts per volt. This high voltage is then filtered, sections regulated, and applied to the Channeltron(R) as indicated by Figures 18 and 19. Since the voltage applied to the inverter (which controls the channel voltage) is proportional to the star magnitude, it is used to drive a "star magnitude" circuit on Board No. 9. Also, the inverter input limit may be readjusted by paralleling D_7 with another zener on Board No. 9 and a connection is made for this purpose. In addition, a test point to check operation of the high voltage section is brought out to connector J_1-F.

Timing Circuits

A simplified block diagram of the timing section is shown in Figure 20. The timing circuits contain an oscillator which is used as the basic timing reference for the entire system. The frequency of the oscillator is fixed by the line scan rate, i.e., the length of time required for the spot to commence at the center, sweep out loop 1 and loop 2, and return to the center. A series of frequency dividers steps down this line frequency to obtain the frame scan signal required for the radial component of the sweep. This frame scan signal is also shifted 90° to provide a quadrature frame scan signal. The combination of these two frame scan frequencies, impressed upon the deflection yokes, define the azimuth scan. The higher line scan frequency, generated by the oscillator before division, defines the radial oscillation or line scan.

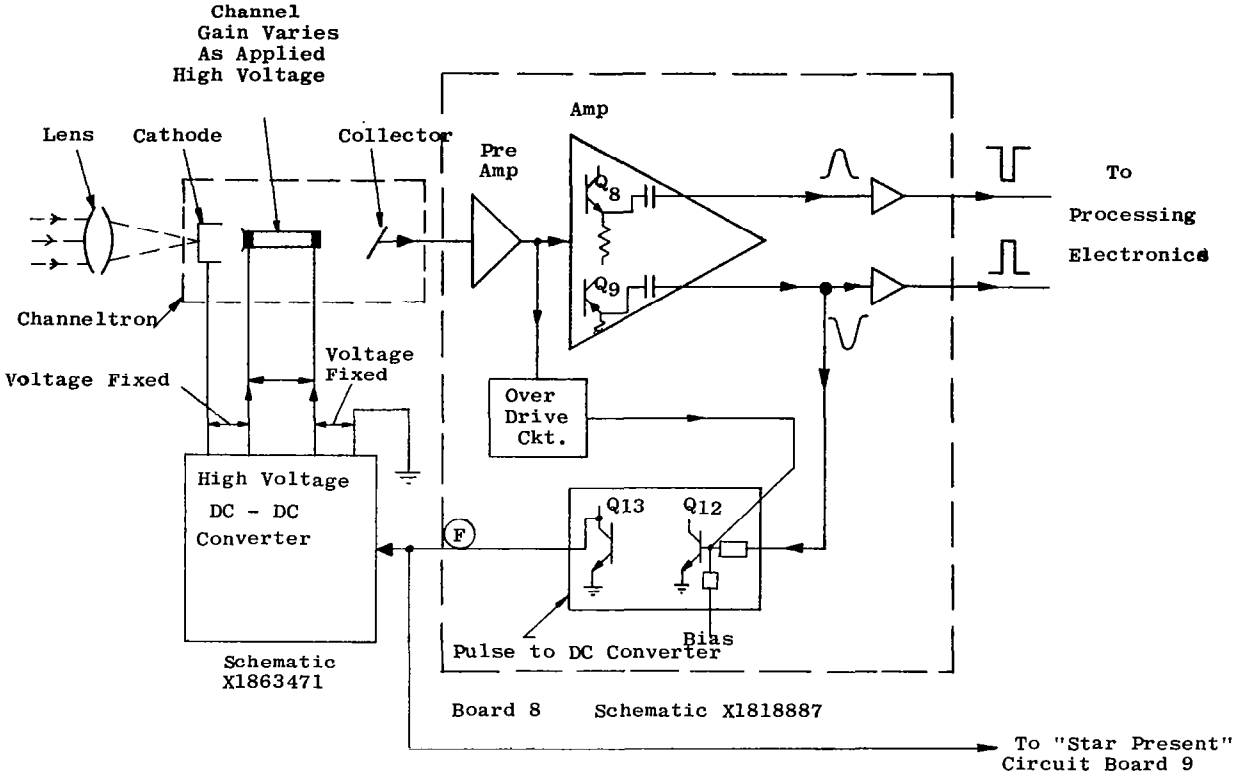

High Voltage DC Servo

FIGURE 18

The sine wave signals from the timing section are combined to form separate pitch and yaw signals suitable for use in the magnetic deflection yoke. As shown previously the fixed deflection coils, mounted coaxially with the Channeltron®, perform the equivalent function of a mechanically rotating yoke and associated motor drive with much less weight and power consumption, and with the inherent reliability associated with non-moving parts.

The developed equations for the scan requirements show that the timing sine waves must be combined in multiplicative fashion to give the proper pitch and yaw coil currents. The scan generation may thus be thought of as an electrical resolver, yielding pitch and yaw scan components whose resultant is the equivalent of a scan developed by a sine wave current in a rotating deflection coil.

1) $r = r_o \sin n\phi$ (n - leaved rose), desired scan

$\phi = 2\pi Ft.$

n = even integer

ϕ = azimuth angle of scan

r_o = radius of photocathode

F = frame frequency

t = time

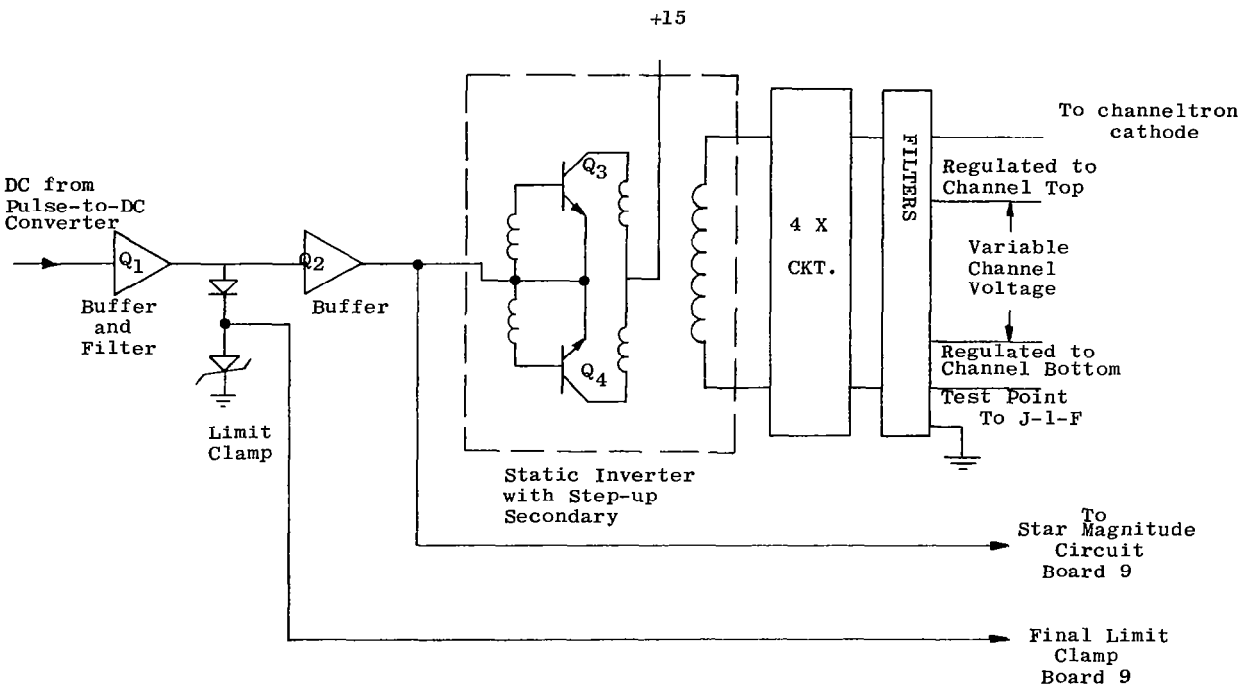

High Voltage DC-to-DC Converter

FIGURE 19

2) $r = r_o \sin 2\pi n Ft.$

since $y = r \sin \phi$

and $x = r \cos \phi$

3) $y = r_o \left\{ \sin (2\pi n Ft) \right\} \left\{ \sin (2\pi Ft) \right\}$

4) $x = r_o \left\{ \sin (2\pi n Ft) \right\} \left\{ \cos (2\pi Ft) \right\}$

Since scan deflections are proportional to deflection currents, currents in accordance with equations 3 and 4 must be applied to the y and x coils.

Figure 21 is a photograph of some of the printed circuit boards used in the tracker. The timing section board is the second from the left in the upper row. The Texas Instrument flat packs of the 500 series, used for frequency division and for the exclusive OR function, are on the right-hand half of the board; the large capacitor is the tuning capacitor of the LC oscillator. It is of the wound polystyrene dielectric variety to compensate the temperature coefficient of the wound toroid visible immediately above it.

In the delivered trackers this board is designated Board No. 1, and is located immediately behind Board No. 0. (the board on the upper left in the photograph), the output circuit board. It is, therefore, the second board from the tracker mounting surface. The timing circuit board generates only the timing signals; that is, the square waves used to provide demodulation. Where these signals are required as sine waves, (for example, as inputs to the magnetoresistive bridge modulators), they are first passed through active filters located elsewhere in the tracker (See paragraphs on active low pass filters in the section on Miscellaneous Circuits).

The timing section is discussed further in the section on Demodulation.

Magnetoresistive Multiplier

The magnetoresistive multiplier is shown schematically in Figure 22. It consists of a core of magnetic material upon which is wound a small coil. One input is applied to the coil. The other input is applied across the half-bridge formed by the two magnetoresistors. The magnetoresistors are high-impedance, thin film, fully encapsulated elements which are commercially

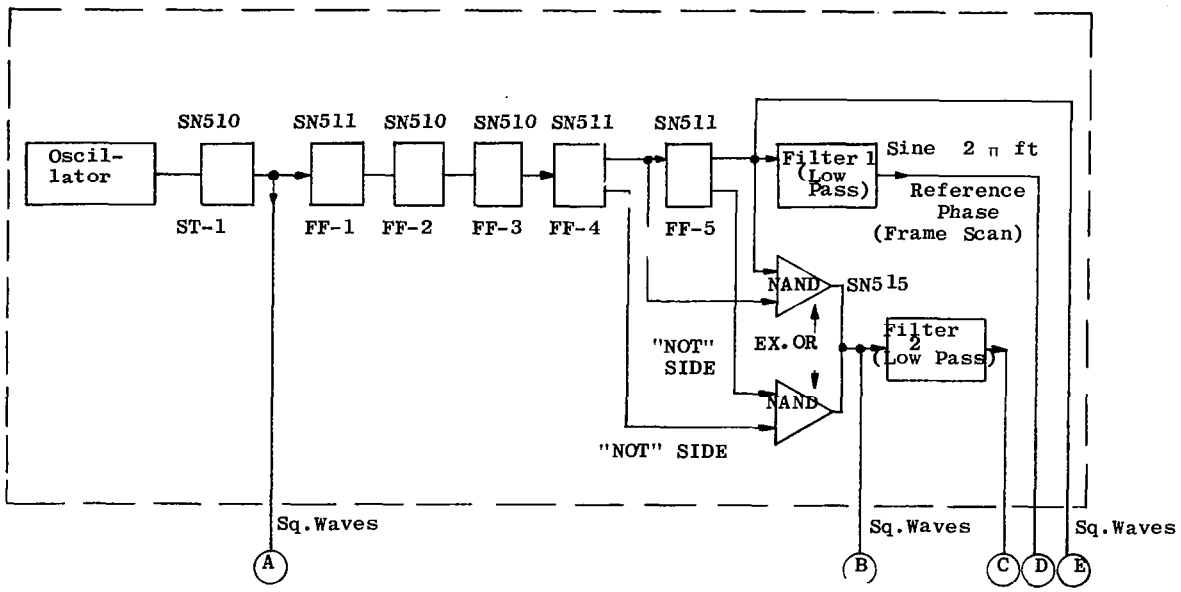

Timing Section Block Diagram

FIGURE 20

available. They feature low noise and are non-inductive. The permanent magnet biases the core to 1/2 of rated field. As a current is applied to the magnetic input, the flux in one leg goes up and goes down in the other. The bridge is now unbalanced with respect to bridge excitation. As the input current to the magnetic circuit is reversed, the unbalance in resistance occurs but in the opposite sense. The resultant output is proportional to the product of the two inputs.

These multipliers are supplied by American Aerospace Products, and the present star tracker is believed to be one of the first applications of this class of device. The original breadboard version of the star tracker has been operated well over a thousand hours without failure. Inherently rugged, these multipliers are uniquely applicable to this class of service.

The figure shows a single magnetoresistive multiplier. In actual practice a pair of these multipliers is used. This matched pair is located on Board No. 7 of the trackers furnished.

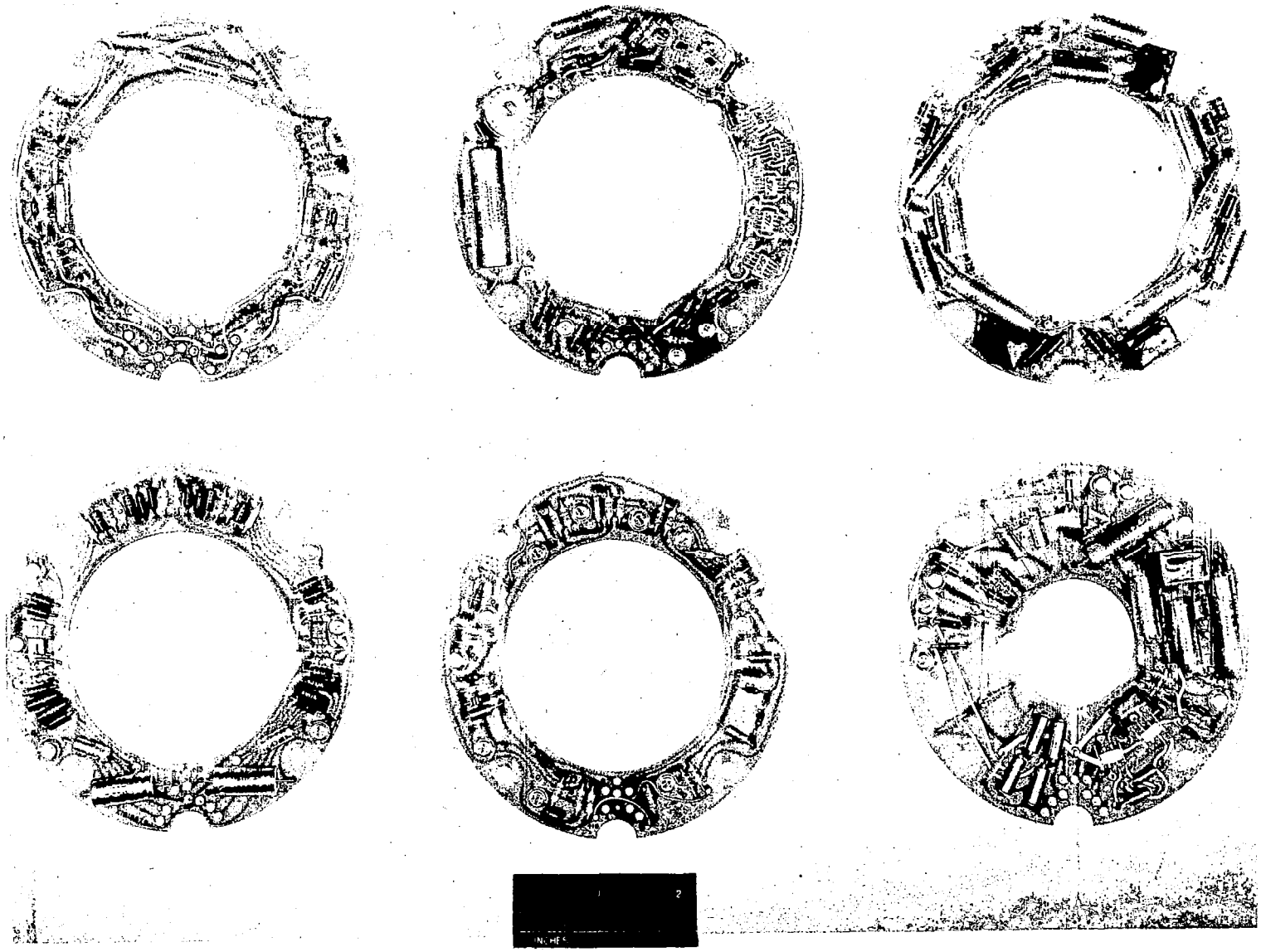

Printed Circuit Boards

FIGURE 21

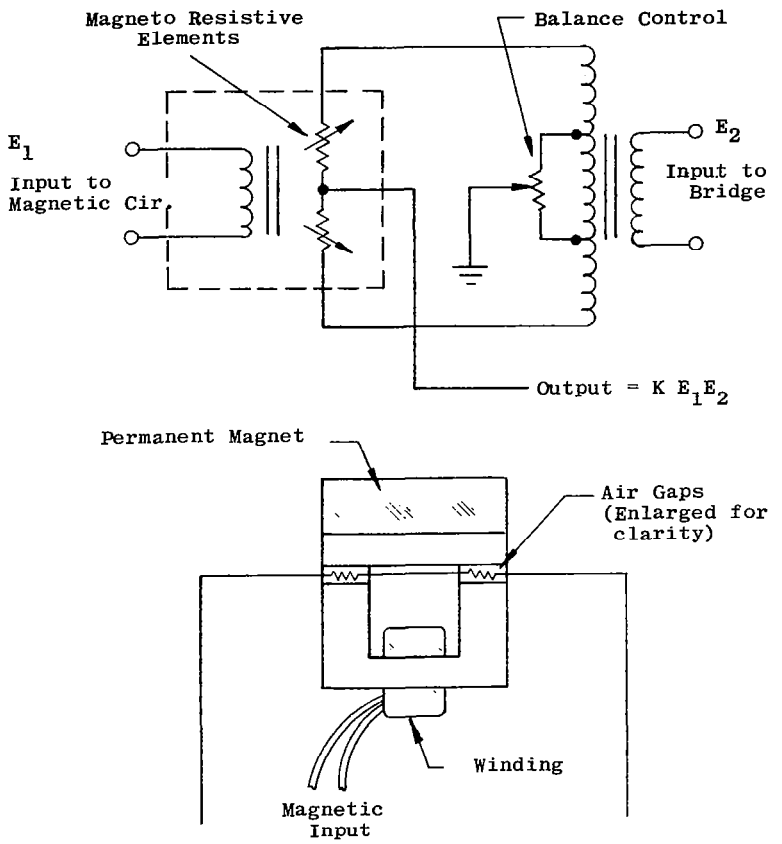

Magnetoresistive Bridge

FIGURE 22

The filtered 400 cps sine wave reference signal is applied to a unity gain amplifier. The amplifier output is phase-split by a center tapped transformer which supplies the E_2 bridge input signals to both multipliers in parallel, forming a bridge circuit. One multiplier accepts the 25 cps sine signal as E1, the other multiplier accepts the 25 cps cosine signal as E1. The output lead from each multiplier thus contains a modulation product which has the form of a 400 cps carrier frequency modulated at a 25 cps rate with the modulating frequency shifted, in one signal, 90 degrees from the other, as in Figure 3. After subsequent amplification these two signals are applied to the X and Y deflection coils, and produce the scan pattern already described. The coil-driving amplifiers are physically located in a potted assembly surrounding the image dissector photomultiplier.

Analysis of Scan

The scan investigates the field for star sources by an oscillation in zenith along a diameter which is slowly rotating. The diameter rotates once in space completing the cycle of events, carrying with it the multiple zenith oscillation; the rotation in azimuth opening the zenith oscillation into lobes or "petals". The complete cycle entails one "frame". The smaller time required for two zenith oscillations from center to two opposite points on the circumference and return, is called the "line scan" time. The zenith travel varies as a sinusoidal function of time and in general the ratio $\frac{\text{line scan frequency}}{\text{frame frequency}}$ is an even integer.

In Figure 23, the scan reaches the circumference at all odd-numbered times. A pair of petals, (for example, the petals generated at times 1 and 3,) are due to one sinusoidal line scan. The uniform azimuthal advance is seen to give width to the petals as well as to advance the petal tips. There is an interlace feature; during the first half of the frame the complete cathode is encompassed symmetrically but leaves excessively wide gaps. The second half of the scan fills in these gaps assuring an overlap of coverage at the circumference.

The scan is generated by two stationary orthogonal deflection coils. Since deflection in each axis is proportional to the coil current in that axis, each axis is proportional to the coil current in that axis, each current waveform may be considered to be equal to the projection in each axis of the time record of the scan of Figure 23.

Consider the scan deflection circuit as shown schematically in Figure 24. The applicable waveforms are shown in Figure 25.

The output of multiplier 1 is $(\sin 2\pi F_2 t)(\sin 2\pi F_1 t)$ and that of multiplier 2 is $(\cos 2\pi F_2 t)(\sin 2\pi F_1 t)$. The instantaneous amplitude of the resultant, since the two are applied in space quadrature, is

$$A = \left\{(\sin 2\pi F_1 t)^2 \left[(\sin 2\pi F_2 t)^2 + (\cos 2\pi f_2 t)^2\right]\right\}^{1/2}$$

$$A = \sin 2\pi F_1 t)$$

The instantaneous amplitude is thus equal to the instantaneous value of the higher frequency, or "line-scan" frequency.

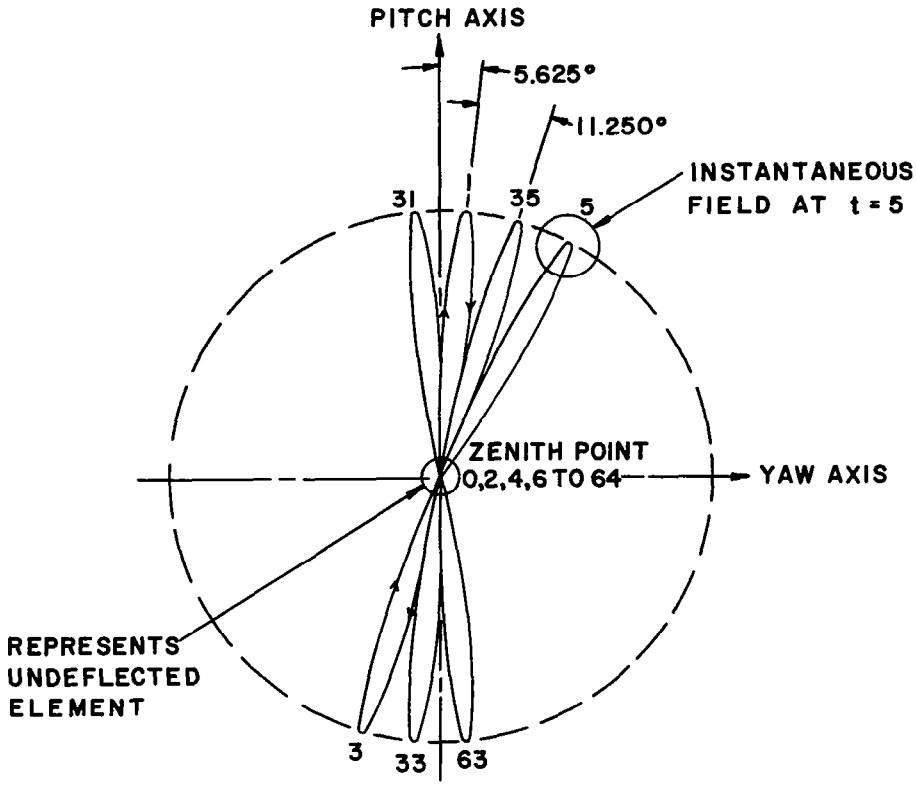

TRAJECTORY OF CENTER OF SCANNING ELEMENT FOR $\frac{\text{RADIAL SCAN FREQ}}{\text{FRAME SCAN FREQ}} = 16$

Partial Scan Pattern

FIGURE 23

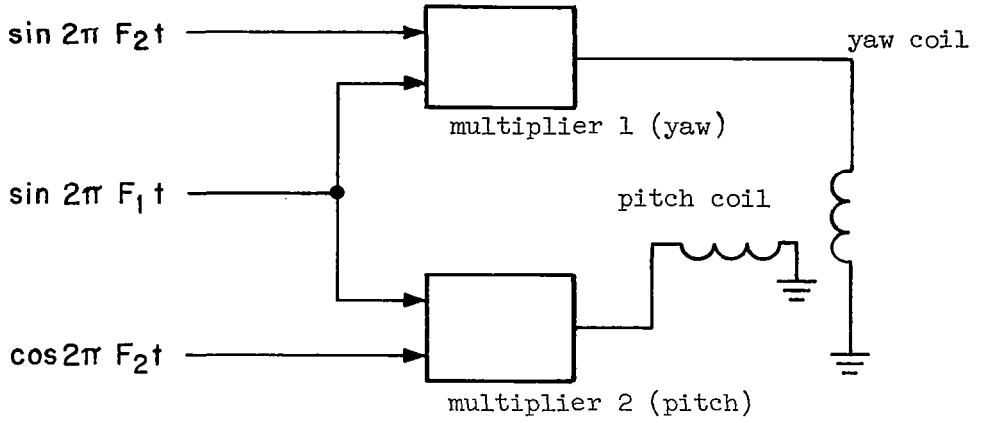

Scan Generation Schematic

FIGURE 24

The angle that the resultant deflection vector makes with a reference is equal to

$$\phi = \tan^{-1} \frac{\sin 2\pi F_2 t}{\cos 2\pi F_2 t}$$

$$\phi = 2\pi F_2 t$$

The aximuth angle of the scan is therefore a uniformly increasing function with period $\frac{1}{2 F_2}$ seconds.

The circuit therefore will give the required deflection and each of the deflection waveforms is generated as the product output of analog multiplier devices. The line scan waveform is an input to each multiplier and either the sine $2\pi F_2 t$ or cosine $2\pi F_2 t$ becomes the second input, the latter signals causing the effective scan rotation.

For a star exactly at boresight point, there are two pulses per line scan, their centroids occurring exactly at reference time. No pulse motion occurs due to changing scan azimuth.

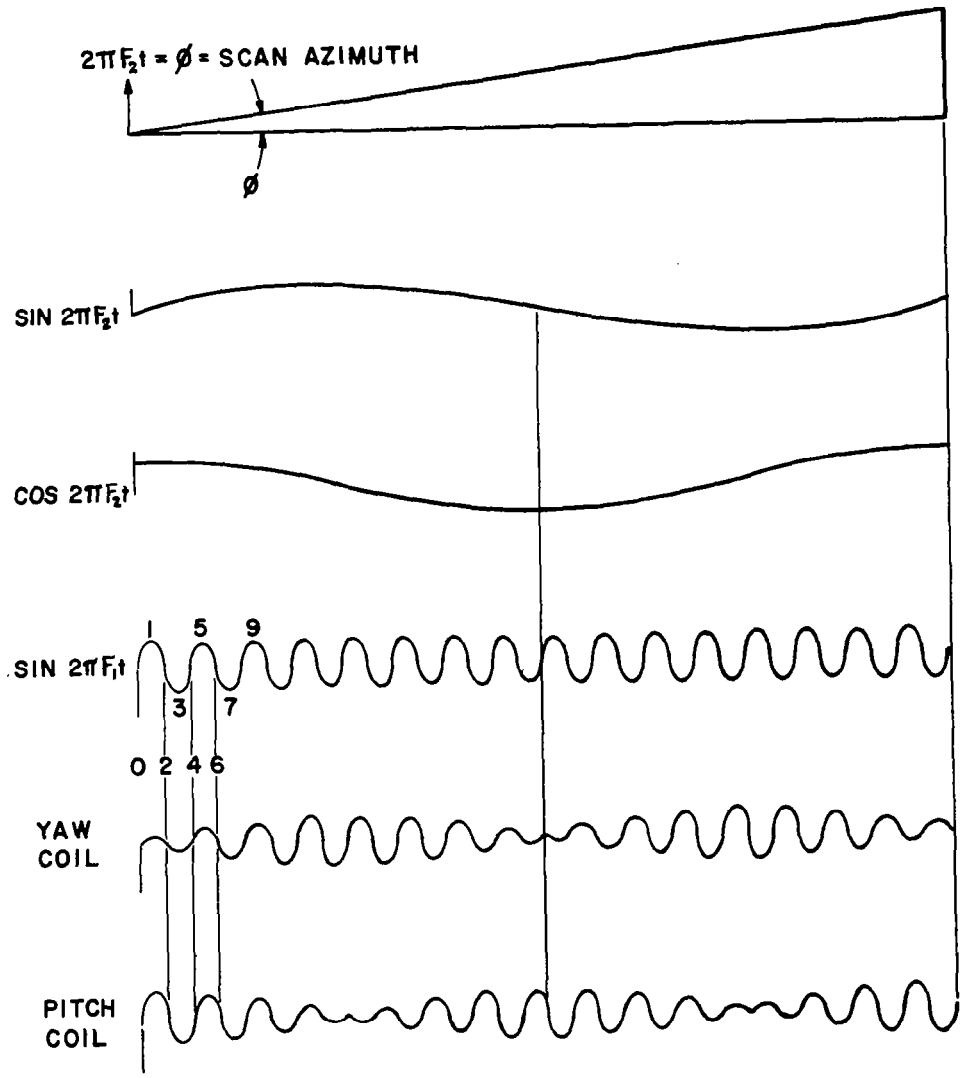

Wave Forms, Scan

FIGURE 25

For a star not at boresight but within the proportional region, the pulse timing throughout the frame varies from pulse to pulse, a reflection of the changing scan azimuth. The scan in this case may be approximated by its central portion, which resembles the spokes of a wheel. On these spokes the scan zenith velocity in terms of optical field degrees/sec is a constant and therefore the pulse motion is proportional to the component of star displacement along the spoke. Therefore there is a cyclical change in pulse motion encompassing two maxima and two null points. The maxima are of opposite sense and the demodulator will distinguish between them. Figure 26 shows the geometry controlling the pulse motion.

The video pulse train is demodulated with respect to the reference signal and its output filtered. The action occurring on demodulation of a single pulse is instructive. In this case the output of the demodulator is a composite double pulse which shows a net positive or negative pulse area proportional to pulse advance or retard. Figure 27 shows that the measurement is independent of the pulse width. The operation is linear with pulse motion as long as the reference zenith time is contained within the pulse. This requirement will be met for all pulses, for a star within the proportional region. The net pulse areas throughout the frame will be converted to an analog voltage by the low pass filter.

In Figure 28, targets 1, 2, and 3 are located along a constant azimuth line at various zeniths. The star azimuth is colinear with the scan at times t = 6. The demodulation is the equivalent of a multiplication of a square wave of unit positive and negative half-amplitude. The demodulator output for target 1, on axis, has frequencies of F_1 and higher present. The filter, which is a low-pass type with passband including F_2, has no output. If the star is at location 2, the demodulator output, reflecting measurements of pulse motion contains an amount of F_2 signal proportional to zenith motion. The maximum point of the filter output sinusoid occurs when scan azimuth coincides with star azimuth. In this way the phase of the filter output, the analog modulation, is 90° away from the star azimuth angle. For star 3, outside the proportional region, the video pulse train contains only a few pulses, reflecting more of an acquisition rather than tracking function. The pulses contain no coincidence with the reference transitions, and therefore proportionality of demodulator output amplitude with zenith angle is lost. The azimuthal data suffers no degradation, however.

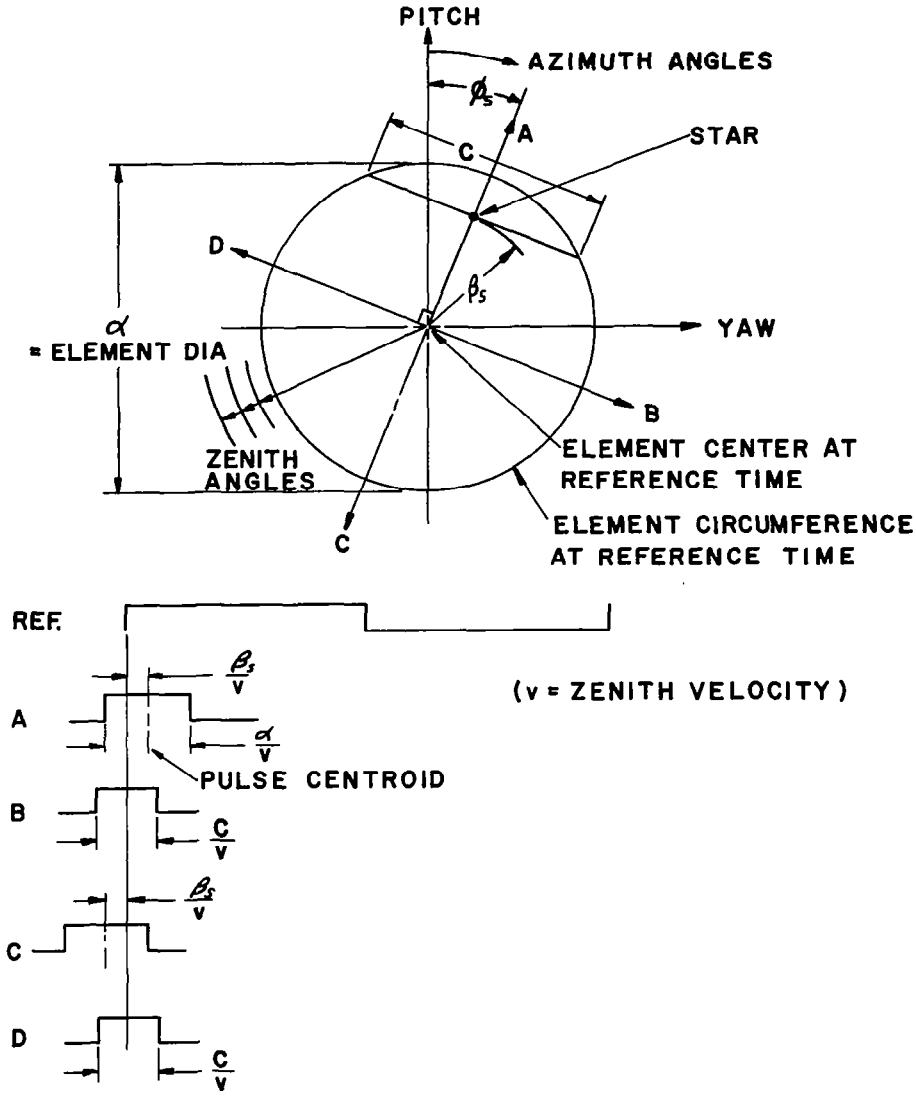

Geometry Affecting Pulse Motion

FIGURE 26

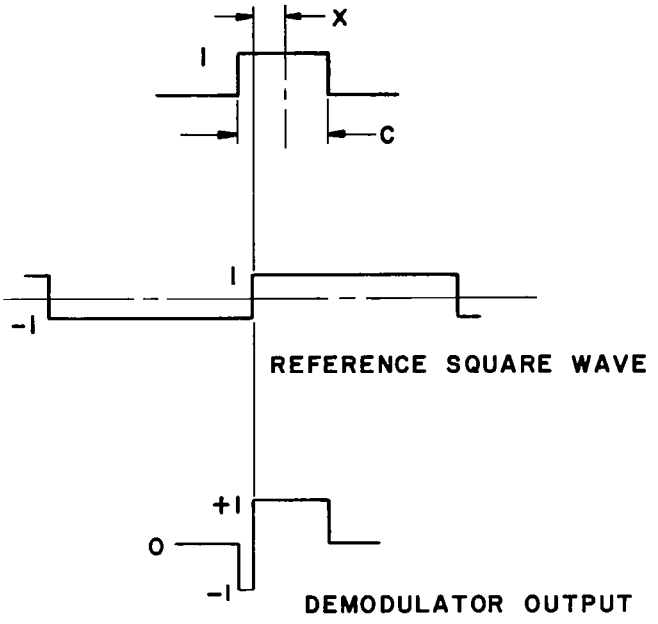

$$\text{POSITIVE AREA} = \frac{C}{2} + X$$

$$\text{NEGATIVE AREA} = \frac{C}{2} - X$$

$$\Delta = \frac{C}{2} + X - \left(\frac{C}{2} - X\right) = 2X = \text{POS AREA} - \text{NEG AREA}$$

Measurement of Pulse Motion

FIGURE 27

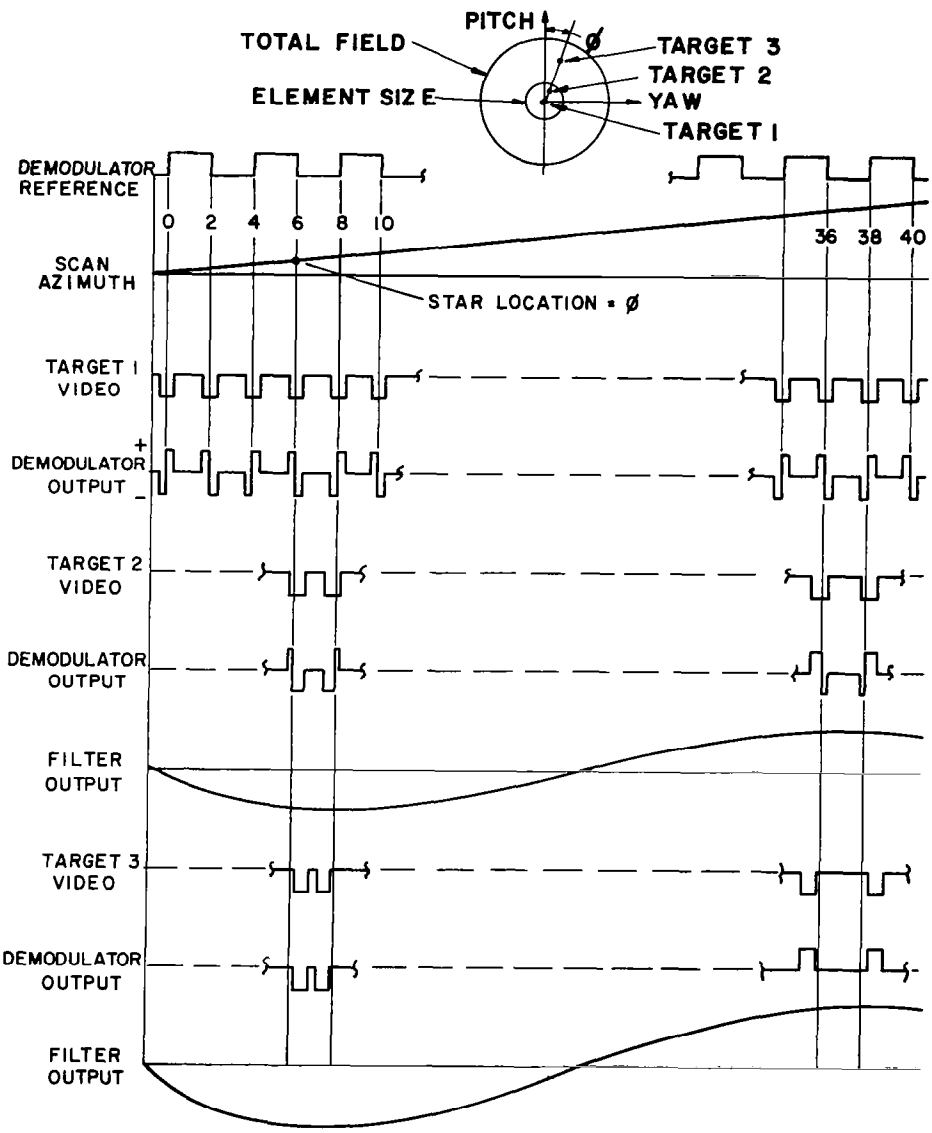

Wave Forms, Demodulator and Filter

FIGURE 28

Demodulation - Resolving

The variable phase analog modulation may be converted to pitch error by multiplying by the sine of $2\pi F_2 t$, or to yaw error by multiplying by the cosine. The actual instrumentation is by switching type demodulators using square rather than sinusoidal reference waveforms. The average value of output for such a device, with input $A \sin (2\pi F_2 t+\alpha)$ and reference square wave which equals -1 for $0 < t < \frac{1}{2F_2}$, and +1 for $\frac{1}{2F_2} < t < \frac{1}{F_2}$, is

$$F_2 \int_0^{\frac{1}{2F_2}} -A \sin (2\pi F_2 t+\alpha)dt + F_2 \int_{\frac{1}{2F_2}}^{\frac{1}{F_2}} A \sin (2\pi F_2 t+\alpha)\, dt$$

$$= \frac{-2A}{\pi} \cos \alpha$$

This output is therefore the negative of the product of amplitude and $\cos \alpha$. The other demodulator with reference shifted 90°, will be the orthogonal component.

Scanning Considerations

The system has very low sensitivity to null shift due to changes in electronic components. This is due to the ac coupling to the deflection coils and to the use of ac signals throughout the processing of error signals. The final resolution to dc pitch and yaw error signals is done at a high enough level to require no further amplification.

The star location will be faithfully reproduced in two dimensions within the proportional region. In the rest of the field, the star location will be approximated by the intersection of the actual star location vector and the circle defining the proportional region. This type of saturation will provide slewing of the star into the proportional region whereupon proportional nulling will occur. The output characteristic is therefore compatible with the usual 2-axis control system.

Demodulation

The demodulator circuitry is located on Board No. 5.

As shown in Figure 29, synchronous demodulator No. 1 is synchronously switched from the reference flip flop FF-1, so that the Texas Instrument Solid Circuit demodulators are alternately in the open circuit or short circuit condition, i. e., SN 354A (1) open and SN 354A (2) closed in one state of FF-1 and SN 354A (1) closed and SN 354A (2) open in the other state of FF-1. Thus, any positive video signal present during the even numbered scan loops is transferred to the demodulator output and any inverse video signal is transferred to the output during the odd numbered scan loops. The output from synchronous demodulator No. 1 is shown in Figure 30. The demodulator output is fed into active filter No. 4 (Figure 31), and the output obtained is shown in Figure 30.

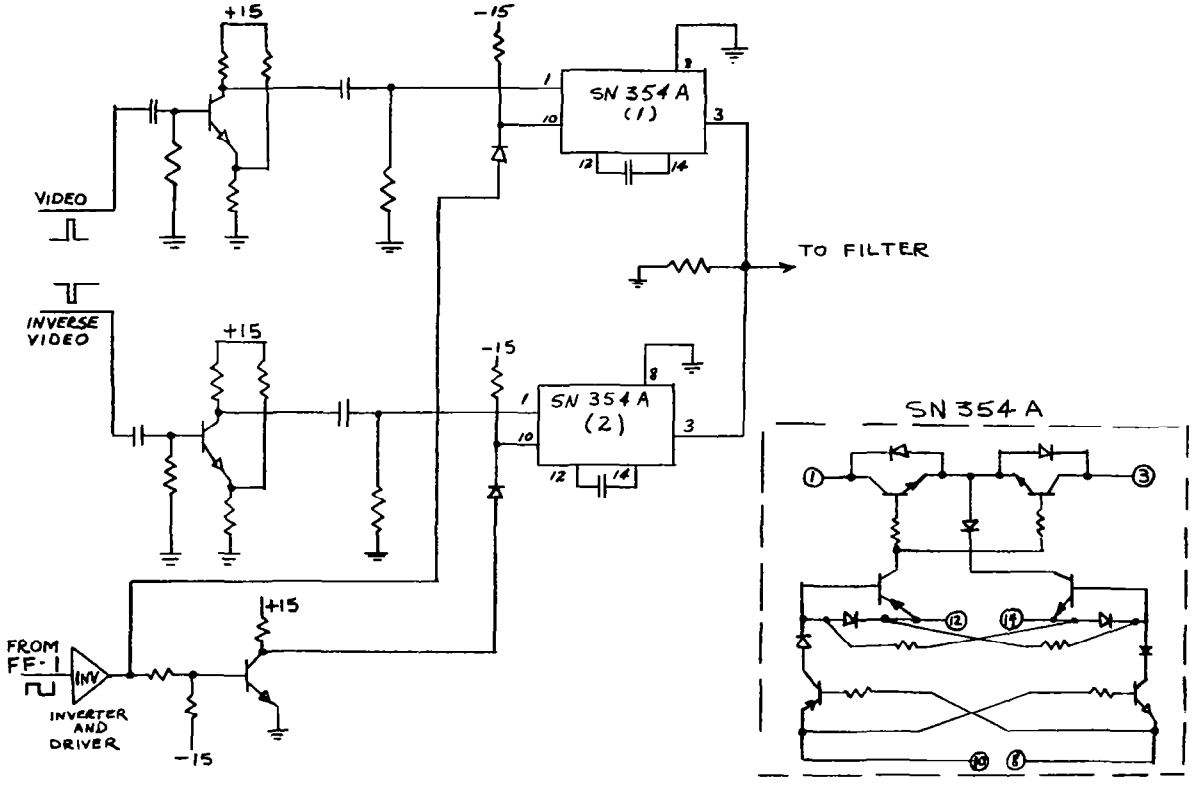

Synchronous Demodulator No. 1

FIGURE 29

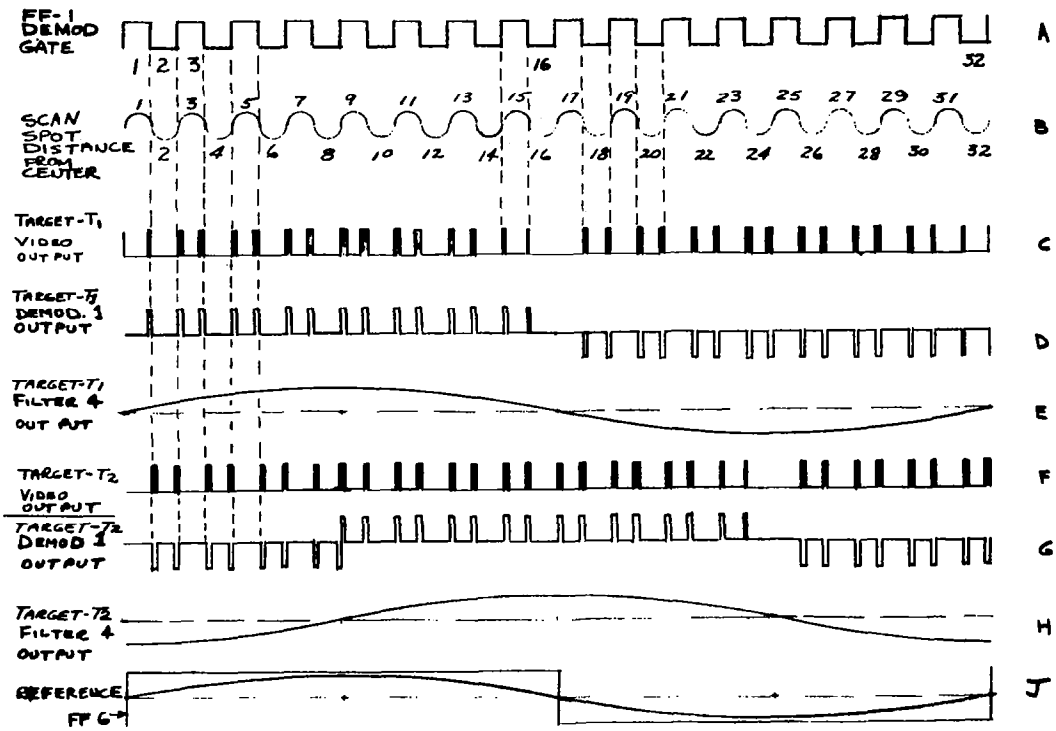

Demodulation Signals

FIGURE 30.

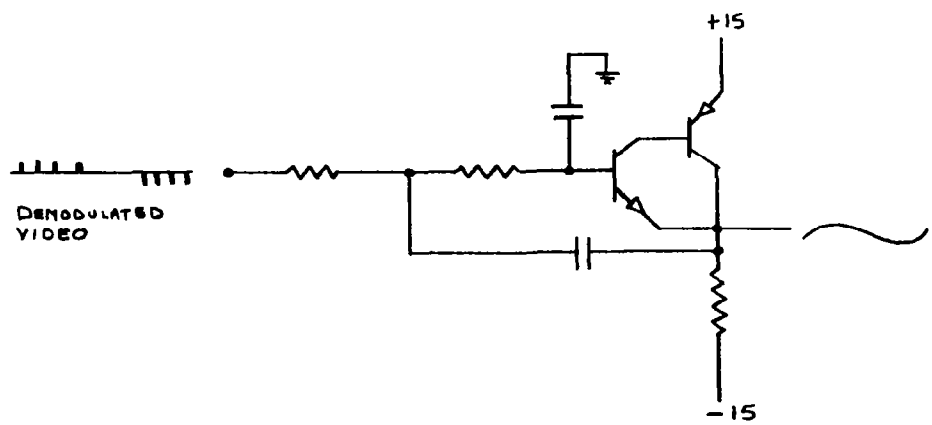

Active Filter No. 4

FIGURE 31.

The filtered output from demodulator No. 1 and filter No. 4 has a fundamental component equal to the scan frame frequency. This output, after phase splitting and amplification is fed into two full wave synchronous demodulators made up of Texas Instrument solid circuit demodulators (Figure 32). One of the full wave demodulators, No. 2, comprising SN 354A (3) and SN 354A (4), is switched at the reference frame frequency and phase by the flip-flop FF-6 and its compliment. The other full wave demodulator, No. 3, comprising SN 354A (5) and SN 354 (6) is switched at the reference frame frequency and 90° after FF-6 by using FF5 and FF6 to drive a Texas Instrument solid circuit "exclusive OR".

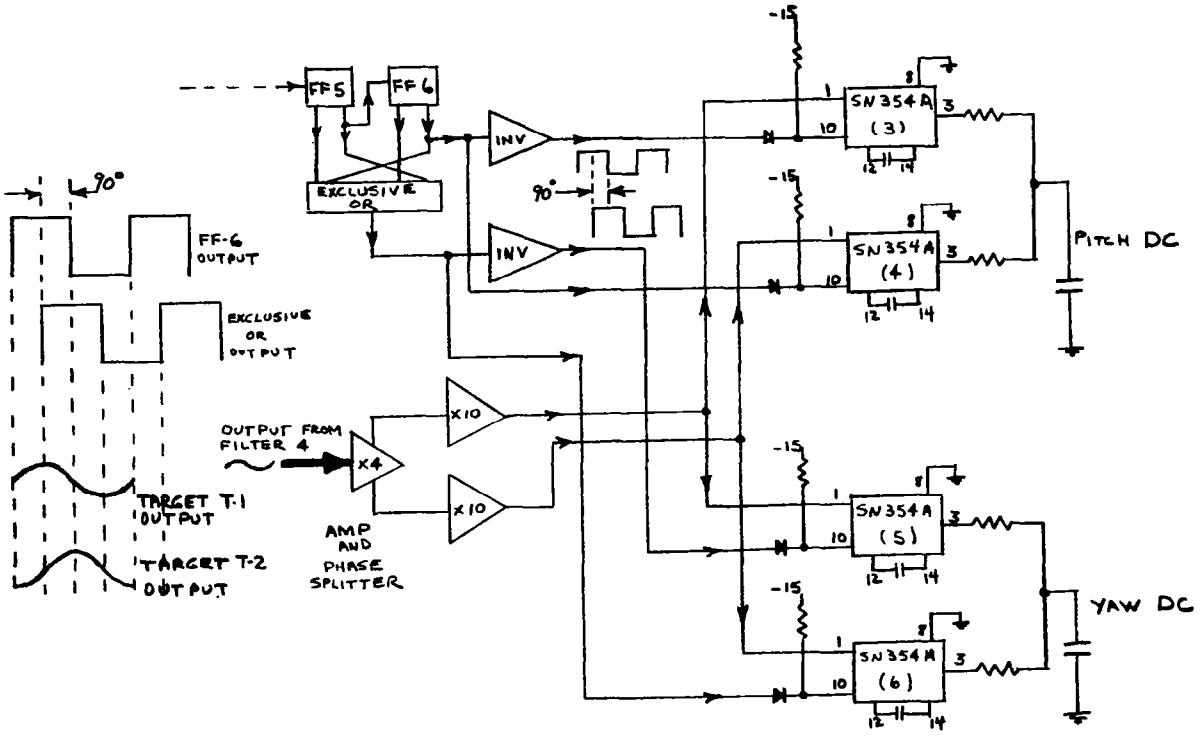

Synchronous Full Wave Demodulators No. 2 and 3

FIGURE 32

Thus, the filtered video output is demodulated by demodulator No. 2 to obtain pitch information and by demodulator No. 3 to obtain yaw information. With the target at T_1 (See Figure 33), the reference demodulating switching voltages and the dc yaw and pitch voltages are shown in Figure 34.

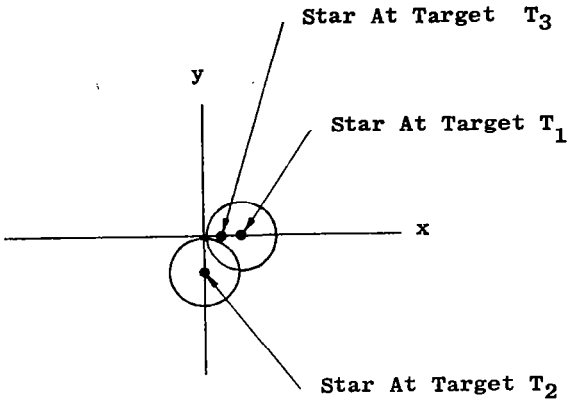

Target Location

FIGURE 33

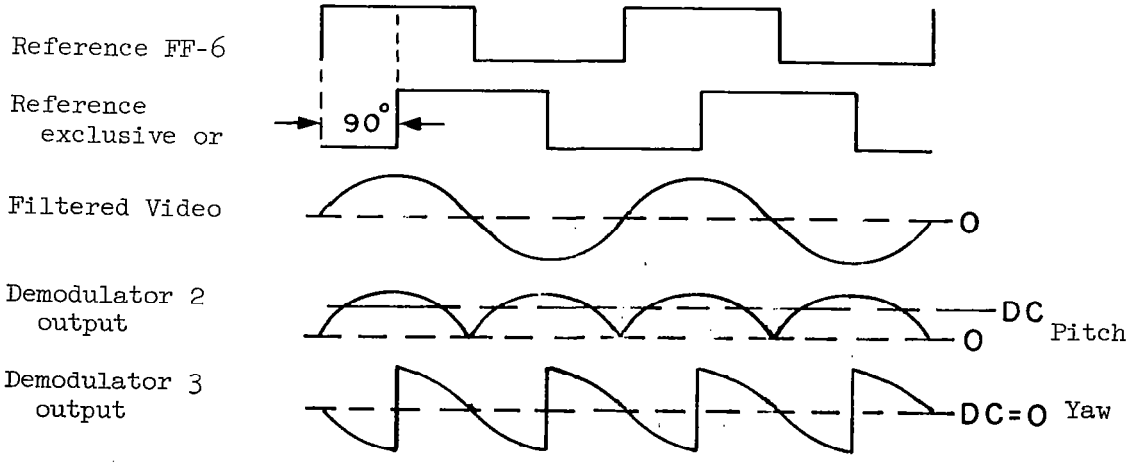

Target at T_1

FIGURE 34

Similarly, if the target star was detected at T_2 (See Figure 35) the video output, Demodulator 2 output, and Filter 4 output would be shown by Figure 30, F, G, and H respectively. The output of Filter 4 with the target at T_2 has been shifted by 90^o from the output of Filter 4 with the target at T_1. With the target at T_2, the reference demodulating switching voltages and DC Yaw and Pitch voltages are shown.

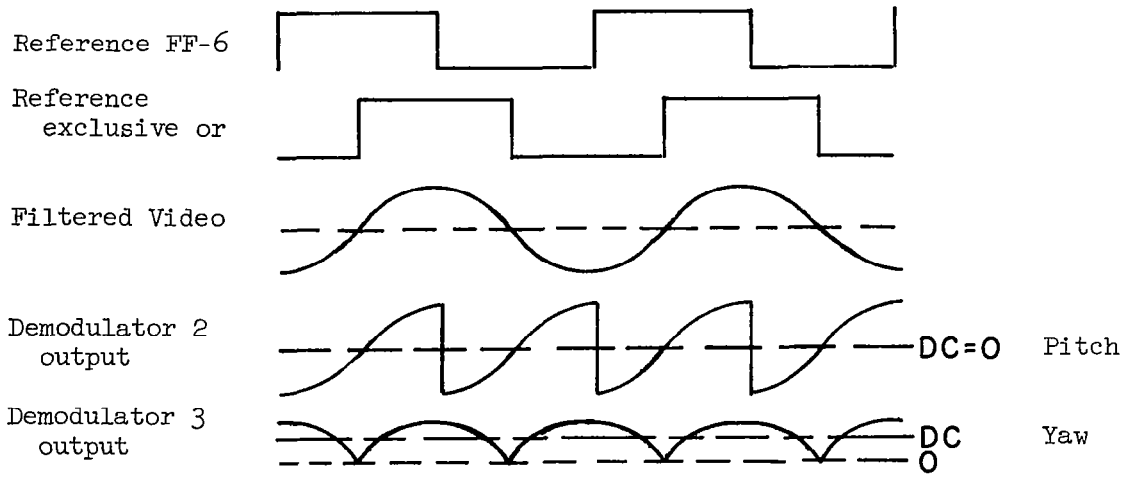

Target at T_2

FIGURE 35

The two cases just illustrated are simple ones in that targets along single axes have been used; however, it is apparent that a star or planet off axis would be a combination of the two cited cases where each of the demodulators (demodulator No. 2 and demodulator No. 3) would extract its in-phase component and give an average dc value.

If Target T_1 were allowed to slide over to Target 3 and a comparison made between the fundamental components of the video outputs, we would see where the addition of the small opposite polarity spikes to the T_3 demodulated output would reduce the magnitude of the fundamental component and consequently the magnitude of the DC Pitch signal. This is the operation of the star and planet tracker in the proportional region, and zero output results when the star or planet is in the center of the field of view and the positive and negative halves of the demodulated pulse are each 50% of the video pulse width.

The timing section uses an oscillator driving a flip-flop type of frequency divider. The output of the last flip-flop is a square wave of frame-scan frequency. In order to develop a 90° phase shift, a logical gate consisting of 2 NAND's driven by the last two stages is used, giving as output a 90° displaced phase shift. Filters 1 and 2 are identical 2 state R-C low-pass filters giving exactly 180° phase shift. Filter 3 is also a 180° phase shift low-pass filter. The sine wave signals will be used in scan generation and the square wave signals in demodulation.

Miscellaneous Circuits

Active low pass filters. All of the active filters incorporated into the star tracker are of the same basic design, and are built up of active filter segments of the type shown in Figure 36.

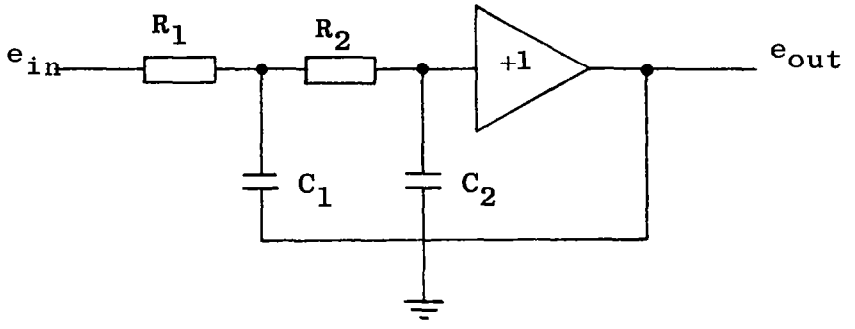

Active Filter Segment

FIGURE 36

The transfer function for the filter segment is given by:

$$\frac{e_{out}}{e_{in}}(S) \cong \frac{1}{R_1R_2C_1C_2S^2 + (R_1 + R_2)C_2S + 1} = \frac{\omega_o^2}{S^2+2\zeta\omega_o S+\omega_o^2}$$

$$\omega_o \cong \frac{1}{(R_1 R_2 C_1 C_2)^{1/2}}$$

$$\zeta \cong \frac{(R_1+R_2)\ C_2\ \omega_o}{2} = \left(\frac{R_1+R_2}{2}\right)\left(\frac{C_2}{R_1 R_2 C_1}\right)^{1/2}$$

The active filter segments are tuned to 400 cps and 25 cps with a damping factor of $\zeta = 0.4$ from which a slight gain is obtained at the frequency F_o.

The nominal values used in the tracker are:

(A) 25 cycle filter			(B) 400 cycle filter		
R_1	=	100K	R_1	=	100K
C_1	=	$0.16\,\mu f$	C_1	=	$0.01\mu f$
R_2	=	100K	R_2	=	100K
C_2	=	$0.0256\mu f$	C_2	=	$0.0016\mu f$

(A) $$\omega_o \cong \frac{1}{(100\text{x}10^3 \times 100\text{x}10^3 \times 0.16\text{x}10^{-6} \times 0.0256\text{x}10^{-6})^{1/2}}$$

$$\omega_o \cong 156.2$$

$$F_o \cong \frac{156.2}{2\pi} \cong 25 \text{ cps}$$

$$\zeta \cong 100K \left[\frac{0.0256}{0.16\ (100K)^2}\right]^{1/2}$$

$$\zeta = 0.4$$

(B) $$\omega_o \cong \frac{1}{(100\text{x}10^3 \text{ x } 100\text{x}10^3 \text{ x } 0.01\text{x}10^{-6} \text{ x } 0.0016\text{x}10^{-6})^{1/2}}$$

$$\omega_o \cong 2500$$

$$F_o \cong \frac{2500}{6.28} \cong 400 \text{ cps}$$

$$\zeta \cong 100K \left[\frac{0.0016}{0.01\ (100K)^2}\right]^{1/2}$$

$$\zeta \cong 0.4$$

The phase shift at the frequency F_o or ω_o is found from:

$$\frac{e_{out}}{e_{in}} = \frac{\omega_o^2}{S^2 + 2\zeta\omega_o S + \omega_o^2}$$

$$S = j\omega_o$$

$$\frac{e_{out}}{e_{in}} = \frac{\omega_o^2}{\omega_o^2 + j^2\omega_o^2 + 2j\zeta\omega_o^2} = \frac{\omega_o^2}{2j\zeta\omega_o^2}$$

$$\frac{e_{out}}{e_{in}} = \frac{1}{2j\zeta}$$

which is recognized as a 90^o phase lag in each filter segment.

There are four active filters in the star tracker, three on Board No. 2 and one on Board No. 5. Each active filter is composed of two of the described active filter segments connected in cascade. The phase relationship and voltage magnitudes of the active filter signals compared to the timing signals is shown in Figure 37.

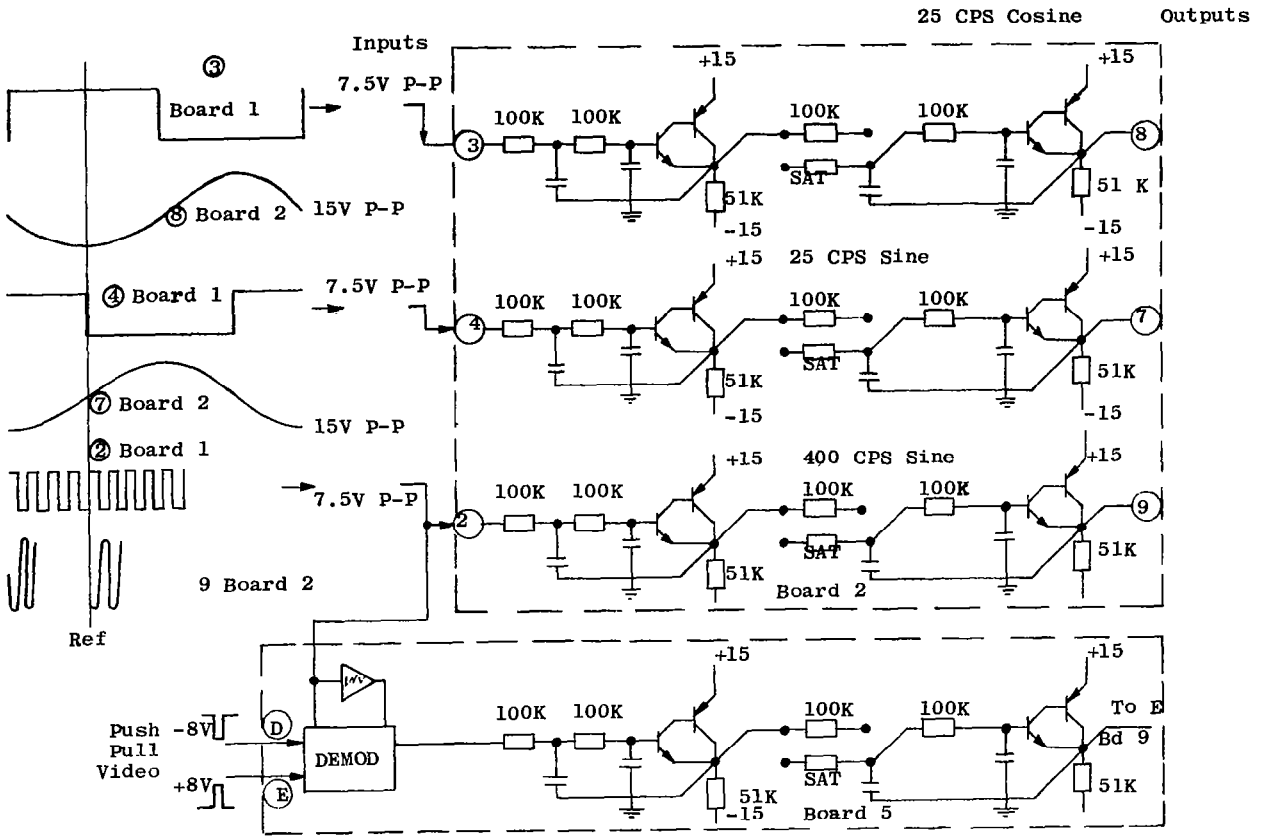

Active Filter Circuits

FIGURE 37

Theoretically, each of the cascaded active filters will have a phase shift of 180°. Due to the tolerances of the resistors and capacitors, however, it is unusual to obtain a 180° phase shift without some sort of trimming. This final "trimming in" is obtained by the use of the select-at-test (SAT) resistors as shown in the diagram. The SAT's may be connected in series or parallel with the adjacent 100K ohm resistor depending upon whether a slight lag or lead is needed to trim the filter in.

The Fourier expansion of the square wave driving the active filters is:

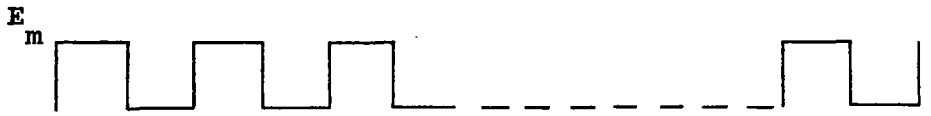

$$E = \frac{2E_m}{\pi}\left\{\frac{\pi}{2} + \sin \omega t + \frac{1}{3}\sin 3\omega t \text{ ----} \frac{1}{m}\sin m\omega t\right]$$

The third harmonic is the component that requires the most filtering, and at the output of the filter will be below the fundamental by $\frac{1}{3}$ x Filter Attenuation - 24DB per octave, or (-9.5 - 38)DB $\cong$ -47.5 DB. Thus, the filter outputs will contain less then 1% third harmonic distortion and much less of the higher harmonics.

25 CPS Information Amplifier and Gain Switching

The star tracker X-axis and Y-axis output error signals are obtained by full-wave demodulating the 25 cps output of the 25 cps active filter on board No. 5 (schematic drawing No. X1856346). Two gain stages on Board No. 5 and a resistance attenuator network on Board No. 9 (schematic drawing No. X1896329, sheet 2) are incorporated between the 25 cps active filter and the output demodulators (Board No. 0, schematic drawing No. X1856353) to obtain the proper output error signal gradient.

The first gain stage utilizes transistors Q8 and Q9 and generates push-pull outputs, and the gain (either output) is equal to $\frac{R_{19} + R_{20}}{R_{19}} = 4.3$. The second gain stage also generates push-pull outputs to drive the full-wave demodulators and is comprised of transistors Q_{10}, Q_{11}, Q_{12}, and Q_{13}. The gain of this stage is equal to $\frac{R_{29} + R_{30}}{R_{29}} = \frac{R_{32} + R_{31}}{R_{32}} = 10.4$. The gain of the two stages, then, is approximately 45. The resistance attenuator network has transmission properties depending upon whether the star is (1) within the tracker proportional zone or (2) outside the proportional zone but within the tracker field of view or (3) outside the field of view.

If the star is within the proportional zone the coincidence detector and the proportional region detector circuits on board 9 (See Figure 38) have triggered Q_4 (Board No. 9) into a short circuit configuration (Q_7- open-circuited). Under these conditions the 25 cps gain is equal to $\frac{R_8}{R_8 + R_9} \times 45$, and the proportional region gradient may be adjusted to the desired value by selection of R_9.

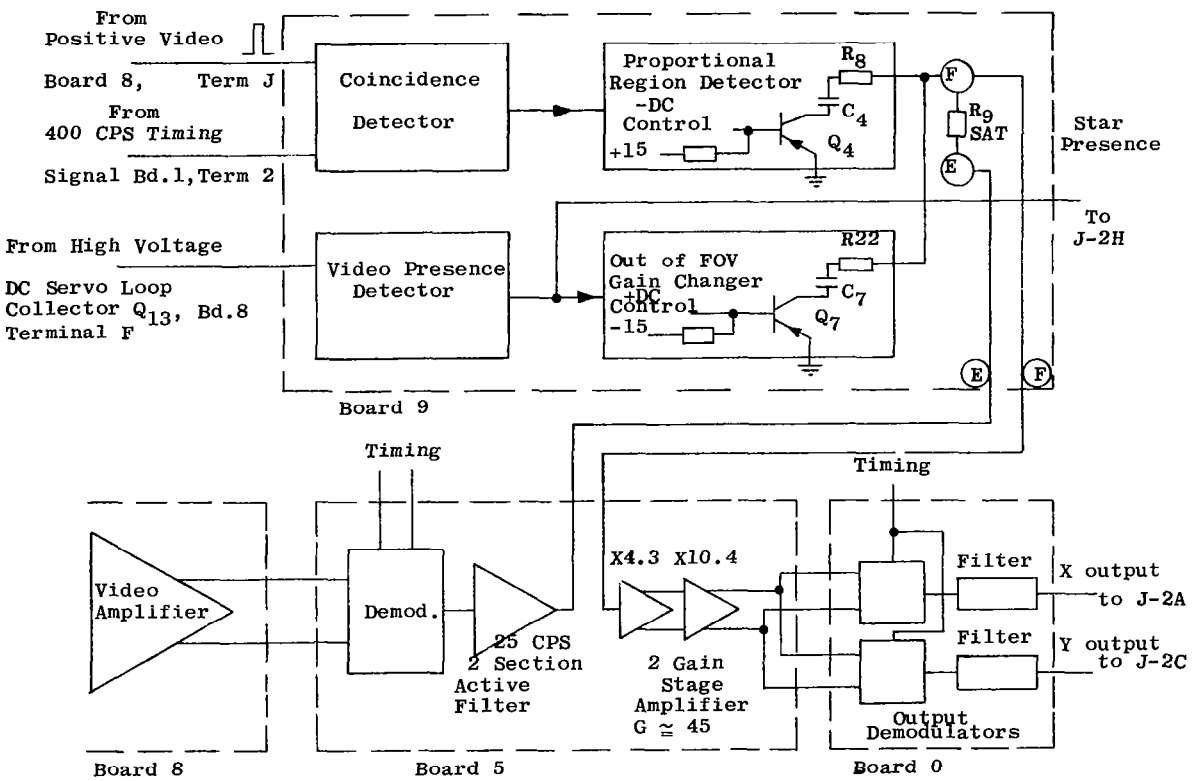

25 CPS Information Channel

FIGURE 38

If the star is within the field of view, but outside the proportional zone, transistors Q_4 and Q_7 (Board No. 9) are both open-circuited and there is no attenuation and the 25 cps gain is 45.

If the star is outside the field of view the "star present" signal is off and transistor Q_7 is triggered into a short-circuited configuration (Q_4 -open). Under these conditions the 25 cps gain is $\frac{R_{22} \times 45}{R_{22} + R_9}$. Thus, outside the field of view where the channel voltage is at a maximum for maximum star sensitivity for weak star detection, the noise voltages on the X and Y output lines can be kept low by reducing the 25 cps gain.

Star Present Detector

When a star enters the field of view of the tracker, video pulses are coupled from the video amplifier to the pulse-to-dc converter in the high voltage dc servo loop. The dc voltage at the output of the pulse-to-dc converter will then rise from its star "not present" level of -12 volts in a more positive voltage direction. When this dc voltage reaches approximately -8 volts it turns on a "Schmitt trigger" on Board No. 9 (schematic drawing No. X1856346, sheet 2) which will switch the "star present" terminal (J_2 G) voltage from its zero to five volt state. The Schmitt Trigger will remain on until the voltage level at the output of the pulse-to-dc converter falls more negative then the -8 volt level.

The Schmitt trigger circuit on board No. 9 is comprised of transistors Q_5 and Q_6. VR_2 acts as a dc level translator between the pulse-to-dc-converter and the Schmitt trigger. R_{23}, C_5, and C_6 act as a low pass filter to prevent the trigger circuit from being sensitive to fluctuations on the pulse-to-dc converter output voltage.

The "star present" Schmitt trigger also turns off the gain control transistor Q_7, Board No. 9, during a star present condition and on during a star not present condition to alter the 25 cps gain on Board No. 5 as described in the preceding section.

Coincidence Detector and Proportional Region Detector

If the positive video signal and the 400 cps timing signal from terminal 2, Board No. 1, are fed into the inputs of a 2 input AND gate, the AND gate will produce a maximum number of output pulses during one scan frame when the star is at boresight, a decreased number of output pulses per frame when at the edge of the proportional zone, and a minimum number of pulses per

frame when at the edge of the field of view.

These output pulses are used to trigger a "one shot" made up of transistors Q_2 and Q_3, with the pulse width output of the one shot being controlled by C_2. The negative polarity output pulses of the one shot are fed into a RC filter made up of R_5 and C_3. By adjusting C_2, R_5, C_3, and R_6, the gain control transistor Q_4, which is reverse biased by resistors R_7 and R_{16}, is made to fire on-or-off when the star is at the edge of the proportional zone by the negative dc voltage developed across C_3. This proportional region gain changer will alter the 25 cps gain on Board 5 as described previously.

Multiplier Coil Current Amplifiers

Board No. 6 (schematic drawing No. X1856370) contains two identical multiplier coil current amplifiers. A simplified drawing of the upper amplifier on the schematic is shown in Figure 39.

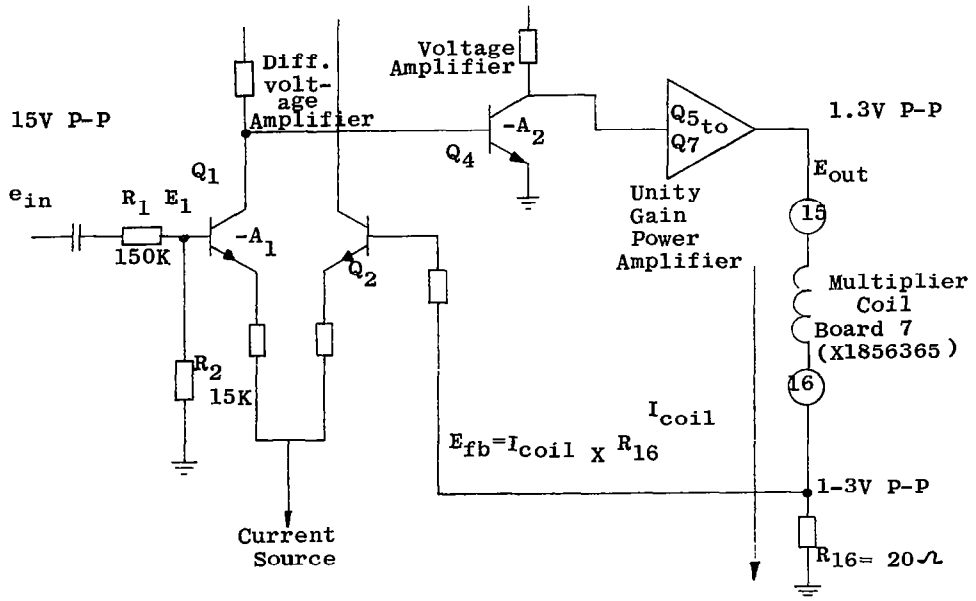

Coil Drive Amplifiers

FIGURE 39

The voltage e_{in} from the 25 cps filter on Board No. 2 is fed into the amplifier at the base of transistor Q_1, and amplified by the differential amplifier consisting of transistor Q_1 and Q_2. The output of the differential amplifier is further amplified by transistor Q_4 which is coupled to a unity gain buffer amplifier. The buffer stage then drives the current through the multiplier coil. The multiplier coil current is returned to ground through a resistor R_{16}. The voltage at the junction of the multiplier coil and resistor R_{16} is then fed back to the base of the differential amplifier transistor Q_2. The current in the multiplier coil may be found by the solution of the following equations.

$$\left[E_1 - I_{coil} \times R_{16}\right] \times A_1 \times A_2 = e_{out} \qquad (1)$$

$$I_{coil} (R_{16} + \mathbf{Z}\,coil) = e_{out} \qquad (2)$$

$$E_1 A_1 A_2 - I_{coil} A_1 A_2 R_{16} = I_{coil} (R_{16} + \mathbf{Z}\,coil)$$

$$I_{coil} = E_1 \frac{A_1 A_2}{A_1 A_2 R_{16} + R_{16} + \mathbf{Z}\,coil} = \frac{E_1}{R_{16} + \dfrac{R_{16} + \mathbf{Z}\,coil}{A_1 A_2}}$$

$$\text{if} \quad \left|R16\right| >> \left|\frac{R_{16} + \mathbf{Z}\,coil}{A_1 A_2}\right|$$

$$I_{coil} \cong \frac{-E_1}{R16} \cong \frac{R_2}{R_1 + R_2} \frac{e_{in}}{R_{16}}$$

Thus, the high open loop gain of the feedback amplifier eliminates any phase shift due to the reactive component of the coil impedance and the result is a stable voltage-to-current amplifier.

The input to the amplifier is approximately 15 volts peak-to-peak and the output voltage across the feedback resistor R_{16} is approximately 1.3 volts peak-to-peak, for a coil current of approximately $\pm$ 32.5 milliamperes.

Multiplier Two-Phase Voltage Amplifier

Board No. 7 (schematic drawing No. X1856365) contains a voltage amplifier with an output transformer containing two opposite phase secondary windings for excitation of the bridge circuits within the two multipliers. R_{12}, at the input to the first stage buffer transistor Q_5 is adjusted for proper temperature compensation of the multiplier M_1, output characteristic. Transistors Q_1 and Q_4 provide unity gain power amplifiers to drive the output transformer. The input to the amplifier is approximately 15 volts peak-to-peak, and the output at each of the push-pull transformer secondary windings is approximately 8 volts.

OPTICAL CONSIDERATIONS

The tracker was designed to accept various optical heads without internal modifications. To satisfy the Aerobee FACS, an 8^{o} field of view was employed. Figure 40 shown typical photomultiplier characteristics.

Since the usable photocathode diameter is 0.5 inch (12.7 mm) and an 8^{o} field of view was required, this fixed the focal length at

$$f = \frac{12.7}{\tan 8^{o}} = 90 \text{ mm}$$

for this application. Because the energy available is so low the maximum optical aperture was desired, but the requirements of light weight and installation flexibility precluded the use of very large optics. Although several F:1 systems were considered using in-house computers, the need for the smallest circle of confusion (to preclude further degeneration of the curve of Figure 40 (D) dictates the choice of photographic quality optics, and these are not obtainable in lightweight F:1 systems. An F:2 system was therefore employed.

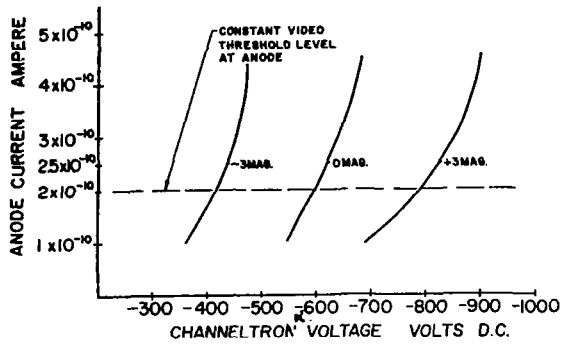

(A)Photomultiplier Voltage vs. Star Magnitude

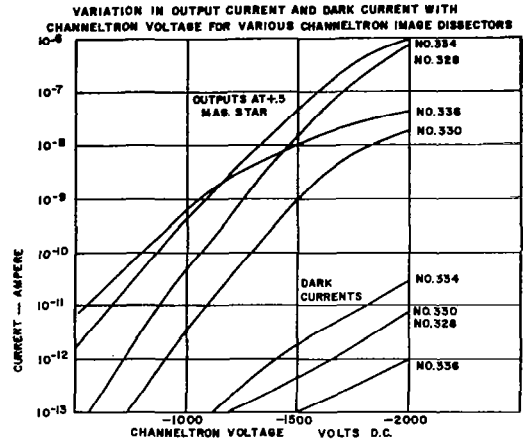

(B)Dark Current Variations

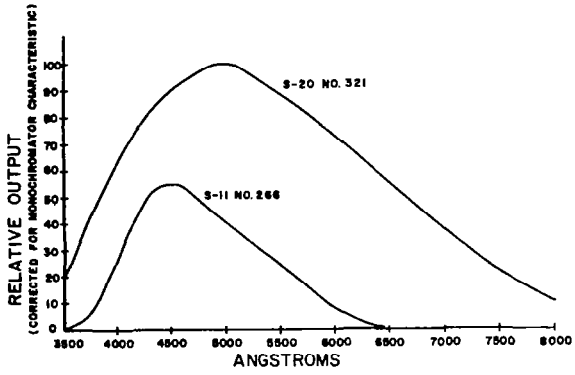

(C)Spectral Responses of S-11 and S-20 Photocathodes

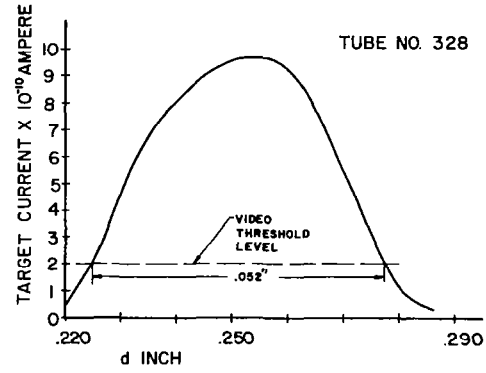

(D)Instantaneous FOV Dimensions

Photomultiplier Characteristics

FIGURE 40

If the video input threshold is set at 2×10^{-10} amperes, then, referring to Figure 40 (D) the effective spot diameter becomes 0.052 inch, and since 0.5 inch on the photocathode surface corresponds to 8 degrees, then the instantaneous field of view of the image dissector is

$$\frac{dF}{D} = 50 \text{ minutes of arc}$$

where d is the effective spot diameter, D the photocathode diameter, and F the field of view subtended by the photocathode in the image plane of the lens. In the unique scanning system employed the instantaneous field of view also defines, at boresight, the proportional zone of Figure 1 (B). The 50

minute value is a compromise to insure an instantaneous field of view sufficiently large to permit tracking the center of illumination of the planets (Table 2) yet sufficiently small to permit separation by at least 50 minutes of arc.

TABLE 2

Planet Targets

PLANET	DIAMETER IN ARC SECONDS	MAX. APP. MAG.
Mercury	6.45	-0.2
Venus	16.82	-4.08
Mars	9.18	-1.94
Jupiter	37.94	-2.4
Saturn	17.44	+0.8

Figure 41 is a plot of calculated photocathode currents obtainable for various star intensities with a 45 mm diameter objective and several photocathode efficiencies; the calculation assumes that a G_0 class star of third magnitude provides 2.5×10^{-4} watts/cm^2 in the wavelength interval from 3500 to 6500 angstroms; 80% transmission is assumed. For simplification the average number of electrons per second is also indicated, one ampere being equal to 1.6×10^{19} electrons per second by definition.

The optics supplied with both trackers are Ernst Leitz Summicron 1:2/90 systems. These are six element lens systems which include anti-reflection coatings. The lenses, as supplied by Leitz, will not withstand the vibration environment specified unless the rear threaded lens support is epoxy bonded to the forward barrel. This has been done in the trackers.

Figure 42 is a photograph of the components of the optical head assembly. The image dissector is cemented within an armco iron, copper plated holder with a silastic silicone rubber potting compound. The holder registers on an alodyned aluminum coil support which contains the deflection coil, an armco iron shroud with netic-conetic liners, and a rubber cushioning washer which accepts the edge of the photocathode faceplate. The coil support

in turn registers against the tracker mounting plate, to the other side of which the telescope is registered. The completely assembled optical head assembly has been shown in Figure 6.

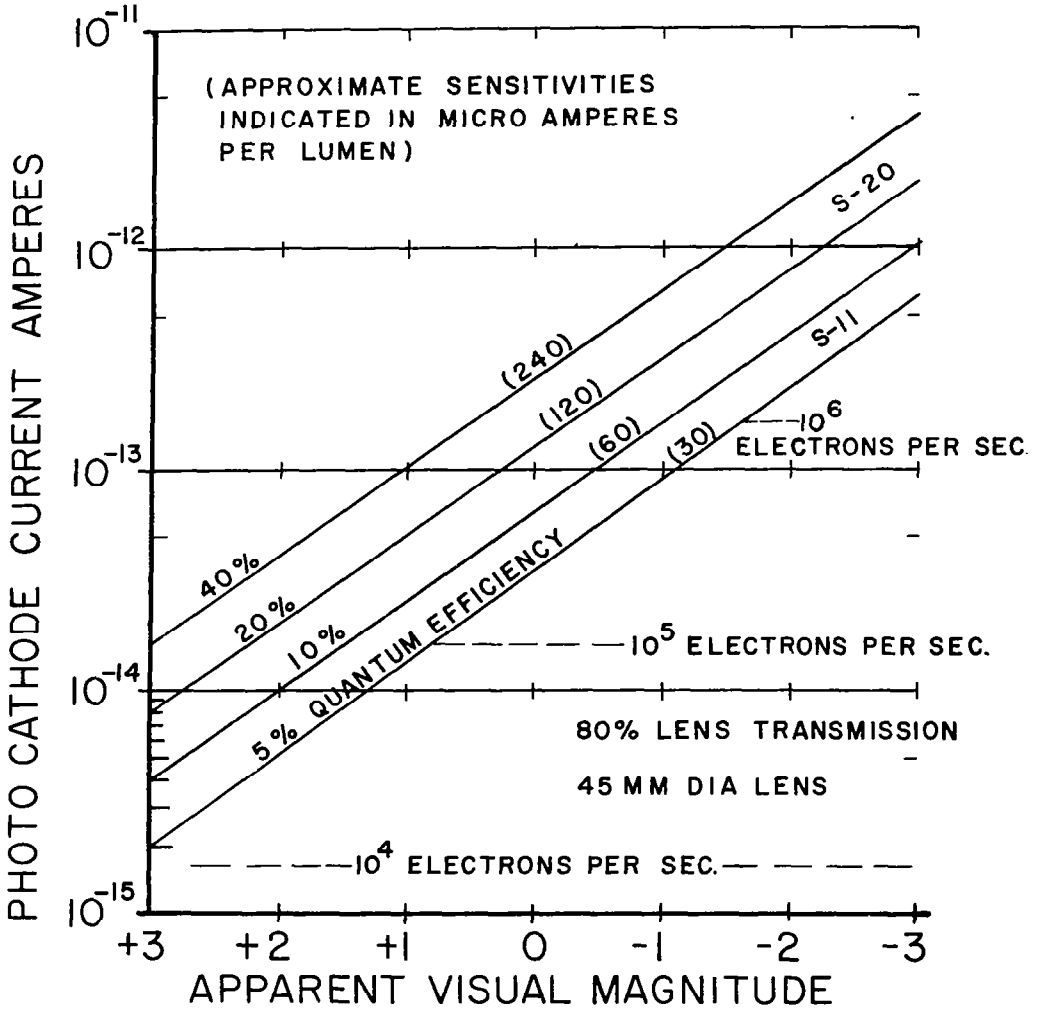

Photo Cathode Currents Available From Star Targets

FIGURE 41

Optical Head Components

FIGURE 42

Channeltron® Characteristics

Typical characteristics of Channeltron® image dissectors produced by this laboratory for star tracking applications are shown in Table 3. Although the initial 200 units incorporated S-11 photocathodes, present production is limited to S-20 photocathodes. The relative spectral response of these cathodes, obtained with a Bausch and Lomb monochromator incorporating a 1350 grooves per millimeter grating, are shown in Figure 40 (C).

Figure 44 is a plot of the anode current obtained as a point source of light is moved across the 0.5 inch diameter photocathode surface in the absence of deflection signals. This is the projection, through the tube's electrostatic lens system, of the detector aperture upon the photocathode, and is useful not only as a measure of the accuracy with which the Channeltron® element has been positioned behind the aperture but also discloses any distortions in the electrostatic lens. The scanning spot "diameter" is determined by the width of this curve; ideally, with perfect electrostatic focusing and an infinitely small point source, this curve would be rectangular, and the scanning spot could then be considered to have an absolute diameter; in practice, however, malfocusing in both the optical system of the tracker and in the electrostatic lens of the detector, and finiteness of the light source result in the bell-shaped characteristic shown. The anode current selected as the threshold thus fixes the effective scanning spot diameter, and not the diameter of the aperture placed between the electron multiplier and the focus of the

electrostatic lens, except in a gross manner. Since the effective spot diameter defines the instantaneous field of view of the tracker, variations in and about the thresholding value, whether due to noise or other signal fluctuations, have a marked effect upon tracker performance. With the deflection circuits operative the shape of the video signal pulses generated in response to a star target is determined by the shape of this curve, and subsequent pulse standardization must necessarily reflect any jitter occurring at threshold.

In the present application the Channeltron (R) voltage supply is electronically servoed in response to star magnitude signals to maintain a constant output current at the anode electrode with star presence (Figure 40 (A)). This was done to permit establishing a minimum threshold level to reject, from the video processing electronics, those signals produced by a second star simultaneously in the tracker field of view, provided the second star was separated from the target star by at least one visual magnitude. Several hundred thousand of these Channeltron (R) elements have already been produced at Bendix for various military and space projects; the Channeltrons (R) used in these image dissectors have typical electron multiplication factors of between 10^5 and 10^6; channel resistances range from 70 to 300 meghohms. Because the Channeltron (R) voltage is automatically adjusted for stellar magnitude, these channels are never operated in the saturated mode; i.e., there is no appreciable limiting of anode current by channel resistance.

The basing diagram in table 3 gives the basing connections used in all these tubes, whether S-11 or S-20 photocathodes. Later models incorporate a special focusing electrode to help minimize the spot rise distance; however, none of these later tubes were incorporated into the delivered trackers. The outline dimensions are shown in drawing No. X1863496 (Figure 43).

Signal-to-Noise

The scan produces one video pulse each time the effective spot diameter traverses the electron image of the target star on the photocathode. Since we are scanning at a rate that permits sweeping one photocathode diameter in 1.25 millisecond (half a 400 cps period), and since the effective spot diameter is approximately 10% of the photocathode diameter, only 125 micorseconds are available, on the average, in which to form the video pulse. Referring to Figure 41 an extremely good S-20 photocathode will produce, for a +3 magnitude star, approximately 100,000 electrons per second; thus, in the time available to form the video pulse only 12 electrons, on the average, are available at the photocathode. A typical S-11 photocathode will yield only 1.5 electrons in this time. Near boresight, where beam velocity is high, only

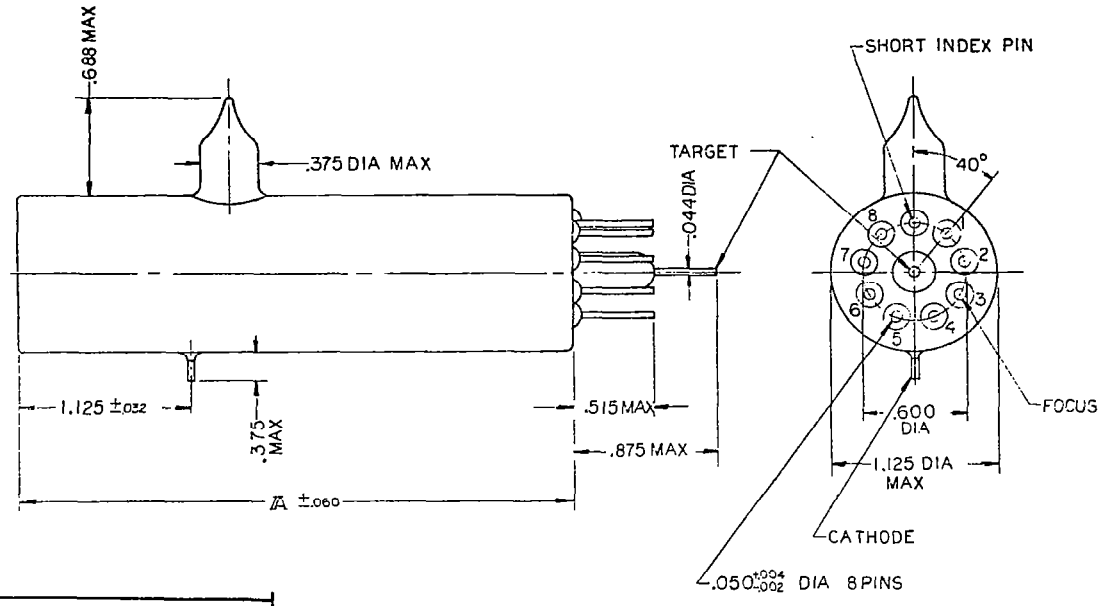

Image Dissector Tube Outline Drawing

FIGURE 43

80 microseconds of "dwell time" are available. A dependency upon electron arrival times is therefore inherent in signal production from such weak star targets which may not be compensated for by Channeltron ® gain or subsequent amplifier gains. With brighter stars, of course, the effect of such shot noise limiting of tracker accuracy is reduced; at +0.5 magnitude, ten times this number of photocathode electrons is available.

It is convenient, in specifying star tracker accuracies, to use that angular offset from null which yields a signal-to-noise ratio of unity. Figure 44 is a plot of tracker accuracies for a variety of Channeltron ® image dissectors using the F:2 optics and the full 8^{o} field of view. Figure 45 shows the effect of decreasing the angular size of the scan. These experimental results agree closely with calculated signal-to-noise ratios based upon shot noise limiting at the photocathode. For planet tracking, as well as for tracking most navigational stars the tracker provides adequate accuracies; for weak stars, however, performance is compromised by the short time available for the scanning beam to dwell upon the star target electron image.

TABLE 3

Channeltron® Image Dissector* Specifications

PHOTOCATHODE	
Faceplate	7056 glass
Spectral response	S-20
Active cathode diameter	18 mm
Luminous sensitivity	120 ua/lumen min.
	140 ua/lumen average
Radiant sensitivity	0.06 amp/watt at 5000 Å (nom.)
Quantum efficiency	15% at 5000 Å
CHANNEL MULTIPLIER	
Resistance	1×10^8 to 6×10^8
Design voltage	2,000 volts dc
Design current	5×10^{-7}
Current gain	10^5 average
OVERALL CHARACTERISTICS	
Anode sensitivity	15 amp/lumen average
Total dark current	10^{-10} amp at 20° max.
OVERALL LENGTH	3 5/8 inches
O.D.	1.125 inches
Weight	1.5 ounces

* Focus fixed type No. X1903152-1, adjustable type No. X1903152-2.

TABLE 3 (CONT)

Channeltron® Image Dissector Specifications*

SPOT SIZE	0.050 d. nominal
Deflection sensitivity	2 mm per gauss
VOLTAGES	
Collector	0
Channel - Output end	-50 V
Channel - Input end and lens assembly	-2050 V
Cathode	-2550 V
Focus electode	-2200 to -2550 V

BASING DIAGRAM

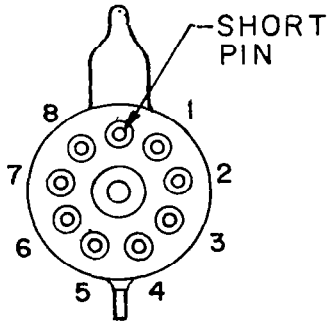

Lens #1, #4, #7

Sb generator #2

Channel output end - #5 & #8

Focus electrode - #3 & #6

Target - center lead

Cathode - side lead

Note: Focus electrode exists in Type 1903152-2 tubes or tubes with Serial Nos. 400 and up.

*Focus type No. X1903152-1, adjustable type No. X1903152-2.

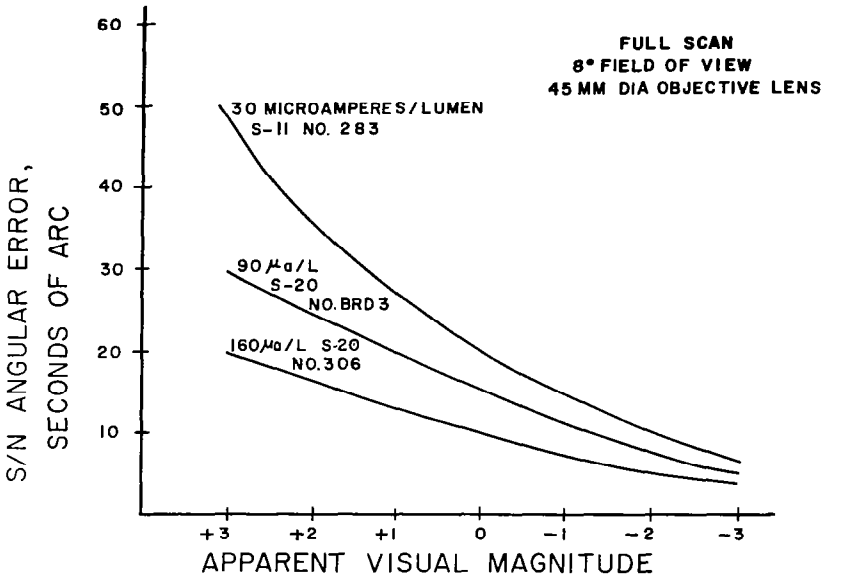

Angular Error vs Star Magnitude

FIGURE 44

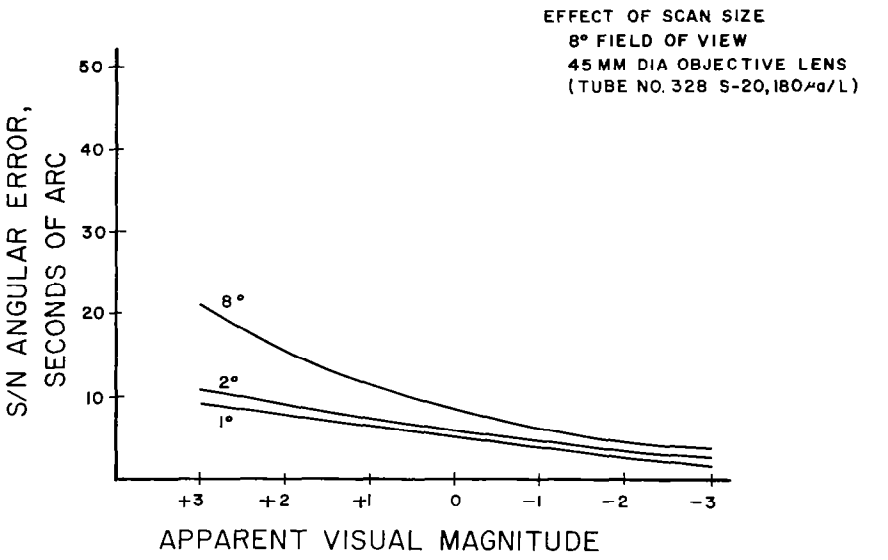

Effect of Scan Size

FIGURE 45

During the course of the program, a detailed investigation of signal-to-noise conditions was carried out both experimentally and analytically. The following section discusses the analytical aspects of signal-to-noise ratios in the present tracker.

Signal-To-Noise Analysis

This section summarizes the results of a study aimed at formulating the RMS of the equivalent angular noise output of an image dissecting star sensor due to shot noise current emanating from the photocathode. The equivalent angular noise would combine with the true angular error for a servoed star tracker and would thus be the angular noise input to the servo.

The formulation states the RMS of the equivalent angular noise in terms of star magnitude, its effective photon wave length, and the principal parameters of the subsystems. The subsystems are the entrance optics, the phototube, and the signal processing electronics.

The scope of the analysis is restricted to stars at a boresight angle within the angular subtense of the image dissector's scanning spot and to stars of magnitude such as to yield electrons at average rates so that individual electrons cannot be resolved by the photosensor bandwidth.

While thermal as well as shot noise is present, experimental results point to the former as negligible.

Finally, the analysis excludes the effects of shot noise other than from a star near boresight, and thus its applicability is restricted to star tracking outside the atmosphere.

Definitions of parameters. Referring to Figure 46, it may be noted that there are designated a total of thirteen independent parameters (in parentheses), of which two are star parameters and eleven are system parameters. The flow line symbols refer to the quantities which are to be successively formulated in terms of the star and system parameters.

Star Parameters

m - visual magnitude of star

λ - Effective wavelength of star radiation (approximately the centroid wavelength of the spectrum)

System Parameters

D	-	optical entrance lens diameter
δ	-	rise angle of electronic image of star
α	-	instantaneous field of view or limiting aperture
Q	-	over-all quantum efficiency of entrance lens and phototcathode
f_R	-	radial scan frequency - also fundamental of radial scan demodulator
θ_T	-	total angular field of scan
N	-	number of pulses per scanning frame
B_P	-	noise bandwidth of video amplifier
a	-	ratio of threshold to peak currents
B_F	-	noise bandwidth of frame scan filter
B_ϵ	-	noise bandwidth of error signal filter

Signal processing. A rosette scan pattern is generated by setting the frequency of crossed electron deflecting magnetic fields and the voltage generating the electrostatic focussing field. The scan pattern is then the locus of points in the photocathode from which photoelectrons can be potentially collected. Photoelectrons are actually collected by the tube anode when the scanning spot, or instantaneous field of view, crosses the focussed star image on the photocathode. Thus the steady electron emission from the star image is modulated by the scan pattern.

If there were no bandwidth limiting (due to the video amplifier), no electron malfocussing inherent in the phototube, and no shot noise, the scan would result in a series of rectangular pulses of current, each pulse being generated as the scanning spot crossed the focussed image of the star on the photocathode. Owing to the limiting bandpass of the amplifier alone, the rectangular pulses would would be rounded off. Experimental results indicate, however, a series of rounded off trapezoidal pulses. The inference is that the input pulse train to the video amplifier is a series of trapezoid-like pulses, with the rise time of each trapezoid being proportional to the rise angle, or image diameter,

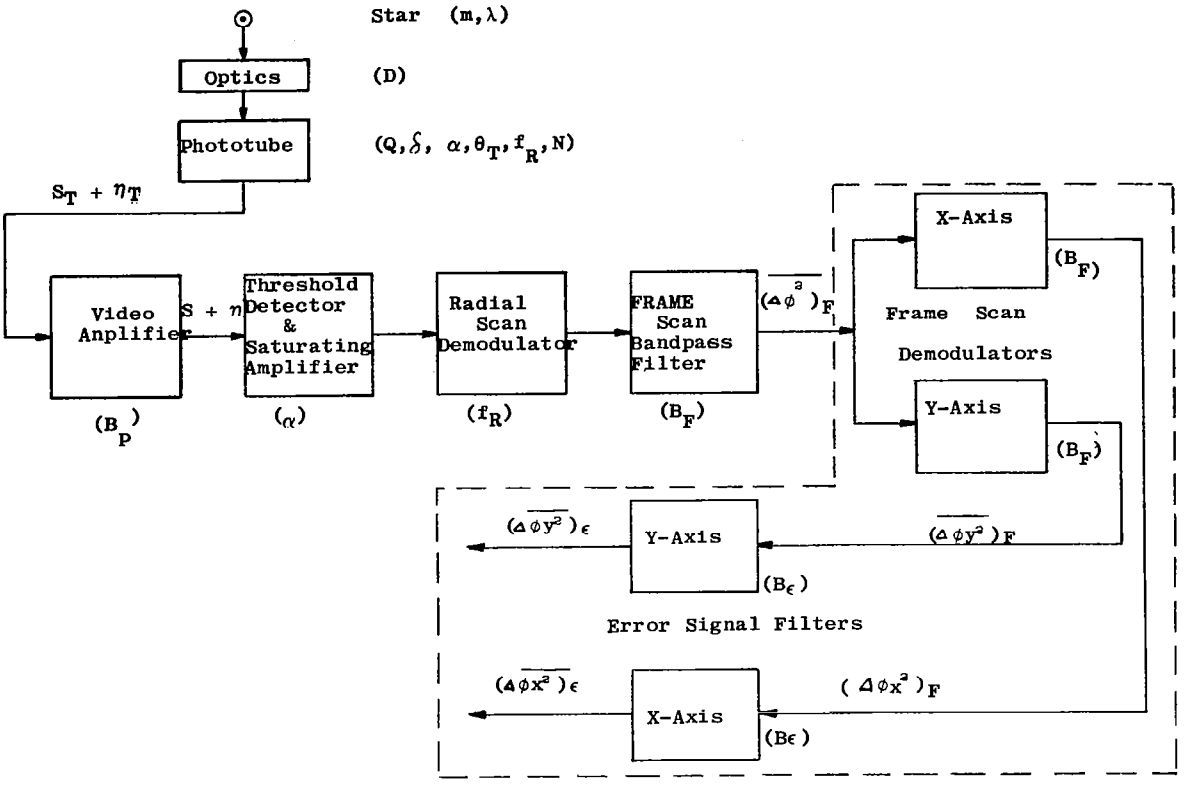

Analysis System Diagram

FIGURE 46

associated with imperfect electron focussing, and inversely proportional to the velocity of the scanning spot as it crosses the star image.

The amplified trapezoid pulse train is fed into a threshold detector which passes only that part of each pulse exceeding the threshold. (See Figure 46.) Its purpose is to exclude tracking of other stars within the total field of view which are fainter by a specified amount than that of the strongest star. A saturating amplifier then amplifies the series of excess pulses to some fixed saturation level. The result is a series of rectangular pulses whose edges reflect the threshold crossings of the amplified trapezoidal train. As will be seen, the direction of the star image is obtained from the series of threshold crossing times of the trapezoid pulse train, one scanning frame in length.

The rectangular train is then demodulated by effectively being multiplied by a unit square wave at a fundamental frequency equal to the radial frequency

of the scan. The output train thus suffers sign reversal at each instant the scan crosses boresight or sweep center. The demodulated train is then passed through the frame scan bandpass filter. This filter with a flat bandpass has a sharp cut-off at the frame scan frequency, and thus has a smoothing time equal to half the period of the frame. If there are N lobes in the rosette scan pattern, there will be N pulses per frame for a star near boresight. This filter output will then be a continuous averaging over the last $\frac{N}{2}$ pulses of the demodulated train input. The result will be a sine wave with a period equal to the frame scan period, an amplitude proportional to the star's boresight angle, and a phase equal to the star's azimuth. The amplitude and phase of this sine wave are equivalent in information to the x- and y- coordinates of the star image. These coordinates are detected by demodulating in parallel the sine wave by two square waves each with a fundamental equal to the sine wave frequency, and with a time separation equal to one fourth the frame period. The frame scan demodulators thus act as resolvers.

Referring to Figure 46, the four boxes enclosed by the dotted envelope effectively vector the star image in two dimensions, relative to the boresight axis. That is, the direction of the image relative to boresight is found by these four boxes. The magnitude of image displacement is found only to a proportionality constant. Referring to Figure 47, a geometric analogue of the signal processing is shown, for a star image off boresight, but within the radius of the scanning spot diameter. The figure is a figure of revolution which is generated by rotating the successive trapezoidal pulses comprising a frame through the successive pass angles of the rosette scan, with the axis of rotation being the boresight axis. The axis of the figure of revolution which is at the centroid of the series of threshold crossings on the circular threshold contour, corresponds with the location of the star image relative to the boresight axis. It can be shown that for these threshold crossing points as intersections of a circle (the threshold contour) with uniformly angularly spaced lines intersecting at the boresight axis (the passes of the rosette scan), its centroid vector referred to the boresight axis, points in the same direction as the center of the circular threshold contour which is the location of the star image.

Having noted the one to one correspondence between the series of threshold crossing events and their spatial coordinates in an electronic image, the centroid of these equivalent coordinates is effectively found by the combined action of the radial scan demodulator and the frame scan filter. The sign reversals acting on the thresholded train by the demodulator are equivalent to sector balancing in sequence of the electronic image. The frame scan filter continuously averages the balanced sequence over half the period of the frame. The filter output is resolved by the two phased square wave demodulators.

(A) EQUIVALENT ELECTRONIC IMAGE
OF FRAME BANDPASS FILTER OUTPUT
(PERSPECTIVE VIEW)

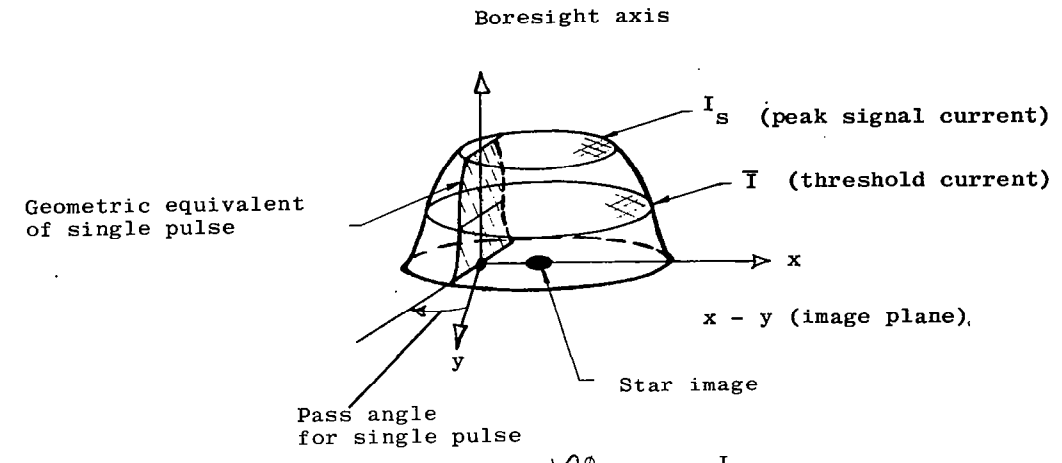

(B) TOP VIEW SHOWING
RANDOM RADIAL EDGE
JITTER DUE TO SHOT
NOISE

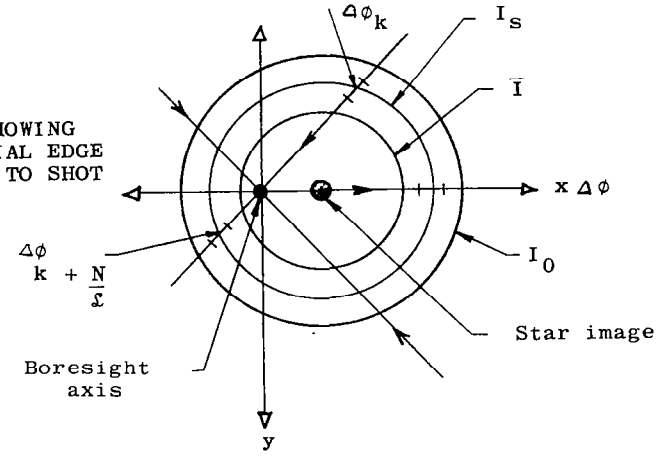

Electronic Image Equivalents

FIGURE 47

The two demodulator outputs are then proportional to the x- and y- coordinates of the equivalent threshold contour. (It should be noted that interleaving of the scan pattern results continuously in a nearly symmetrical array of passes within a half-period. Were this not so, the instantaneous centroid would oscillate about the threshold contour's centroid.)

Noise processing. An inference that can be drawn from the preceding observations is that if the timing of threshold crossing events can determine, down to a point, the star image, in the noise-free case, the random time jitter of these events due to the presence of noise, will in turn result in an equivalent spatial jitter in the location of the star image.

Shown in Figure 48 are the signal trains as corrupted by shot noise, under the assumption that the number of electrons per pulse for the input train to the video amplifier is much greater than that resoluble in time by the amplifier. In this case, the shot noise may be considered as modulated by the signal pulses in a statistical mean square sense. With s(t) as the amplifier output signal train, the instantaneous ensemble average of the shot noise, $\overline{n(t)^2}$, is related to the unmodulated shot noise, $\overline{n_o(t)^2}$, (that is the shot associated with the peak signal level) as

$$\overline{n(t)^2} = \frac{s(t)}{I_s} \overline{n_o 2} \qquad (1\text{-a})$$

with

$$\overline{n_o{}^2} = 2eI_sB_P \qquad (1\text{-b})$$

or

$$\overline{n(t)^2} = 2es(t)\,B_P \qquad (1\text{-c})$$

(In Equation 1, e is the electron charge: I_s is the peak of the signal current.) Then averaged over all instants, t_k, at threshold current, $\bar{I}$, the mean square of the noise sampled at threshold is:

$$\overline{n_k{}^2} = 2e\bar{I}B_p = 2\,eaI_s\,B_p \qquad (1\text{-d})$$

where $a = \frac{\bar{I}}{I_s}$ is the threshold ratio, and

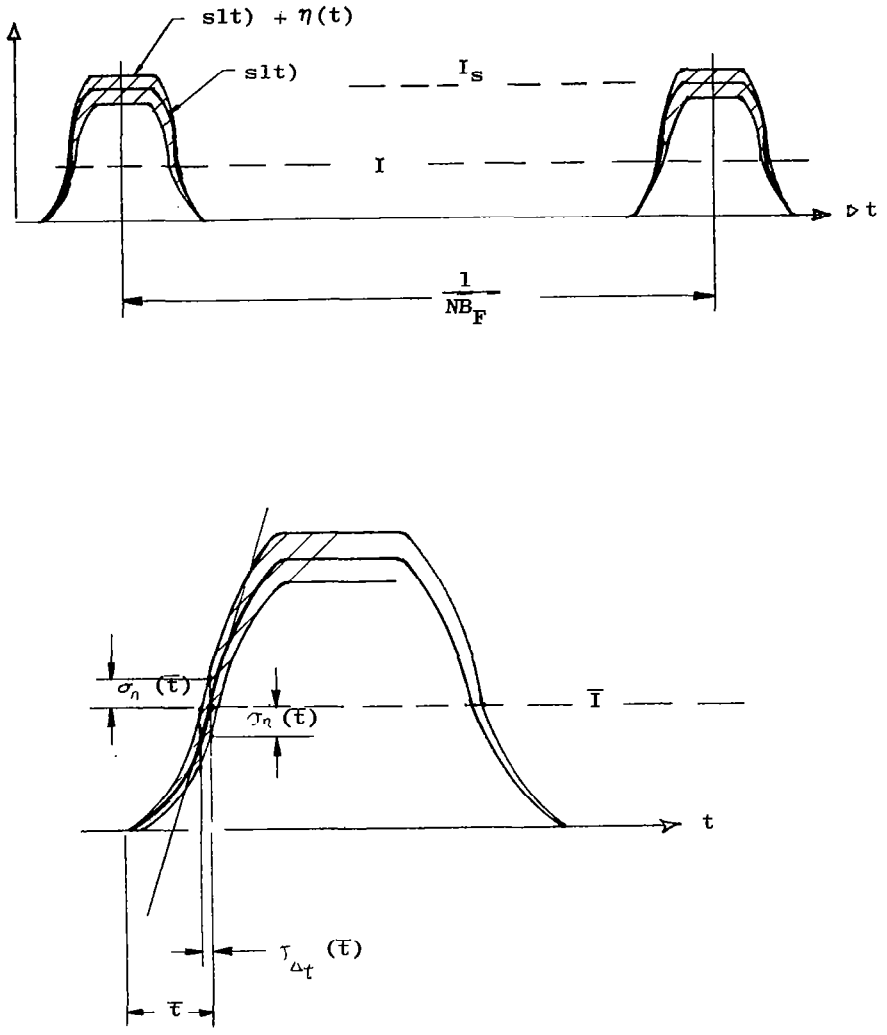

Signal Waveforms Plus RMS Noise

FIGURE 48

B_P is the noise bandwidth of the video amplifier. The noise bandwidth, B, of a linear filter, G(jf), is defined as

$$B = \frac{1}{\left|G(jo)\right|^2 2} \int_o^\infty \left|G(jf)\right|^2 \, df \qquad (1\text{-}e)$$

For unity dc gain, the noise bandwidth would be simply the frequency integral of the filter spectral power window,

$$\left|G(jf)\right|^2 = G(jf)\; G^*(jf) \qquad (1\text{-}f)$$

In considering the equivalent radial angular fluctuation of the electronic image centroid as passed by the frame scan filter, there will be an averaging of the jittered samples of $\frac{N}{2}$ pulses, or N threshold crossings, in its smoothing time. (Note there are 2N such crossings per frame for an N lobe rosette.) Referring to Figure 47, $\Delta\phi_k$ is the random equivalent radial jitter at the kth threshold crossing due to the noise sample, n_k. Taking note that the only likely correlation between the random samples will be those pairs on opposite sides of the threshold contour, corresponding to the threshold crossings of leading and trailing edges of a signal pulse, we have

$$\Delta\phi_k = \omega_s \Delta t_k \qquad k = 1, \ldots, \frac{N}{2} \qquad (2)$$

$$\Delta\phi_k + \frac{N}{2} = -\omega_s \Delta t_k + \frac{N}{2}$$

where ω_s is the scan angular velocity at sweep center and can be stated in terms of the radial scan frequency and total field of view as

$$\omega_s = \pi f_R \theta_T \qquad (3)$$

The opposite signs in (2) reflect the fact that a lag in the time jitter will be equivalent to an outward radial displacement from the threshold contour on one side of this contour, while on its opposite side $\left(\text{at } K + \frac{N}{2}\right)$, it will produce an inward displacement. The same is true, of course, for a lead time jitter.

The samples of time jitter are related to the noise samples, n_k, by

$$\Delta t_k = -\frac{n_k}{\dot{s}_k}, \quad \text{for all k,} \qquad (4\text{-}a)$$

adopting the convention that for a lag jitter, Δt_k is positive, and for a lead it is negative. But it should also be noted that the signal slopes on opposite sides of the output pulses of the video amplifier are approximately opposite in sign, i.e.

$$\dot{s}_k \quad + \quad \frac{N}{2} \quad = \; - \; \dot{s}_k \tag{4-b}$$

Hence, $$\Delta\phi_k \qquad \Delta\phi_k \quad + \quad \frac{N}{2} \quad = \left(\frac{\omega_s}{\dot{s}_k}\right)^2 \quad n_k \qquad n_k \quad + \quad \frac{N}{2} \tag{4-c}$$

Now, noting that the small samples of radial jitter, at photosensor bandwidth, B_P, must be considered as vectors in determining these results on the filter's equivalent centroid error, the random centroid vector error at filter bandwidth, B_F, is (5-a)

$$\vec{\Delta\theta}_F \quad = \quad \frac{1}{N} \sum_{k \,=\, 1}^{N} \Big\backslash \; \vec{\Delta\phi}_k \qquad P$$

The square of the random magnitude is

$$(\Delta\phi^{\,2})_F \quad = \quad \frac{1}{N^2} \sum_{k \,=\, 1}^{N} \sum_{j \,=\, 1}^{N} (\vec{\Delta\phi}_k \; \vec{\Delta\phi}_j) \quad P \tag{5-b}$$

$$(\vec{\Delta\phi}_k \; \vec{\Delta\phi}_j)_P \quad = \quad (\Delta\phi_k \quad \Delta\phi_j)_P \qquad \cos \frac{2\pi}{N} (j-k) \tag{5-c}$$

The mean square is then

$$\overline{(\Delta\phi^{\,2})_F} \quad = \quad \frac{1}{N^2} \sum_{k \,=\, 1}^{N} \sum_{j \,=\, 1}^{N} \cos \frac{2\pi}{N} (j-k) \; \overline{(\Delta\phi_k \, \Delta\phi_j)_P} \tag{5-d}$$

Again assuming there is no noise correlation from pulse to pulse, but only possibly between leading and trailing edges of a single pulse,

$$\overline{\Delta\phi_k \quad \Delta\phi_j}_P = \begin{cases} \overline{\left(\Delta\phi_k^{\,2}\right)}_P = \overline{\left(\Delta\phi_j^{\,2}\right)}_P & , \text{ for } j = k \\ \overline{\left(\Delta\phi_k \quad \Delta\phi_k + \frac{N}{2}\right)}_P & , \text{ for } j = k + \frac{N}{2} \\ \overline{\left(\Delta\phi_{k + \frac{N}{2}} \quad \Delta\phi_k\right)}_P & , \text{ for } j = k - \frac{N}{2} \\ o & , \text{ for } j \text{ none of the above} \end{cases} \qquad (6\text{-a})$$

$$\sum_{k=1}^{N} \sum_{j=1}^{N} \cos \frac{2\pi}{N} (j - k) = \begin{cases} N, \text{ for } j = k \\ -\frac{N}{2}, \text{ for } j = k + \frac{N}{2} \\ -\frac{N}{2}, \text{ for } j = k - \frac{N}{2} \end{cases} \qquad (6\text{-b})$$

Hence, the mean square of the centroid radial angular fluctuation is

$$\overline{(\Delta\phi^2)}_F = \frac{1}{N} \left\{ \overline{\Delta\phi_k^{\,2}} - \overline{\Delta\phi_k \quad \Delta\phi_{k + \frac{N}{2}}} \right\}_P \qquad (7\text{-a})$$

From (2) and (4)

$$\overline{(\Delta\phi^2)}_F = \frac{1}{N} \left[\frac{\omega_s}{\dot{\bar{s}}(t)} \right]^2 \left\{ \overline{n_k^{\,2}} - \overline{n_k \quad n_{k + \frac{N}{2}}} \right\}_P \qquad (7\text{-b})$$

To obtain the mean square of the x- and y- components of the centroid angular error, note that the random components

$$(\Delta\phi_x)_F = \frac{1}{N} \sum_{k=1}^{N} (\Delta\phi_k)_P \cos \frac{2\pi k}{N}$$

$$(\Delta\phi_y)_F = \frac{1}{N} \sum_{k=1}^{N} (\Delta\phi_k)_P \sin \frac{2\pi k}{N} \qquad (8\text{-a})$$

$$\text{Then } (\Delta\phi_x{}^2)_F = \frac{1}{N^2} \sum_{k=1}^{N} \sum_{k=1}^{N} (\Delta\phi_k \, \Delta\phi_j)_P \cos\frac{2\pi k}{N} \cos \frac{2\pi j}{N}$$

$$= \frac{1}{2N^2} \sum_{k=1}^{N} \sum_{j=1}^{N} (\Delta\phi_k \, \Delta\phi_j)_P \left[\cos \frac{2\pi}{N} (k-j) + \cos \frac{2\pi}{N} (k+j)\right] \qquad (8\text{-b})$$

and similarly for $(\Delta\phi_y{}^2)_F$.

Then the mean square of x- and y- components of the centroid radial fluctuation is, by the previous arguments,

$$\left(\overline{\Delta\phi_x{}^2}\right)_F = \frac{1}{2N} \left\{\overline{\Delta\phi_k{}^2} - \overline{\Delta\phi_k \, \Delta\phi_k} + \frac{N}{2}\right\}_P = \left(\overline{\Delta\phi_y{}^2}\right)_F \qquad (8\text{-c})$$

We see that the mean squares of the x- and y- components of the centroid radial fluctuation is half that of radial component, as expected.

Referring to (7-b), the result obtained assuming the random centroid error to be the mean vector combination of sample threshold vector errors, is identical to that obtainable with the magnitude of the centroid error assumed to be a mean scalar combination of sample scalar errors. This is due to the radial symmetry assumed for the alignment of the sample vectors. However, without the vector argument, the result for the mean squares of the components, (8-c), would have required arbitrary assumptions.

Continuing, the mean squares of the equivalent angular noise outputs from the error signal filters, x- and y-, are given by

$$\overline{(\Delta\phi_x{}^2)_\epsilon} = \overline{(\Delta\phi_y{}^2)_\epsilon} = \frac{B\epsilon}{B_F}\ \overline{(\Delta\phi_x{}^2)}_F, \qquad (9\text{-a})$$

and we have for their RMS angular fluctuations for the x- and y- error signal filters,

$$(\sigma^{\phi_x})_\epsilon = (\sigma^{\phi_y})_\epsilon = \left[\frac{\omega_s}{s(t)}\right]\sqrt{\frac{B\epsilon}{2\ NB_F}\left[\overline{n_k{}^2} - \overline{n_k n_{k+\frac{N}{2}}}\right]_P} \qquad (9\text{-b})$$

As previously stated, the frame scan filter with noise bandwidth B_F, is practically flat out to the cut-off frequency, B_F. The video amplifier of noise bandwidth B_P, has a frequency response given approximately by

$$G_p(jf) = \frac{1}{1 + 2\pi\ jfT_P}, \qquad \text{or} \qquad (10\text{-a})$$

$$\left|G_P(jf)\right|^2 = \frac{1}{1 + 4\pi^2 f^2 T_P{}^2}, \qquad (10\text{-b})$$

and a white noise bandwidth given by

$$B_P = \int_0^\infty \frac{df}{1 + 4\pi^2 f^2\ T_P{}^2} = \frac{1}{4T_P}, \qquad (10\text{-c})$$

showing that (10-b) may be written

$$\left|G_P(jf)\right|^2 = \frac{4B_P{}^2}{4B_P{}^2 + \pi^2 f^2} \qquad (10\text{-d})$$

Similarly, the error signal filter, given by

$$G_\epsilon(jf) = \frac{1}{1 + 2\pi\, jf\, T_\epsilon}\,, \qquad (10\text{-e})$$

with a noise bandwidth given by

$$B_\epsilon = \int_0^\infty \frac{df}{1 + 4\pi^2 f^2 T_\epsilon{}^2} = \frac{1}{4T_\epsilon} \qquad (10\text{-f})$$

The video amplifier frequency response alone is relevant to obtaining the mean square and correlated noise as well as the signal slope at threshold.

The mean square of the noise samples, $\overline{n_k{}^2}$, has already been given in (1-d). This equation follows from assuming an effective input noise spectrum from the phototube,

$$S_{n_T}(f) = 2e\bar{I} = 2eaI_s \qquad (11\text{-a})$$

The amplifier output noise spectrum is then

$$S_n(f) = \left|G_P(jf)\right|^2 S_{n_T}\,, \qquad (11\text{-b})$$

and its mean square output,

$$\overline{n^2} = \int_0^\infty S_n(f)\, df = 2e\bar{I} \int_0^\infty \frac{df}{1 + 4\pi^2 f^2 T_P{}^2} = 2eIB_P \qquad (11\text{-c})$$

The pulse edge noise correlation, $\overline{n_k n_k} + \frac{N}{2}$ is the noise autocorrelation for delay equal to the time interval between threshold crossings for a leading and trailing edge of a pulse.

Designating this interval as t_P, and utilizing a theorem relating the power density spectrum to the autocorrelation as a Fourier transform pair:

$$R_n(\tau) = \int_0^\infty S_n(f) \cos 2\pi f \tau \, df$$

$$S_n(f) = 4\int_0^\infty R_n(\tau) \cos 2\pi f \tau \, d\tau \qquad (12)$$

$$\text{with } R_n(0) = \overline{n^2}$$

$$\overline{n_k n_k} + \frac{N}{2} = R_n(t_P) = \int_0^\infty \frac{2e\bar{I}}{1 + 4\pi^2 f^2 T_P^2} \cos 2\pi f t_P df$$

$$= \frac{e\bar{I}}{2T_P} \exp\left\{ - \left| \frac{t_P}{T_P} \right| \right\} \qquad (13)$$

$$\overline{n_k n_k} + \frac{N}{2} = 2e\bar{I} B_P \exp\left\{ - \left| 4B_P t_P \right| \right\}$$

The interval between threshold crossings, t_P, can be stated in terms of the effective scanning spot diameter, and other system parameters as

$$t_P = \frac{\alpha}{\omega_s} = \frac{\alpha}{\pi f_r \theta_T} \qquad (14)$$

The magnitude of the signal slope at threshold is obtained from the ramp response of a filter given by the amplifier's frequency response (10-a). Modeling the input trapezoid ramp as

$$s_T(t) = \frac{t}{\tau_P} \quad I_s, \quad o < t < \tau_P \tag{15-a}$$

The amplifier output over this interval is then

$$s(t) = \frac{I_s}{\tau_P} \left\{ t - T_P \left(1 - e^{-t/T_P}\right) \right\}. \tag{15-b}$$

Hence, the slope at threshold time, $\bar{t}$, is

$$\dot{s}(\bar{t}) = \frac{I_s}{\tau_P} \left(1 - e^{-\bar{t}/\tau_P}\right) \tag{15-c}$$

The rise time of the input signal slope, τ_P, reflects the imperfect focussing of the phototube, which in turn is specified by a rise angle, independent of the sweep center velocity, ω_s. The relation of the rise angle of the tube, δ, to the rise time is

$$\delta = \omega_s \tau_P \tag{16}$$

The input rise time, τ_P, can be related to the amplifier's output rise time, τ_P' from the constraint,

$$s(\tau_P') = I_s \tag{17-a}$$

and using (14-b)

$$\tau_P = \tau_P' - T_P \left(1 - e^{-\tau_P'/\tau_P}\right)$$

$$\tau_P = \tau_P' - \frac{1}{4B_P}\left(1 - e^{-4B_P \tau_P'}\right) \qquad (17\text{-b})$$

Then using (15), the tube rise angle, δ, can be found.

A direct measurement of δ is available. This consists of fixing the scan at foresight (eliminating the sweep), and observing the error signal level as a simulated star is successively moved through the spot diameter. The succession of signal levels versus star boresight angle should yield the rise angle. Having obtained the rise angle, independent of amplifier output measurements which would depend on (16) and (17), the threshold time, t, is found by using (15-b) evaluated at $\bar{t}$. Assuming $e^{-\bar{t}}/T_P << 1$

$$s(\bar{t}) = \bar{I} = aI_s \cong \frac{I_s}{\tau_P}\,\bar{t} \qquad (18\text{-a})$$

Hence,

$$\dot{s}\,(\bar{t}) \cong \frac{I_s}{P}\left[1 - \exp - (4aB_P\ \tau_P)\right] \qquad (18\text{-b})$$

Substituting (11-c), (13), (14), (15-c), (16), and (18-b) into (9), there results for the RMS equivalent angular noise output for each axis.

$$(\sigma\Phi_x)_\epsilon = (\sigma\Phi_y)_\epsilon = \frac{\delta}{1 - \exp - \left(\frac{4aB_P\delta}{\pi f_r\ \theta T}\right)} \sqrt{\frac{B_e B_P}{N\ B_F}\ \frac{ea}{I_s}\left[1 - \exp - \left(\frac{4B_P\alpha}{\pi f_R\ \theta_T}\right)\right]} \qquad (19)$$

The minus sign under the radical indicates that as the correlation of leading and trailing samples of noise at threshold crossings increases, a reduction in system effective angular noise occurs. This is compatible with the observation that the leading and trailing slopes of the signal pulses are opposite in sign, and, therefore, if the pulse is so short as to permit significant threshold noise correlation per pulse, the leading and trailing edges of the pulses coming out of the threshold detector will jitter in opposite directions. Equivalently, the pulse centroid of these pulses will not be jittered, and since the first demodulator sector balances these pulses, the result would indeed be a reduction of output angular noise as the edge noise correlation is increased. As will be indicated in the following section, in practice, the edge noise correlation is quite negligible, and the term is omitted hereafter.

There remains the requirement of expressing the ratio of the electron charge, e, to the peak signal current, I_s, in terms of the star magnitude, m, its effective photon wavelength, λ, and the entrance aperture, D, of the optics optics.

According to Abate*, the collected radiant power, P, is related to star visual magnitude, m, and entrance diameter, D by

$$P \text{ (watts)} = \frac{1.57 \times 10^{-12} \; D^2}{2.51^m} \text{ (inches}^2\text{)} \qquad (20\text{-a})$$

With p as the average photon rate collected, pe as the average electron rate emitted by the photocathode, Q as the over-all quantum efficiency of entrance optics and photocathode, then for photons of effective wave length, λ,

$$P = p \frac{hc}{\lambda}$$

$$p_e = Q p_e \qquad (20\text{-b})$$

$$I_s = p_e$$

and

$$\frac{e}{I_s} = \frac{hc}{PQ\lambda} \qquad (20\text{-c})$$

* "Star Tracking and Scanning Systems, Their Performance and Parametric Design" - I.E.E.E., Trans, Aero. and Nav., Sept., 1963

The product of Planck's constant and the vacuum velocity of light is

$$hc = 19.8 \times 10^{-20} \text{ watt-sec. - microns,} \qquad (20\text{-d})$$

the microns being used in compatibility with the photon wavelength, λ, in microns.

$$\sqrt{\frac{e}{I_s}} = \sqrt{\frac{hc}{PQ\lambda}} = \frac{3.6 \times 10^{-4}}{D} \sqrt{\frac{2.51^m}{Q\lambda}} \qquad (20\text{-e})$$

Where as before, D is in inches, λ is in microns, and m is the star's visual magnitude.

Hence, the end result is

$$(\sigma^{\phi}x)_{\epsilon} = \frac{3.6 \times 10^{-4}}{D} \left[\frac{\delta}{1 - \exp-\left(\frac{4aB_P\delta}{\pi f_r \theta_T}\right)}\right] \sqrt{\frac{2.51^m aB_{\epsilon} B_P}{Q\lambda \; NB_F}} = (\sigma\phi y)_{\epsilon} \qquad (21)$$

The output RMS angular noise given by (29) will be in arc seconds, with δ in the numerator in arc seconds, and with δ and θ_T in the denominator in radians.

All parameters except the amplifier noise bandwidth, B_p, are either limited by state of the art capabilities, e.g., Q and δ, or by operational requirements, e.g., B_{ϵ} and θ_T, which, in turn, impose constraints on NB_F and f_R. Note also that D is limited by size and weight considerations, while m and λ are environmental constraints. Given these parameters, however, a trade-off in the video amplifier bandwidth, B_p, is available, as shown by (21) If (21) is differentiated with respect to B_p and the derivative set equal to zero, a minimum RMS angular error will result, indicating the trade-off between degrading the input pulse slopes and blocking the noise. The optimum bandwidth, B_p, resulting from the derivative constraint,

$$\exp - \left(\frac{4a\delta}{\pi f R \theta_T} \sqrt{B_P}\right) = \left(1 + \frac{8a\delta}{\pi f R \theta_T} \sqrt{B_P}\right) - 1 \qquad (22\text{-a})$$

turn out to satisfy the constraint,

$$\frac{4a\delta}{\pi f_R \theta_T} \quad \triangle B_P = 1.26 \qquad (22\text{-b})$$

(Again, this follows from assuming that the threshold time is much greater than the amplifier time constant, or that the slope of the output is practically the same as the slope of the input, when threshold is reached.)

Finally it may be noted from (21) that for all parameters fixed except B_P, the RMS angular error goes to infinity as $\frac{1}{\sqrt{B_P}}$, as B_P goes to zero, and as $\sqrt{B_P}$, as B_P goes to infinity. Therefore, the RMS error is more sensitive to amplifier bandwidth on the low side of optimum than on the high side.

Numerical evaluations are as follows.

$a = \frac{\bar{I}}{I_s} = 0.4$	(threshold ratio)
$Q = 0.05$	(quantum efficiency)
$\lambda = 0.5\mu$	(photon wavelength of star)
$\delta = 15$ arc minutes	(rise angle of electronic image)
$D = 2$ inches	(optical aperture)
$f_R = 400$ cps	(radial frequency of scan)
$\theta_T = 8^o = 0.14$ radians	(total field of view of scan)
$\omega_s = \pi f_R \theta_T = 176$ rad/sec	(sweep center angular velocity)
$\alpha = 0.01$ radians	(scanning spot diameter above threshold)
$t_p = \frac{\alpha}{\omega_s} = 57\mu$ s	(threshold interval within output pulse)

$N = 32$ (number of pulses per frame)

$B_F = 25$ cps (noise bandwidth of frame scan filter)

$B_\epsilon = 5$ cps (noise bandwidth of error signal filter)

Referring to (22-b), and for the above values,

$\hat{B}_P = 31,500$ cps (optimum noise bandwidth for video amplifier).

Referring to (19)

$$\exp -\left(\frac{4\hat{B}_p \alpha}{\pi f_r \theta T}\right) = 0.00085,$$

and thus the edge noise correlation is 0.085% of the mean square noise for optimum amplifier bandwidth.

To show the dependence of the RMS angular error (in arc seconds) on amplifier noise bandwidth, B_p, and star magnitude, m, for the above values inserted into (21),

$$(\sigma \Phi x)_\epsilon = \frac{5.1 \times 10^{-2}}{1 - \exp(-.00004 B_P)} \sqrt{2.51^m B_P} \qquad (23)$$

Table 4 indicates the per axis RMS error in arc seconds using (23).

The results show a noncritical dependence on amplifier bandwidth for even a third magnitude star. Again, these results reflect the assumption of time to threshold being large compared to the amplifier time constant.

To show, on the other hand, the dependence on the electronic rise angle, δ, the limit of (21) as δ approaches zero, is

$$(\sigma \Phi x)_\epsilon = \frac{3.6 \times 10^4}{D} \times \frac{\pi f_r \theta_T}{4} \sqrt{\frac{2.51^m}{Q \lambda a} \frac{B_\epsilon}{N B_F B_P}} \qquad (24)$$

TABLE 4

Per Axis RMS Error

B_p	m			
	3	2	0	-3
10×10^3	65.0	39.5	15.6	3.9
20×10^3	52.0	33.8	13.0	3.25
$31.5 \times 10^{3*}$	51.0	32.3	12.7	3.18
40×10^3	51.2	32.5	12.7	3.20
50×10^3	54.0	34.0	13.7	3.38

$*B_P$

Equation (24) shows that for the signal input train to the amplifier a series of rectangular pulses, the RMS output error is directly proportional to the sweep center angular velocity, $\pi f_R \theta_T$. This contrasts with the weak dependence for the input train with a rise angle, $\delta \geq \frac{\pi f_R \theta^T}{4aB_P}$ as shown by (21). As Table 5 indicates, for a sweep center angular velocity = 176 radians/sec., and all other parameters the same as well, the improvement for a faint star is significant. In arc seconds,

$$(\delta\phi x)_\epsilon = 1.25 \times 10^3 \sqrt{\frac{2.51^m}{B_P}}, \qquad (25)$$

for $\delta = 0$.

Now considering the average interval between photoelectrons and the resolving time of the video amplifier, the following is noted:

TABLE 5

Per Axis RMS Error Improvement

B_p	m	
	3	-3
10 x 10^3	50	3.12
20 x 10^3	35.5	2.22
31.5 x 10^3	28	1.75
40 x 10^3	25	1.56
50 x 10^3	22.3	1.39

The average number of electrons per second,

$$P_e = \frac{I_s}{e} = \frac{PQ\lambda}{hc} = 8 \times 10^6 \frac{D^2 Q\lambda}{2.51^m} \qquad (26)$$

for D inches and λ in microns. For m = +3, and the other parameters as previously evaluated,

$$P_e = 5 \times 10^4 \text{ electrons/sec.}$$

and the average interval,

$$t_e = \frac{1}{P_e} = 2 \times 10^{-5} \text{ sec.}$$

The smoothing time or limit of time resolution of impulse events for a linear filter of noise bandwidth, B_P, is

$$\Delta t_P = \frac{1}{2B_P}$$

and for B_p at optimum = 31,500 cps.

$$\Delta t_P = 1.6 \times 10^{-5} \text{ sec.}$$

With such a bandwidth, the amplifier should resolve most individual electrons as individual output impulses. This is occasionally observed; however, contrary to the requirements for signal modulated noise, the results predicted by (23) agreed quite well with noise measurements for a magnitude 3 star. No explanation can be offered as a theory for predicting sensor angular error for the low signal to noise ratio case, i.e., for resoluble electrons is not now available.

The average number of electrons per pulse for a magnitude 3 star, and for the total field of view = 8^o is surprisingly small. This number,

$$\bar{n}_P = p_e t_p = 5 \times 10^4 \times 57 \times 10^{-6} = 2.8 \text{ electrons}$$

This implies that the number per frame and thus the minimum number to vector the star image relative to boresight is

$$N\bar{n}_p = 32 \times 2.8 \cong 90 \text{ signal electrons}$$

Thus a surprisingly small number of electrons can yield, without further filtering, $\frac{B_F}{B_\epsilon}$ $(\delta\phi x) = 5 \times 51$ arc seconds = 114 arc seconds - RMS.

To continue the numerical evaluations:

$$(\delta\phi x)_\epsilon = \frac{3.6 \times 10^{-4}}{D} \left[\frac{\delta}{1 - \exp -\left(\frac{4aB_p\delta}{\pi f_{R\,\theta T}} \right)} \right] \sqrt{\frac{2.51^m \; aB_\epsilon \; B_p}{\Omega \lambda N B_F}}$$

D = 2 in. (optical aperture)

δ = 15 arc min. = 4.5×10^{-3} rad. (electronic rise angle)

f_R = 400 cps (radial scan frequency)

$m = 3$ (star magnitude)

$\lambda = 0.5$ microns (star photon wavelength)

$N = 32$ (no. of pulses per frame)

$B_F = 25$ cps (frame scan filter noise bw)

$B_\epsilon = \frac{\pi}{2} \times 5 \text{ cps} = 7.8$ cps (error signal filter noise bw)

$B_p = 47 \times 10^3$ cps (video amplifier noise bw)

$a = \frac{I}{I_s} = 0.4$ (threshold ratio)

$Q =$ quantum eff.

$$\sqrt{\frac{2.51^m \; aB_\epsilon \; B_D}{Q\lambda N B_F}} = \frac{76}{\sqrt{Q}}$$

$$\frac{raB_p\delta}{\pi f_R \theta_T} = \frac{0.27}{\theta_T}$$

For the previous evaluations, the RMS angular jitter per axis, $(\delta\phi x)_\epsilon$, in arc seconds, depends on total field of view, θ_T, and quantum efficiency as shown in Table 6.

TABLE 6

RMS Angular Jitter

Q	θ_T		
	0^o	2^o	8^o
.05	55	55	59
.25	24.6	24.6	26
.5	17.4	17.4	18.4

The results predicted agree quite well with some experimental results which are for a B_p = 47,000 cps, and all other parameters as stated, $(\delta \phi x)_\epsilon$ = 60 arc seconds for m = 3, and 15 arc seconds for m = 0. (Note the table for B_p = 50,000 cps.)

The conclusion is that the analysis is essentially sound, and that short of improving the tube by reducing its smearing diameter, δ, increasing its quantum efficiency, or of costly additional signal processing methods such as delay line filtering between the amplifier and threshold detector, the star sensor system's performance cannot be expected to improve significantly.

MEASUREMENT PROCEDURES

The Multipurpose Star Tracker is furnished with two AN connector plugs; one, with six pins, is designated J-1 and the other, with ten pins, is designated J-2. External connections are made to the two connectors for the purposes of (a) supplying power to the tracker, (b) supplying star tracker error signals to the control system, (c) supplying "star magnitude" and "star present" signals to the telemeters and (d) furnishing additional test voltages for monitoring during check-out or trouble shooting.

External connections as shown in Figure 49 should be sufficient to obtain star tracker output characteristics and give enough information to assure proper operation of various sections of the tracker.

The various pin connections and their relationship to proper tracker operation are summarized in Table 7 and detailed in the following text.

Connector J-1

Pin A: plus (+) 15 volt terminal of DC Power Supply No. 1.

Pin B: minus (-) terminal of DC Power Supply No. 1.

Pin C: minus (-) 15 volt terminal of Power Supply No. 2.

Pin D: plus (+) terminal of Power Supply No. 2.

TABLE 7

Tracker Terminal Designations

PLUG - PIN	FUNCTION	CONNECTION
J-1 A	+	External Connection
B	-	
C	-	External Connection
D	+	
	15 V Power Supply	
E	Chassis Ground	
F	High voltage Test Point	High Voltage Supply Brn-Orn wire
J-2 A	Vertical (Y-Axis) Error Signal	Board No. 0 Term. 5
B	Ground	
C	Horizontal (X-Axis) Error Signal	Board No. 0 Term.6
D	Neg. Video Pulse	Board No. 8 Term.D
E	Star Magnitude	Board No. 9 Term J
F	25 CPS Information Filter	Board No. 5 Term.A
G	25 CPS Square Wave Timing	Board No. 2 Term.3
H	Star Present Signal	Board No. 9 Term.G
J	Deflection Feedback Horizontal	Board No. 3 Term.F
K	Deflection Feedback Vertical	Board No. 3 Term.E

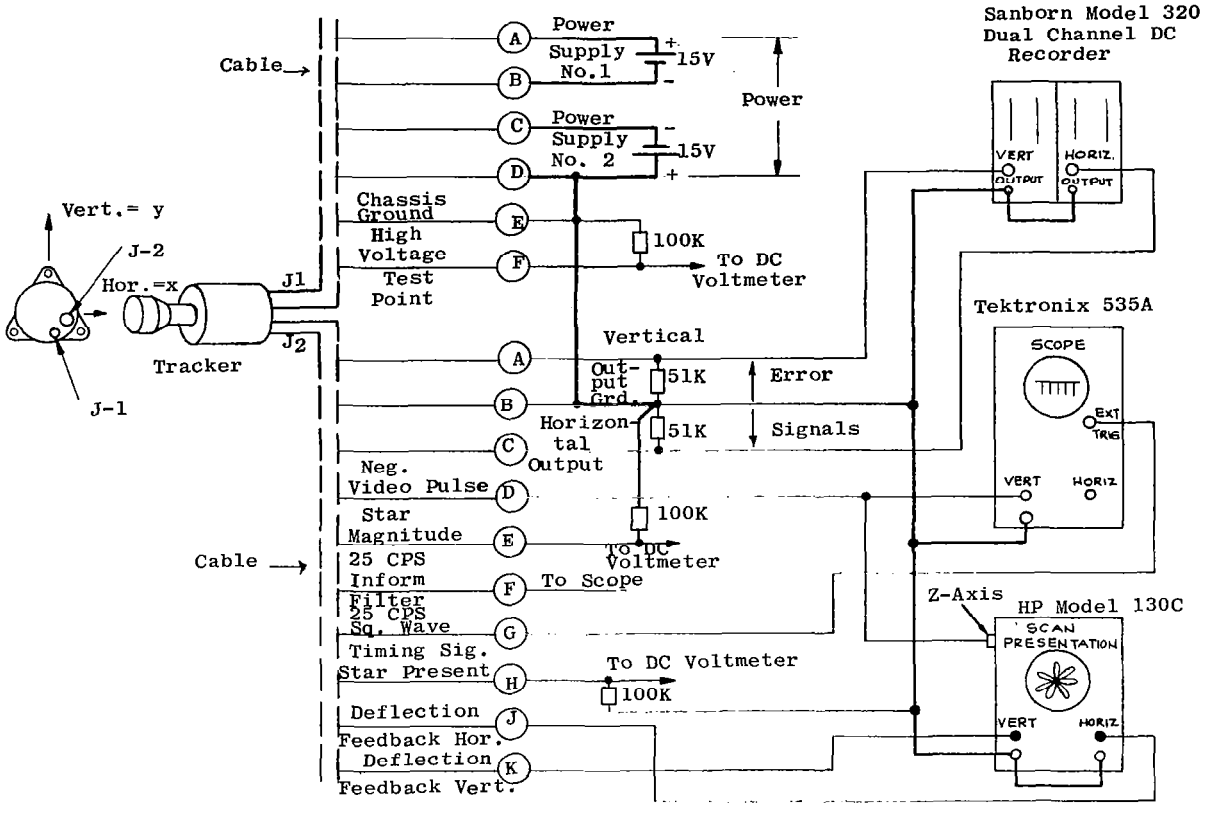

System Test Setup

FIGURE 49

Both of the above dc power supplies should be of the regulated, low output impedance, current limiting type. The positive supply (Pin A) will draw approximately 180 milliamperes dc, and negative supply (Pin C) approximately 120 milliamperes dc. In order to handle peak current demands, the current limiting controls on both power supplies should be set to approximately 450 milliamperes.

Pin E: Shield and chassis ground.

Pin F: High voltage test point. External termination one hundred thousand (100,000) ohms. Under normal operating conditions, this voltage will be approximately -2 volts, but will vary depending upon star magnitude. If no voltage is measured here, probable malfunctions are no high voltage or an open channel.

Connector J-2

Pins A, B, C: Pin A is the vertical (y-axis) error signal and Pin C is the horizontal (x-axis) error signal. Both outputs are returned through Pin B, which is also reference ground. The output error signals can be monitored and their characteristics obtained by connection to a dual channel recorder, as shown in Figure 49, or by the use of any accurate dc voltmeter. Representative star tracker output characteristics are shown in Figure 50.

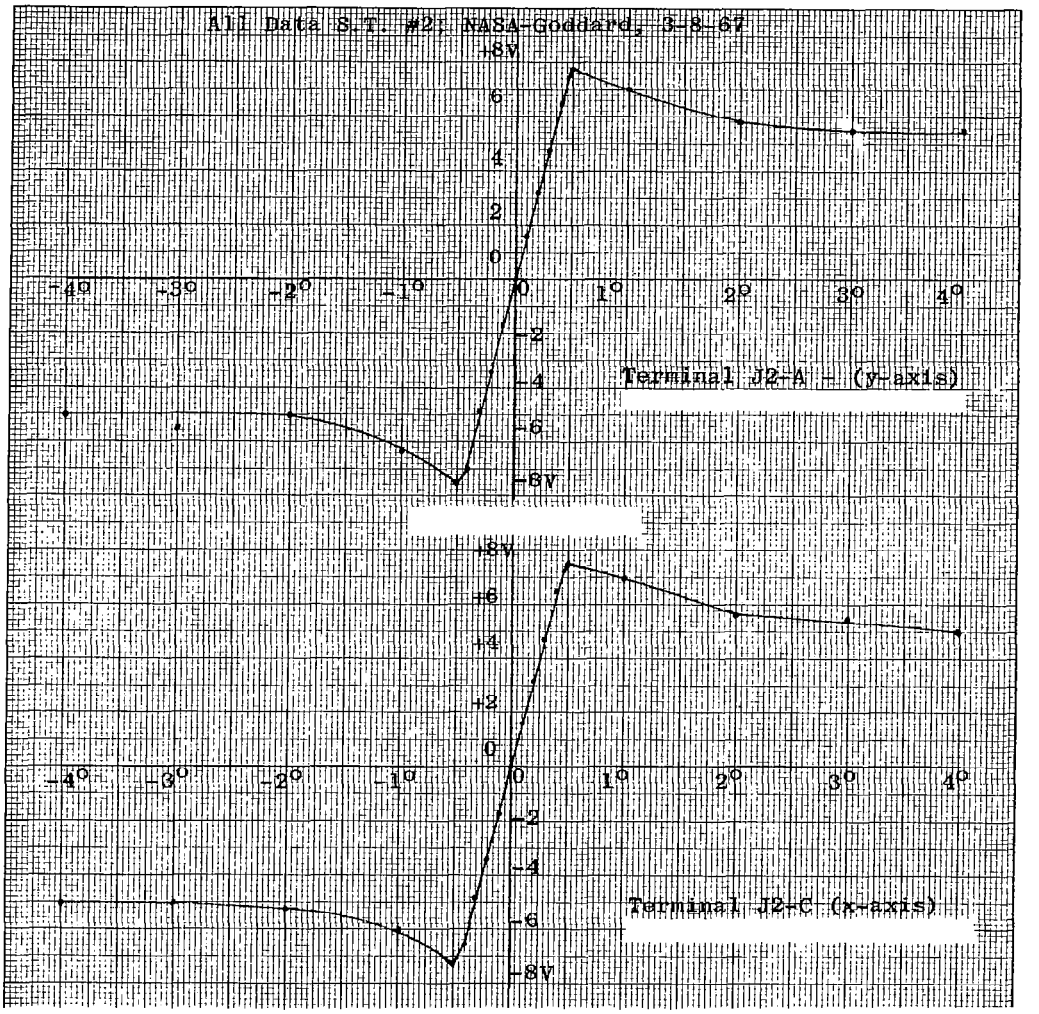

Output Vs Star Position

FIGURE 50

Pin D: Pin D is the negative video signal and can be monitored with a Tektronix Type 535A or equivalent oscilloscope. Representative video signals at this pin for various star positions are shown in Figures 51 through 54. All waveforms shown are with the oscilloscope externally (+) triggered by the 25 cps square wave timing signal from Pin J-2G. The video signal at this pin can also be applied to the Z -axis of the scan-presentation oscilloscope for intensification of the scan pattern to aid in locating the star during testing. Representative scan patterns intensified by the video signals are shown in Figures 51 through 54 for different star positions.

Pin E: Terminate with one hundred thousand (100, 000) ohms. This pin supplies "star magnitude" voltage to a telemeter channel. The voltage will measure from zero to plus (+) five volts for the range of star magnitudes the tracker is designed to operate over. A representative curve of star magnitude voltage for various star magnitudes is shown in Figure 55.

Pin F: 25 cps information filter. This 25 cps signal will vary in magnitude and phase as a function of star position. Its relationship to star position is best monitored by applying the signal to the vertical input of an oscilloscope that is externally triggered (+) by the 25 cps timing signal obtained from Pin J-2G. Representative waveshapes obtained at Pin J-2F are shown in Figures 51 through 54 for various star positions.

Pin G: 25 cps square wave timing signal. This signal is obtained by dividing down from the 800 cps oscillator. Thus, it is used to monitor operation of the timing section. In addition, it can be used to trigger the oscilloscope and maintain a time reference when viewing other test signals. The signal obtained at Pin J-2G is shown as a reference waveform in Figures 51 through 54.

Pin H: Terminate with one hundred thousand (100, 000) ohms. This pin supplies a "star present" signal to a telemeter channel. Under "no star" conditions the voltage will be 0 ± 0.5 volts and under "star present" conditions the voltage will be 5 ± 0.5 volts. This may be measured with any acurate high impedance voltmeter or recorder.

J-25 25 CPS TIMING
5 V/CM 5 MILLISEC/CM

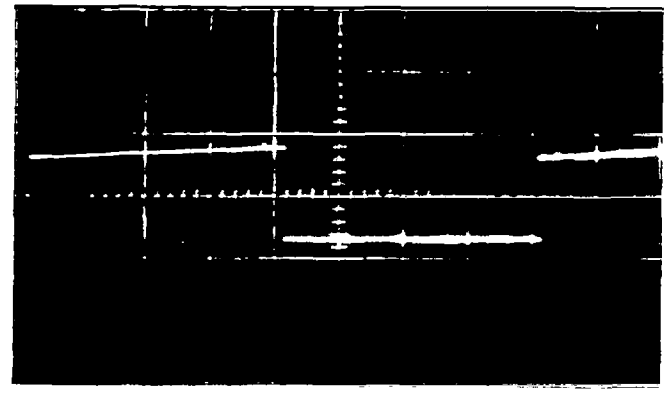

STAR AT BORESIGHT

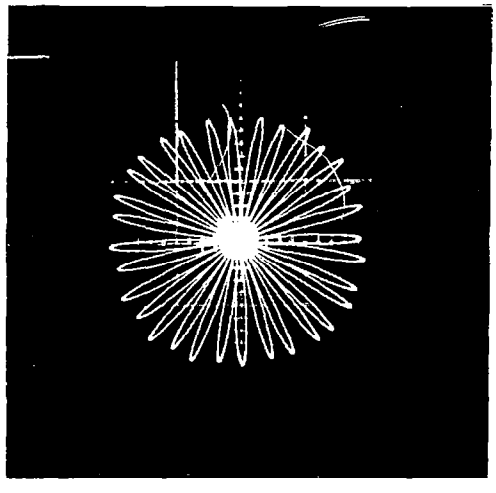

J-2D NEGATIVE VIDEO PULSE
5 V/CM 5 MILLISEC/CM

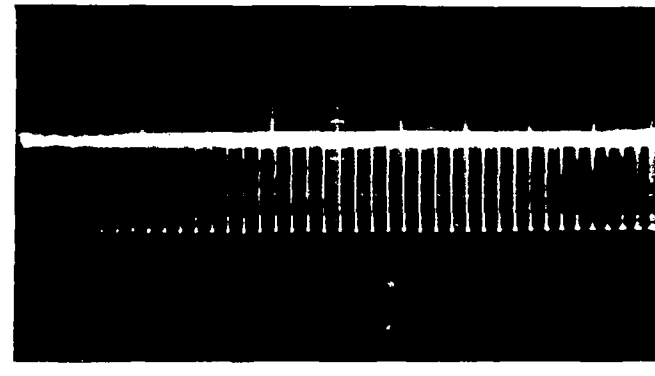

J-2F 25 CPS INFORMATION
5 MILLISEC/CM

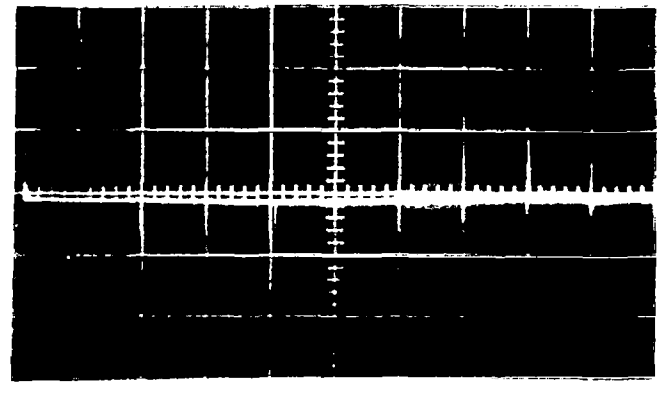

Wave Forms With Star
At Boresight

FIGURE 51

J-2G 25 CPS TIMING
5 V/CM 5 MILLISEC/CM

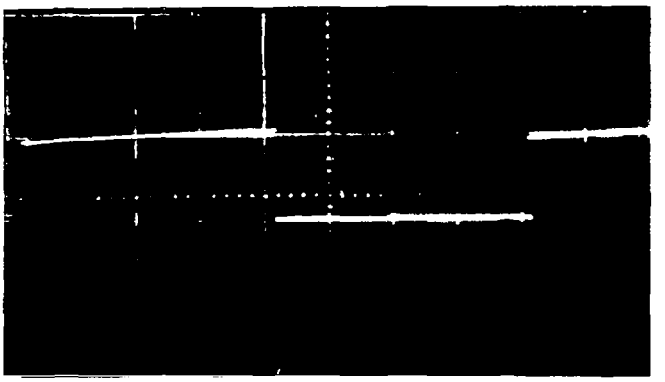

STAR OFF BORESIGHT
HORIZONTALLY (X-AXIS)

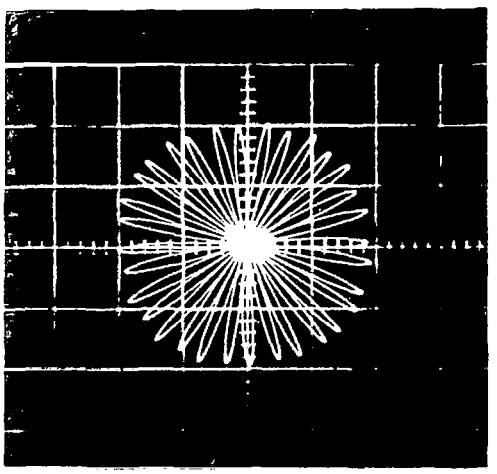

J-2D NEGATIVE VIDEO PULSE
5 V/CM 5 MILLISEC/CM

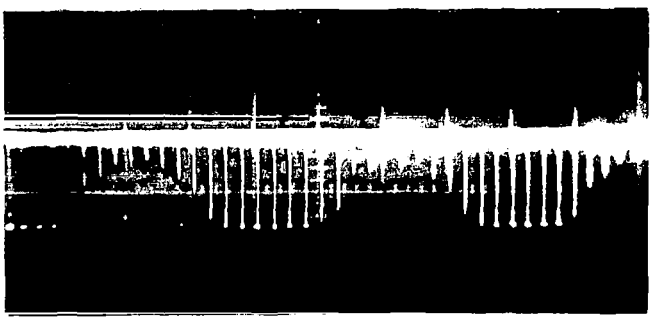

J-2F 25 CPS INFORMATION
5 MILLISEC/CM

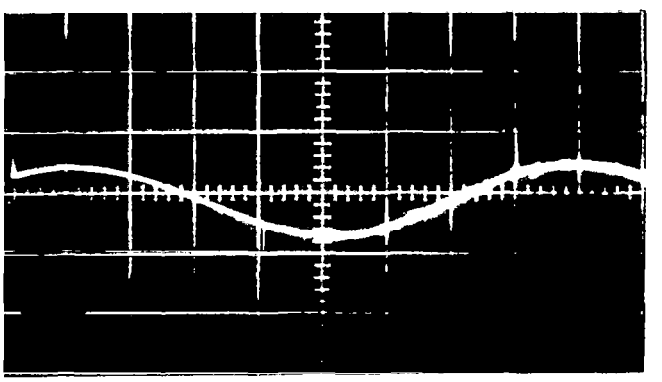

Wave Forms With Star Off
Boresight Horizontally

FIGURE 52

J-2G 25 CPS TIMING
5 V/CM 5 MILLISEC/CM

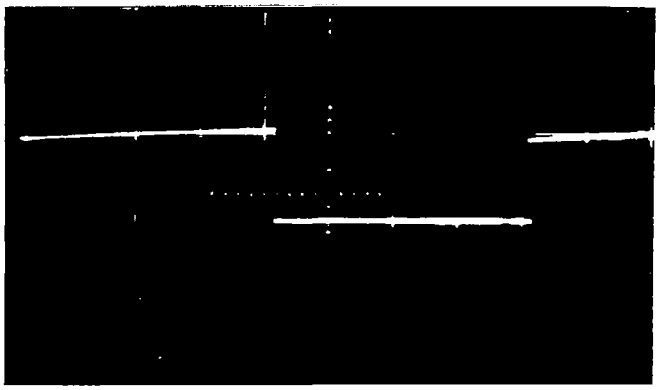

STAR OFF BORESIGHT
VERTICALLY (Y-AXIS)

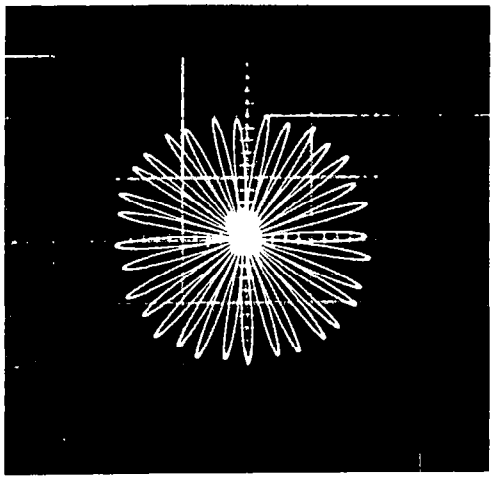

J-2D NEGATIVE VIDEO PULSE
5 V/CM 5 MILLISEC/CM

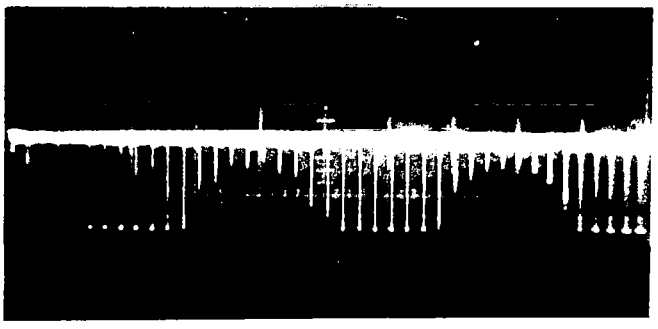

J-2F 25 CPS INFORMATION
5 MILLISEC/CM

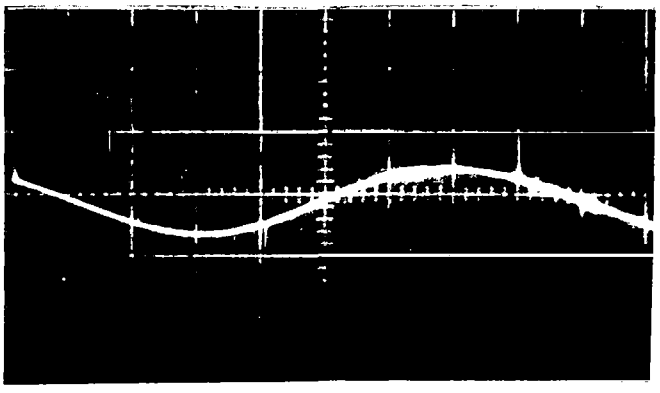

Wave Forms With Star Off
Boresight Vertically

FIGURE 53

J-2G 25 CPS TIMING
5V/CM 5 MILLISEC/CM

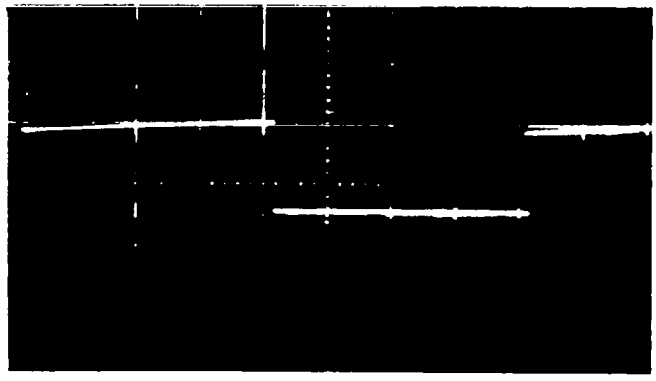

STAR OFF BORESIGHT
HORIZONTALLY (X-AXIS)
and
VERTICALLY (Y-AXIS)

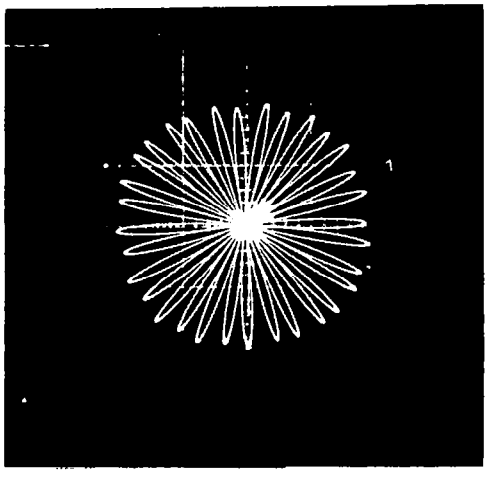

J-2D NEGATIVE VIDEO PULSE
5 V/CM 5 MILLISEC/CM

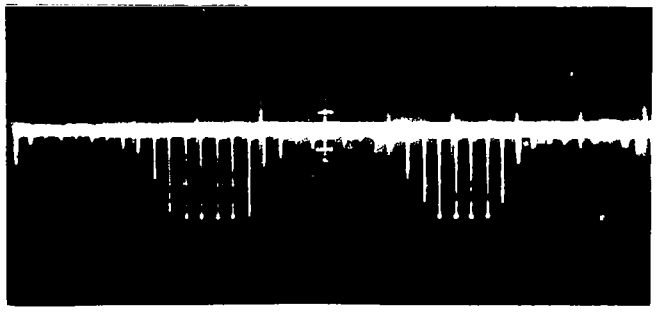

J-2F 25 CPS INFORMATION
5 MILLISEC/CM

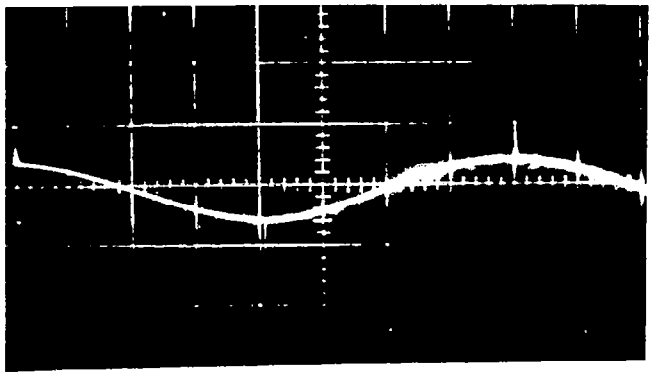

Wave Forms With Star Off
Boresight In Both Axes

FIGURE 54

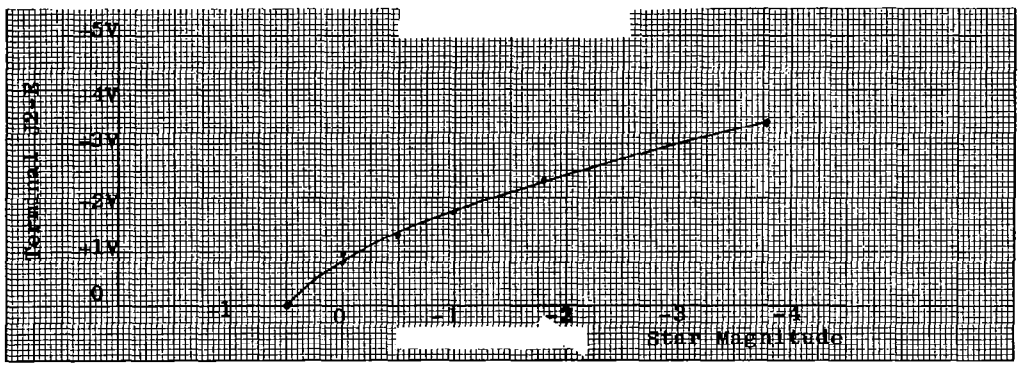

Star Magnitude Voltages

FIGURE 55

Pins J and K: Pins J and K are internally connected to the feedback resistors in the current amplifiers driving the x and y deflection coils. By externally connecting Pins J and K to the vertical and horizontal amplifiers of an oscilloscope, the multilobed current scan driving the deflection coils may be presented as an aid in checking star tracker operation. By simultaneously applying the negative video signal obtained from Pin J-2D to the " Z -axis" of the oscilloscope to intensify the beam, the star position may be "seen" on the oscilloscope and aid in positioning the test star to a desired point in the field of view. The multilobed scan pattern intensified by the negative video signal is shown in Figures 51 and 54 for various star positions. The waveforms of the voltages across the deflection amplifier feedback resistors, Pins G and H are shown in Figure 56 with the oscilloscope again externally triggered (+) by the 25 cps timing signal from Pin J-2G.

The wiring from the two connector plugs to the internal portion of the star tracker is shown in Figure 49.

J-2G 25 CPS TIMING
5 V/CM 5 MILLISEC/CM

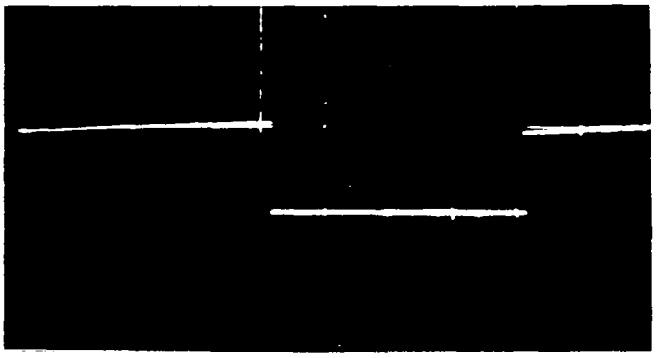

J-2J DEFLECTION FEEDBACK X AXIS
5 MILLISEC/CM

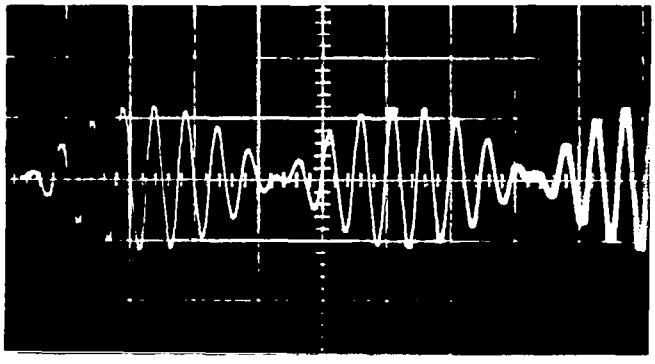

J-2K DEFLECTION FEEDBACK Y-AXIS
5 MILLISEC/CM

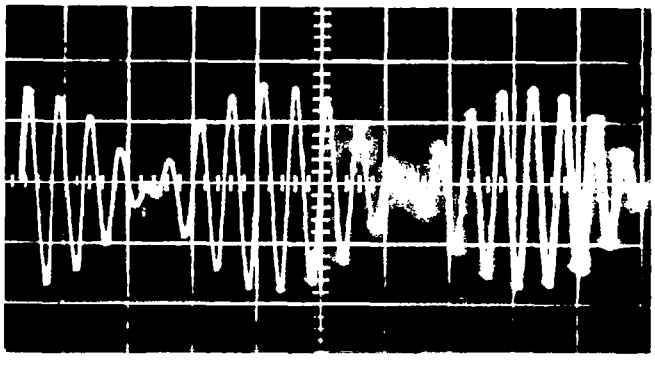

Deflection Signals

FIGURE 56

CONCLUSIONS

The Multipurpose Star and Planet Tracker will track most of the navigational stars and the center of illumination of the visible planets. The pointing accuracy is necessarily limited by the star class and magnitude. It will track a +0.2 magnitude G_0 class star with a pointing accuracy of 25 seconds of arc, acquiring it at the edge of its relatively wide angle field of view and supplying control signals to orient the vehicle into alignment without generating the switching transients associated with two mode systems. This feature alone should make the tracker applicable to vastly simplified control systems of inherently higher reliability than presently employed.

The field of view may readily be changed by a simple internal gain adjustment in the deflection drive amplifier. Thus, if the scan is reduced to 2 degrees, a +3.0 magnitude G_0 class star will be tracked with a pointing accuracy of 20 arc seconds, etc.

The circuits employed are remarkably free of drifts; solid-state components used have suffered no failures in the more than 1000 hours of breadboard operation and packaged tracker operation. This is equally true of the magnetoresistive bridge multipliers and the integrated circuits employed. The only component failure experienced was where least expected, in the dc inverter transformer during vibration.

The Channeltron ® image dissector photomultiplier has been brought to a stage of development where it is competitive with existing image dissectors in operation, and where its inherent ruggedness and high reliability, coupled with the smaller size and freedom from external voltage dividers, should make it applicable to a variety of photodetection purposes.

A great deal of experience has been accumulated by the vendor's organization in star tracking problems and techniques which should provide the stimulus for additional projects of this nature.

RECOMMENDATIONS

In the light of the experience gained in the pursuit of the present project it is possible to make the following recommendations:

1. Decrease the output bandwidth requirement from 5 cps to 1 cps. This will cut the signal-to-noise pointing error in half, and will allow the tracker to be used with existing control systems. This requires that approximately 15 mfd be added across each output terminal.

2. Decrease the scan frequency from 400 cps to 200 cps, and allow for degradation near the edge of the field of view due to decreased overlap of the scanning spot. This requires a change in the filter circuits and adjustment of output gradient.

3. Change from a sine wave "line" frequency to a triangular wave; this will increase "dwell time" on the target, in the proportional region (which is the principal region of interest) by 50%. This involves the substitution of integrators for the existing filters to generate the triangular waves.

4. Substitute a logarithmic amplifier for the existing video amplifier. This minimizes the need for extensive servoing of the high voltage and frees the dc operating point, thus permitting greater adjustment in the positioning of the video pulse threshold value, i.e., permits selection of the threshold at that point of the "pulse rise distance" where there is greatest slope.

5. Alternately, or concomitantly, decrease the field of view.

6. Compare tables 8 and 9 for an indication of the improvement to be expected.

In addition, there are several general suggestions to be made:

The experience with the microcircuited portion of the system has been very good. High density packaging was avoided in this program to enable development to proceed along with final packaging of the two flyable prototypes. A greater use of microcircuits is therefore possible. All the circuits of Boards 3, 6, and 9, for example, could be contained on one board with readily available microcircuits. This, coupled with slightly higher overall density, could yield a tracker embodiment about half the size and weight of the existing tracker. The benefits of the small Channeltron® image dissector over that of large conventional dissectors is not fully exploited in the present tracker design.

The Channeltron® type of image dissector has now reached the stage of development where production of good S-20 cathodes is routine. A sustained effort to incorporate this detector in other star trackers and related devices is therefore desirable, both from the vendor's standpoint and that of the procuring agency.

TABLE 8

Error in Seconds of Arc, Delivered Tracker

MAG	FIELD OF VIEW	
	8^{o}	2^{o}
-3	13	5
0	25	10
+3	58	20

TABLE 9

Error in Seconds of Arc after Modification

MAG	FIELD OF VIEW	
	8^{o}	2.6^{o}
-3	3	3
0	13	6
+3	37	18

BIBLIOGRAPHY

The Bibliography given below contains a list of those papers and publications related directly to the specific project reported upon. No effort has been made to cover the topic of star tracking and trackers, with which the technical literature abounds. Thus, references 1 and 2 are papers presented by members of the Bendix engineering staff on the subject project; references 3, 4 and 6 are papers presented by Bendix personnel on the development of continuous strip electron multipliers of the Channeltron® variety; reference 5 discusses the Channeltron® Image Dissector Photomultiplier, and reference 7 discusses the magneto-resistive bridge multipliers employed for scan generation.

1. G. V. Zito and S. Malkiel; Fourth Int'l. Aerospace Instrumentation Symposium, Cranfield, Bedford, England; March, 1966.

2. G. V. Zito and S. Malkiel; Trans. Twelfth ECCANE, IEEE, Baltimore, Md., 1965.

3. W. C. Wiley and C. F. Hendee; Trans. IRE Nuc. Sci. NS-9, 103; 1962

4. G. W. Goodrich and W. C. Wiley, RSI. 33, 761, July 1962.

5. D. Ceckowski and W. R. Polye; IEEE Int'l. Record, 1964.

6. J. Adams and B. W. Manley, Elec. Eng., March, 1965.

7. T. Baasch; Elec. Prod. Vol. 6, No. 12, 1964.

APPENDIX A

ENGINEERING TEST SUMMARY

TO: G. Zito (2)

THE Bendix CORPORATION
ECLIPSE-PIONEER DIVISION • TETERBORO, NEW JERSEY

ENGINEERING TEST SUMMARY

ETS NO. 6010
PROGRESS
FINAL X
DATE 3/3/67

COPIES TO:
P. Bechberger
E. Meeder
E. Shulton

TEST SPECIMEN DESCRIPTION: Star and Planet Tracker

MFR. OF SPECIMEN	MODEL NO.	SERIAL NO.(S)
Bendix	X-1863465	2

ASSOCIATED PROGRAM OR SYSTEM DESCRIPTION: AEROBEE

TYPE OF TEST	START TEST (DATE)	END TEST (DATE)
Vibration and Shock	2/18/67	2/21/67

TEST ENGINEER: R. Byrd
SUPERVISOR: E. Linhart
COMPREHENSIVE REPORT FOLLOWS: YES ; NO X

OBJECT OF TEST:

To demonstrate compliance with Contract No. NAS 5-3780

Para. 3.3

TEST EQUIPMENT AND IDENTIFICATION:	S/N	Cal.due date
C-125 Vibration Exciter M.B. Electronics	E-39893-63	2 Mon May 67
MB Automatic Random Console	--------	April '67
Accelerometer, Mod.304 M.B. Electronics	297	4-21-67
C-60B Vibration Exciter M.B. Electronics	E-39823-64	4 Wed Mar.'67
M B Amp- Integrator N504	A-35520-64	4 Tue May '67
Accelerometer, Mod. 304	188	4-4-67
HYGE, Type HY-6002 Shock Machine	---	------

TEST SET-UP(S): Accelerometer, Mod. 1211 ENDEVCO 6623 4-17-67

The test specimen was mounted on Vibration and Shock Fixture E.T.D. 6010. The specimen was not powered during this test.

See photos 67-1246, 67-1256 for set up.

DISPOSITION OF SPECIMEN(S):

The test specimen was returned to Dept. 9031.

SHEET 1 OF 7

FORM 10808

THE Bendix CORPORATION

ECLIPSE-PIONEER DIVISION • TETERBORO, NEW JERSEY

ETS NO. 6010

ENGINEERING TEST SUMMARY (CONTINUATION SHEET)

TESTING PERFORMED AND RESULTS:

The test specimen was subjected to 10 g's rms of white noise composed of frequencies from 20 - 2,000 HZ. For a duration on one (1) minute in the longitudinal axis, and then was subjected to 6.2 g's rms of white noise composed of frequencies from 20-2000 HZ for a duration of one (1) minute in the two (2) lateral axes. See Fig. 1-3 for spectrum plots.

The test specimen was also subjected to a sinusoidal vibration of 6 g's rms with a sweep rate of one (1)octave per minute from 20 - 2000 HZ in each of the three axes. The input accelerometer was monitored thru-out the entire testing and all amplitude and resonant frequencies were noted.

The test specimen was then subjected to one 30 g - 11 millisecond half sine shock in the longitudinal axis.

Detailed log sheets are on file in the Engineering Test files.

SHEET 2 OF 7

FORM 10809

THE Bendix CORPORATION
ECLIPSE-PIONEER DIVISION • TETERBORO, NEW JERSEY

K•E SEMI-LOGARITHMIC 359-91
KEUFFEL & ESSER CO. MADE IN U.S.A.
6 CYCLES X 70 DIVISIONS

Fig. 1

AUTOMATIC RANDOM VIBRATION ANALYSIS
MB MODEL T589

ENGINEERING TEST
ETO NO 6010

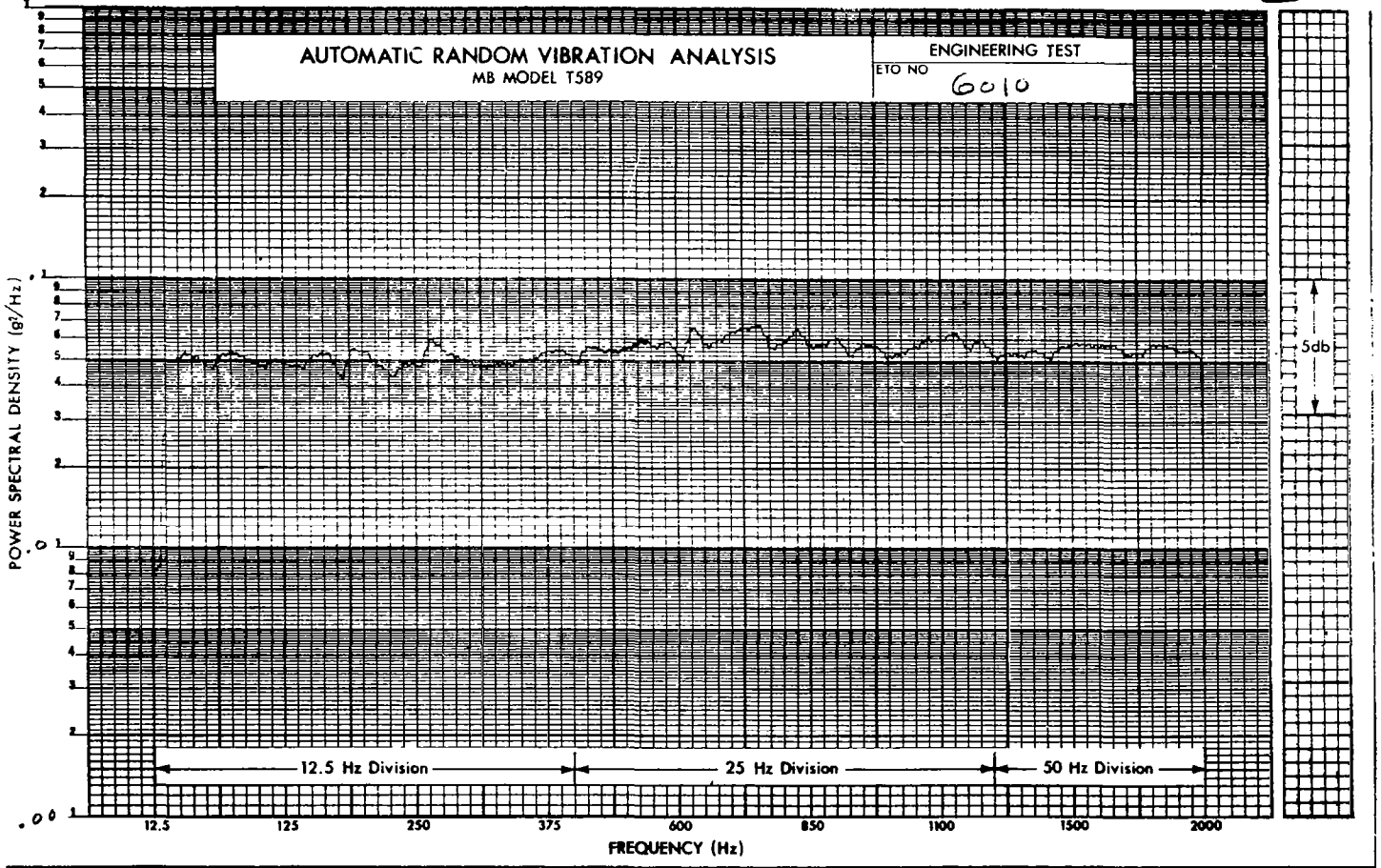

TEST SPECIMEN	VIBRATION AXIS	ACCEL. LOCATION	OVERALL G's rms	DATE	TIME	TEST ENGINEER
STAR & PLANET TRACKER SW-2	#1 LONG.	Fix.	10.0	2-21-67	1455	D.C. Ramsambe

FORM 13961 NS

AL

THE Bendix CORPORATION
ECLIPSE-PIONEER DIVISION • TETERBORO, NEW JERSEY

K•E SEMI-LOGARITHMIC 359-91 KEUFFEL & ESSER CO. MADE IN U.S.A. 8 CYCLES X 70 DIVISIONS

Fig-2

AUTOMATIC RANDOM VIBRATION ANALYSIS
MB MODEL T589

ENGINEERING TEST
ETO NO. 6010

POWER SPECTRAL DENSITY (g²/Hz)

5db

12.5 Hz Division — 25 Hz Division — 50 Hz Division

125 250 375 600 850 1100 1500 2000

FREQUENCY (Hz)

TEST SPECIMEN	VIBRATION AXIS	ACCEL. LOCATION	OVERALL G's rms	DATE	TIME	TEST ENGINEER
STAR & PLANET TRACKER S/N-2	DIR #3	FIXTURE	6.2	2-21-67	1537	D.C. Bransomb

FORM 13961 NS

THE Bendix CORPORATION
ECLIPSE-PIONEER DIVISION • TETERBORO, NEW JERSEY

K•E SEMI-LOGARITHMIC 359-91
KEUFFEL & ESSER CO. MADE IN U.S.A.
8 CYCLES X 70 DIVISIONS

FIG. -3

AUTOMATIC RANDOM VIBRATION ANALYSIS
MB MODEL T589

ENGINEERING TEST
ETO NO. 6010

POWER SPECTRAL DENSITY (g^2/Hz)

5db

12.5 Hz Division | 25 Hz Division | 50 Hz Division

12.5 125 250 375 600 850 1100 1500 2000

FREQUENCY (Hz)

TEST SPECIMEN	VIBRATION AXIS	ACCEL. LOCATION	OVERALL G's rms	DATE	TIME	TEST ENGINEER
STAR & PLANET TRACKER SN-2	LAT. #2	FIXTURE	6.2	2-21-67	1548	DC Ramsey Corp

FORM 13961 MS

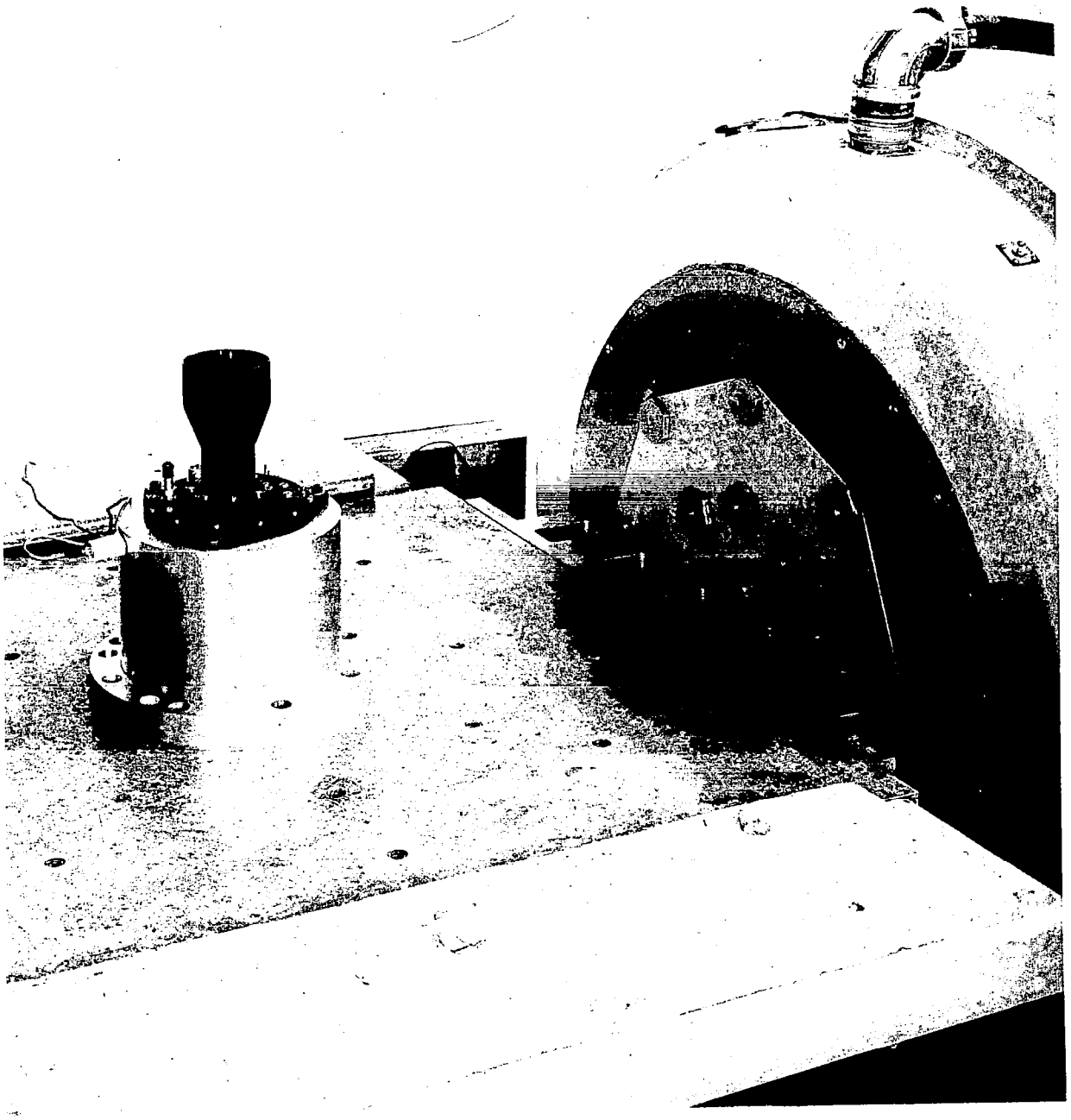

Tracker on Vibration Test Stand

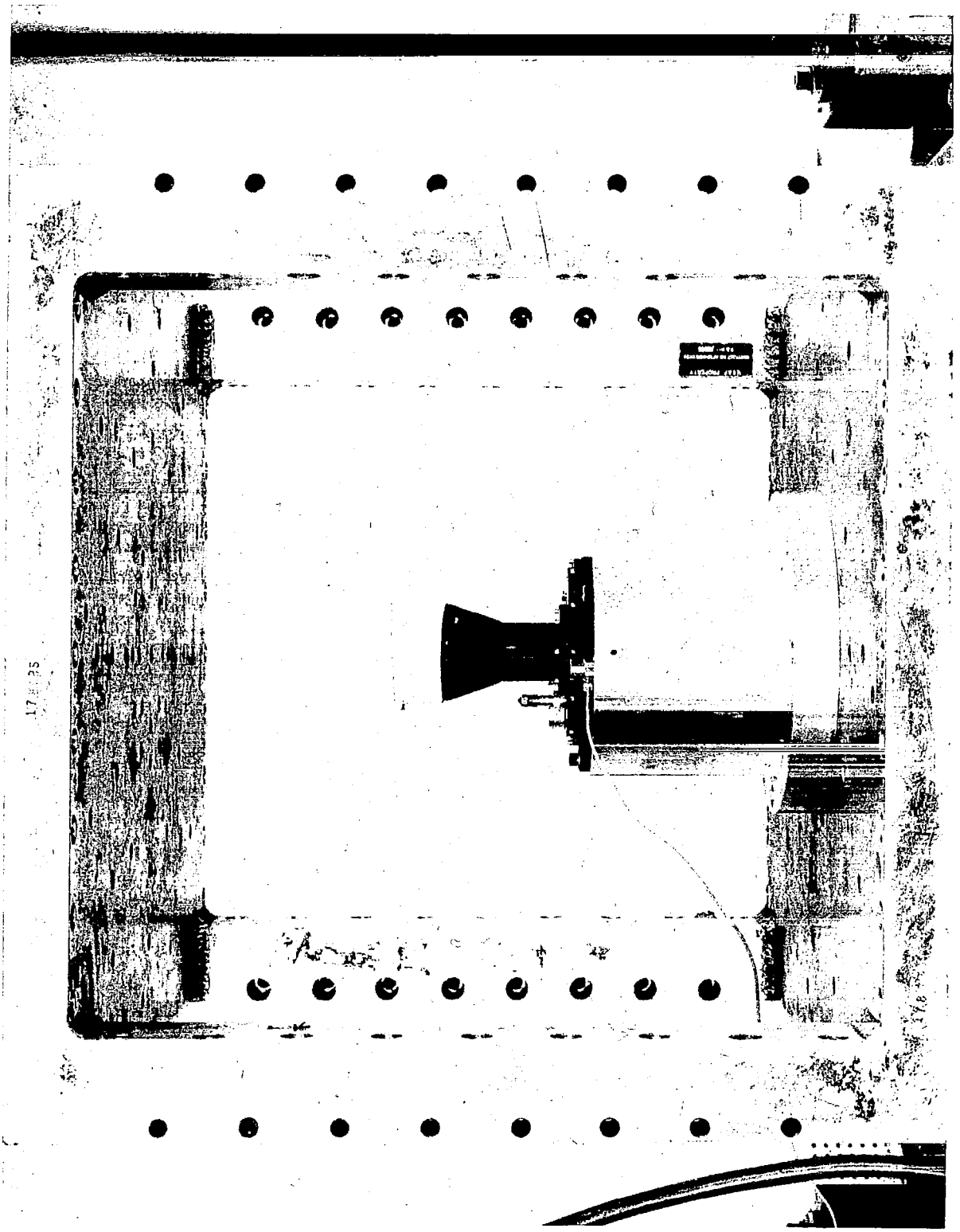

Tracker on Shock Machine